TORSIONAL BEHAVIOUR OF WIRE ROPES FOR KOEPE WINDERS

Jason Minas Yiassoumis

A dissertation submitted to the Faculty of Engineering, University of the Witwatersrand, Johannesburg, in fulfilment of the requirements for the degree of Master of Science in Engineering

Johannesburg, 1992

ABSTRACT

The torsional behaviour of steel wire ropes used on Koepe winders for vertical shafts is analysed. Theoretical models have been developed for the behaviour of both the head and tail ropes after correcting an assumption made by previous researchers regarding the torque in the ropes. The theoretical models utilise experimentally obtained rope properties. The properties were measured from rope samples tested in a laboratory using specially developed equipment and software. Instruments were designed and used for in-situ measurements on an 1800 m deep shaft during a complete return trip. Some of the measurements were affected by unexpected strong torsional oscillations. However the general trends of the measured torsional behaviour were correctly predicted by the theoretical models. Discrepancies are attributed to the difficulties of obtaining true rope properties, to assumptions made in order to obtain a workable model and to inaccuracies in the measured behaviour because of the strong torsional oscillations. Further research is recommended. Nevertheless there is sufficient correlation between the models and the experiments, as well as with other published results, to draw certain conclusions with confidence. In particular the results confirm the adverse effect of hoisting depth, the need to use non-spin ropes and the need for swivels at both ends of freely looped tail ropes. New findings include the importance of balanced frictional torque between the two swivels of a tail rope and the realisation that the rope rotation is caused by the torque difference between the two legs of a head or tail rope and not the absolute value of the torques. The results also emphasize the important role of the torsional stiffness of a rope in relation to its torsional behaviour. The use of theoretical models to design or select ropes suitable for specific Koepe winders is suggested.

Total 14 + 194 pages

The scanned pages from the paper document follow …

8 CONCLUSIONS AND RECOMMENDATIONS

As pointed out by Dr. J.T.D. Fritz previous research included an error in the assumption that the torque in hoisting ropes varies along their length. Assuming constant torque, new theoretical models were developed. The predictions of these models, based on laboratory measurements of rope properties were tested on a working Koepe winder.

Difficulties were encountered during some measurements on a working Koepe winder in the form of strong torsional vibrations. Such measurements involve considerable preparation and coordination with officers on the mine and could not be repeated. Nevertheless an attempt has been made to extract results by analytical manipulation to eliminate the effect of the vibrations.

8.1 Findings Related to the Measured and Calculated Results

Differences between measured and predicted behaviour involved the following:

The head rope rotation measured by the chalk line test, was significantly lower than the calculated value. The difference is attributed to:

a. The assumption made in the theoretical model that the loading and unloading torque tension curves were the same, i.e. hysteresis was neglected.
b. Differences between actual torsional properties of the rope and those measured on a short sample in the laboratory.

The differences between the measured and calculated torque values in both head and tail ropes were substantial. However, these differences could possibly be justified by:

a. The assumptions made in the theoretical model.
b. The fact that measurements were not done in a laboratory under controlled conditions, but on site with unknown factors and assumptions about the test conditions and the rope properties.

Despite the differences between the measured and calculated values, the theoretical models have correctly predicted the trends and direction of the variation of the torque and the rope rotation. The models have therefore correctly qualified but not accurately quantified the ropes' behaviour.

8.2 Findings Related to Previous Work

The work presented in this dissertation has confirmed certain conclusions reached by previous researchers, namely:

The rotation of both head and tail ropes is a function of the square of the hoisting depth.

The head and tail rope portions close to the conveyances are subjected to the greatest lay angle changes. These portions are also subjected to the most severe fatigue loading. Special attention must therefore be given to those portions during rope inspection.

A rope with a zero C factor will eliminate lay angle variations and rope rotation.

On Koepe winders where the tail loop is formed freely without a tail sheave it is necessary to install low frictional torque swivels at both ends of the rope.

The present study has also given theoretical proof to certain opinions and practices adopted by rope users over the years such as the fact that:

A rope with a zero or very low C factor is susceptible to birdcaging problems. A certain amount of positive torque, which tends to tighten the outer strands, is desirable in the head rope.

8.3 New Findings

The following findings, which the author believes to be new, follow from this research:

The lay angle variations and therefore the rope rotation for both head and tail rope are a result of the torque difference in the two sections of the rope and not of the absolute value of the torque in the ropes.

The torsional behaviour of multi-strand non-spin head ropes is more sensitive to the introduction of negative than positive rotation.

Multi-strand non-spin head ropes do not rotate when the conveyances are loaded or unloaded. However triangular stand ropes rotate during these processes.

The variation, with tensile load, of the frictional torque of the swivels on the two legs of a freely looped tail rope must be minimum. This will ensure that both swivels rotate simultaneously during the trip, preventing the two legs of the rope from intertwining.

The following additional findings, supported by the author, are a matter of controversy among rope users:

The fact that both the head and tail rope rotation are functions of the square of the hoisting depth should not be seen as a limitation to the application of the Koepe system to deep level shafts. With proper rope design, rope selection and operating procedures, the problems associated with the torsional behaviour can be overcome.

Lay angle variations and rope rotation can be minimised by appropriate rope design. A rope with a high torsional stiffness or an appropriate shape of torque-tension curves can give the desired results.

Rope life improvements achieved with the installation of non-spin ropes are mainly due to the higher torsional stiffness of these ropes. Their lower torque factor has a lesser influence.

8.4 Recommendations for Further Work

Further research, aimed at improving the quantitative accuracy of predictions of rope behaviour, is recommended. In particular:

Modelling of the torsional behaviour of the ropes taking into account hysteresis effects will increase the accuracy of the calculations. This however will result in a significantly more complex algorithm. The condition of each rope element will depend not only on the torque and tension in the element but also on the torque and tension history.

Further experiments on Koepe winders are recommended to measure the torque variation in both head and tail ropes.

Further investigation into the torsional properties of wire ropes is recommended. Aspects such as variation of the torsional properties of ropes along their length and effective torsional stiffness of a wire rope in service should be investigated.

TORSIONAL BEHAVIOUR OF WIRE ROPES FOR KOEPE WINDERS

Jason Minas Yiassoumis

A dissertation submitted to the Faculty of Engineering, University of the Witwatersrand, Johannesburg, in fulfilment of the requirements for the degree of Master of Science in Engineering

Johannesburg, 1992

DECLARATION

I declare that this dissertation is my own, unaided work. It is being submitted for the Degree of Master of Science in Engineering in the University of the Witwatersrand, Johannesburg. It has not been submitted before for any degree or examination in any other University.

Jason Minas Yiassoumis

..... day of..... 1992

ABSTRACT

The torsional behaviour of steel wire ropes used on Koepe winders for vertical shafts is analysed. Theoretical models have been developed for the behaviour of both the head and tail ropes after correcting an assumption made by previous researchers regarding the torque in the ropes. The theoretical models utilise experimentally obtained rope properties. The properties were measured from rope samples tested in a laboratory using specially developed equipment and software. Instruments were designed and used for in-situ measurements on an 1800 m deep shaft during a complete return trip. Some of the measurements were affected by unexpected strong torsional oscillations. However the general trends of the measured torsional behaviour were correctly predicted by the theoretical models. Discrepancies are attributed to the difficulties of obtaining true rope properties, to assumptions made in order to obtain a workable model and to inaccuracies in the measured behaviour because of the strong torsional oscillations. Further research is recommended. Nevertheless there is sufficient correlation between the models and the experiments, as well as with other published results, to draw certain conclusions with confidence. In particular the results confirm the adverse effect of hoisting depth, the need to use non-spin ropes and the need for swivels at both ends of freely looped tail ropes. New findings include the importance of balanced frictional torque between the two swivels of a tail rope and the realisation that the rope rotation is caused by the torque difference between the two legs of a head or tail rope and not the absolute value of the torques. The results also emphasize the important role of the torsional stiffness of a rope in relation to its torsional behaviour. The use of theoretical models to design or select ropes suitable for specific Koepe winders is suggested.

To my parents, Minas and Helen,
for teaching me that knowledge
is the only wealth that can not
be taken away from me but by God.

Acknowledgements

I wish to express my deep appreciation and sincere thanks to Professor C. Dimitriou for his patient guidance during the preparation of this dissertation. I am also grateful to Dr. J.T.F Fritz for initiating the project and for his advice during the first stages of the work.

I would like to thank Mr. G.F.K. Hecker and Dr. C. Boothroyd for allowing me to use the facilities of the CSIR and for their valuable assistance during the course of my project. Thanks are also due to Messrs. M. van Zyl and M. Holloway for their assistance during the test at West Driefontein winder.

Acknowledgements are also due to the COMRO research organization and the management of the West Driefontein mine for allowing me access to their winder experimentation.

My thanks to Mr. E.J. Wainwright for his assistance in locating reports and publications for my literature investigation and his valuable advice.

I am indebted to Miss L. Catano for the patient preparation of the first draft copies of this dissertation.

I am grateful to my wife Sylvia for her continuous support and understanding during the course of the study, for editing my progress reports and for teaching me how to use a word processor.

Finally I would like to thank the CSIR for their financial support.

CONTENTS Page

DECLARATION		ii
ABSTRACT		iii
DEDICATION		iv
ACKNOWLEDGEMENTS		v
CONTENTS		vi
LIST OF FIGURES		x
LIST OF TABLES		xiii
LIST OF SYMBOLS		xiv
1	INTRODUCTION	1
1.1	Koepe Mine Shaft Hoisting Systems	1
1.2	Definitions	5
1.3	Review of Literature	7
1.3.1	Literature on head ropes	7
1.3.2	Literature on tail ropes	10
1.3.3	Literature involving geometrical analysis	12
1.4	Project	14
2.	TORQUE-TENSION PROPERTIES OF WIRE ROPES	14
2.1	Wire Rope Torque-Tension Machine	16
2.2	Specimen Preparation and Test Procedure	19
2.3	Non-spin and Triangular Strand Ropes	20
2.4	Load Sharing Mechanism in Multi-layer Non-spin Ropes	21
3.	THEORETICAL MODEL OF THE HEAD ROPE	29
3.1	Assumptions and Boundary Conditions	29
3.2	Theoretical Model of the Head Rope Using Constant C and T Factors	33
3.2.1	Lay angle variation	35

CONTENTS Page

3.2.2 Rotation of the downgoing rope - Chalk test 37
3.2.3 Application of the model to a practical example 39
3.3 Theoretical Model of the Head Rope Using Variable C and T Factors 44
3.3.1 Head Rope model algorithm 45
3.3.2 Application of the model to a practical example 47
3.3.3 Influence of the shape of the torque-tension curves 47

4. THEORETICAL MODEL OF THE TAIL ROPE 57

4.1 Assumptions and Boundary Conditions 57
4.1.1 Tail rope loop formed freely without a tail sheave 59
4.1.2 Tail rope loop formed by means of a tail sheave 61
4.2 Theoretical Model of the Tail rope using Constant C and T Factors 62
4.2.1 Application to a practical example 66
4.3 Theoretical Model of the Tail rope using Variable C and T Factors 76
4.3.1 Tail rope mode algorithm 76
4.3.2 Application to a practical example 78

5. ON-SITE MEASUREMENTS ON A KOEPE WINDER 82

5.1 Measurement of Torsional and Tensile Loads During a Trip 82
5.1.1 Head Rope loadcell 83
5.1.2 Tail rope loadcell 83
5.1.3 Calibration of the loadcells 83
5.1.4 Instrumentation and procedure 87
5.2 Analysis of Results 88
5.3 Chalk Test and Lay Length Measurements 89

6. TORSIONAL AND LONGITUDINAL VIBRATIONS OF KOEPE HEAD ROPES 93

6.1 Free Torsional Vibrations of a Koepe Head Rope 93
6.2 Free Longitudinal Vibrations of a Koepe Head Rope 95

CONTENTS Page

6.3	**Comparison Between Experimental and Theoretical Results of the Vibration Analysis**	101
7.	**DISCUSSION**	103
7.1	**Comparison Between Theoretical and Experimental Results: Head Rope**	103
7.1.1	Torque difference	106
7.1.2	Rope rotation	107
7.1.3	Rate of torque change	110
7.1.4	Torsional oscillations	112
7.2	**Comparison Between Theoretical and Experimental Results: Tail Rope**	112
7.2.1	Locked swivels	112
7.2.2	Free swivels	114
7.3	**Summary of Discussion on the Differences Between Theoretical and Experimental Results**	114
7.4	**Discussion on the Behaviour of the Head Rope**	115
7.4.1	Comparison with previous theoretical model	116
7.4.2	Discussion on the C and T factors	116
7.4.3	Discussion on the rope weight, q	119
7.4.4	Discussion on the loading and unloading process of the conveyances	120
7.4.5	Discussion on the lay angle variations	120
7.4.6	Discussion on rotation introduced in the rope	121
7.5	**Discussion on the Behaviour of the Tail Rope**	121
7.5.1	Tail loop formed freely without the use of a tail sheave	121
7.5.2	Tail loop formed by means of a tail sheave	124
7.6	**Comparison Between Constant and Variable C and T Models**	125
7.7	**General Discussion**	126
8.	**CONCLUSIONS AND RECOMMENDATIONS**	127
8.1	**Findings Related to the Measured and Calculated Results**	127
8.2	**Findings Related to Previous Work**	128

CONTENTS

Page

8.3 New Findings 129
8.4 Recommendations for Future Work 130

APPENDIX A CONSTRUCTION DETAILS AND PROPERTIES OF WIRE ROPES 131
APPENDIX B HEAD ROPE MODEL USING CONSTANT C AND T FACTORS 138
APPENDIX C PROGRAM LISTINGS 150
APPENDIX D TAIL ROPE MODEL USING CONSTANT C AND T FACTORS 168
APPENDIX E TORSIONAL AND LONGITUDINAL VIBRATIONS OF A KOEPE HEAD ROPE 178
APPENDIX F POLAR SECOND MOMENT OF AREA OF HEAD ROPE AND EFFECTIVE SHEAR MODULUS 184

REFERENCES 190

LIST OF FIGURES

Figure		Page
1.1	Tower mounted Koepe winders	2
1.2	Ground mounted Koepe winders	3
1.3	Multi-rope Koepe winder	4
2.1	Torque-tension machine	17
2.2	Torque-tension machine data acquisition system	18
2.3	Wire rope specimen	20
2.4	Torque-tension curves of a 44 mm triangular strand rope	23
2.5	Torque-tension curves of a 44 mm non-spin rope	23
2.6	Torque factor of a 44 mm triangular strand rope	24
2.7	Torque factor of a 44 mm non-spin rope	24
2.8	Torsional stiffness of a 44 mm triangular strand rope	25
2.9	Torsional stiffness of a 44 mm non-spin rope	25
2.10	Load elongation curves of a 44 mm triangular strand rope	26
2.11	Load elongation curves of a 44 mm non-spin rope	26
2.12	Variation of the modulus of elasticity of a 44 mm triangular strand rope	27
2.13	Variation of the modulus of elasticity of a 44 mm non-spin rope	27
2.14	Tensile load sharing between inner and outer strands	28
3.1	Configuration of Koepe winder	30
3.2	Interchangeability of the head rope sections	32
3.3	Wire rope element	35
3.4	Chalk line test	38
3.5	Torque in the rope during a trip	40
3.6	Torque difference in the two sections of the rope during a trip	40
3.7	Lay angle deviation at a cross section during a double trip: z_1=25 m	41
3.8	Lay angle deviation at a cross section during a double trip: z_1=50 m	41
3.9	Lay angle deviation at a cross section during a double trip: z_1=207,6 m	42

Figure		Page
3.10	Lay angle deviation at a cross section during a double trip: z_1=875 m	42
3.11	Boundary values of lay angle deviation	43
3.12	Chalk line test	43
3.13	Torque-tension curves of West Driefontein head rope for various end rotations	49
3.14	Twist curves of West Driefontein head rope for various torque values	50
3.15	Relation between initial torque and rotation	51
3.16	Torque in the rope	52
3.17	Chalk line test	52
3.18	Lay angle deviation at a cross section during a double trip: z_1=50 m	53
3.19	Lay angle deviation at a cross section during a double trip: z_1=875 m	53
3.20	Torque in the rope for positive end rotation	54
3.21	Chalk line test for positive end rotation	54
3.22	Torque in the rope for negative end rotation	55
3.23	Chalk line test for negative end rotation	55
3.24	Torque difference at the beginning of the trip	56
3.25	Chalk line test results for the middle section of the rope	56
4.1	Tail rope notation	58
4.2	Tail rope results: Locked swivels	69
4.3	Tail rope results: Swivels with constant frictional torque	70
4.4	Tail rope results: Swivels with variable frictional torque	72
4.5	Tail rope results: Loop formed by means of a tail sheave	74
4.6	Torque in the tail rope for variable C and T factors	80
4.7	Torque in the rope for ten turns positive initial rotation	81
4.8	Torque in the rope for twelve turns negative initial rotation	81
5.1	Head rope attachment	84
5.2	Head rope loadcell	84
5.3	Tail rope suspension gear	85
5.4	Tail rope tensile loadcell	86
5.5	Tail rope torsion loadcell	86
5.6	Data acquisition system	90

Figure		Page
5.7	Results from the second trip	91
5.8	Torque in the head rope during a trip	92
5.9	Torque in the tail rope during a trip	92
6.1	Notation for vibration analysis	98
6.2	Natural frequency of torsional and longitudinal vibration	99
6.3	Solution of equation $\theta.\tan\theta = e$	100
6.4	Recorded vibration frequencies	102
7.1	Head rope torque: experimental and theoretical results	104
7.2	Torque difference at the beginning of the trip	105
7.3	Chalk line test results for the middle section of the rope	105
7.4	Effect of torsional hysteresis on rope rotation	108
7.5	Tail rope torque: experimental and theoretical results	113
7.6	Tail loop rotation	123
A.1	Torque tension curves of a West Driefontein discarded tail rope	135
A.2	Torque factor of a West Driefontein discarded tail rope	136
A.3	Torsional stiffness of a West Driefontein discarded tail rope	137
B.1	Configuration of a Koepe winder	139
B.2	Lay angle deviation	144
D.1	Tail rope notation	169
D.2	Tail rope rotation convention	172
E.1	Free body diagram of a torsionally vibrating rope element	181
E.2	Free body diagram of a longitudinally vibrating rope element	183
F.1	Head rope cross section	187
F.2	Head rope wire notation	188

LIST OF TABLES

Table		Page
3.1	Head rope behaviour	34
3.2	Particulars of West Driefontain No. 5 shaft Koepe winder	39
4.1	Freely suspended tail rope without tail sheave	64
4.2	Tail rope loop formed by means of a tail sheave	65
A.1	Construction details of a 44 mm triangular strand rope	132
A.2	Construction details of West Driefontein head rope	133
A.3	Construction details of West Driefontein tail rope	134
F.1	Head rope construction details	189

LIST OF SYMBOLS

Symbol	Quantity
a	Overrun distance
b	Distance between lower station and tail loop
C	Torque factor of a rope
E	Effective modulus of elasticity of the head rope
G	Effective shear modulus of the head rope
h	Hoisting depth
k	Factor combining the rope properties
L_h	Length of the head rope
L_t	Length of the tail rope
M_d	Dynamic frictional torque of a swivel
M_s	Static frictional torque of a swivel
$M_{1,u}$	Torque in the upgoing rope
$M_{2,u}$	Torque in the downgoing rope
N	Number of turns counted during chalk line test
P	Gross weight of the conveyance plus 50% of tail loop weight
P_t	50% of tail loop weight
q	Weight of the rope per unit length
T	Torsional stiffness a rope
u	Distance travelled by conveyances
z_1	Distance of a rope cross section from the upgoing conveyance
z_2	Distance of a rope cross section from the downgoing conveyance
β	Lay angle
θ	Lay angle deviation
Φ_{in}	Rotation introduced in the rope on installation
Φ_{s1}	Rotation of the swivel of the upgoing tail rope
Φ_{s2}	Rotation of the swivel of the downgoing tail rope
Φ_t	Rotation of the tail rope loop
$\Phi_{1,u,z1}$	Relative rotation of a cross section of the upgoing rope
$\Phi_{2,u,z2}$	Relative rotation of a cross section of the downgoing rope

1. INTRODUCTION

1.1 Koepe Mine Shaft Hoisting Systems

In 1877, the technical director of the Hannover Mining Company (Germany), Friedrich Koepe introduced the first mine shaft hoisting system utilizing a contact friction principle to hoist the conveyances. In the following decades the so-called Koepe winding installation replaced hundreds of conventional drum winding systems. Two types of Koepe winders are in use today. The tower mounted winder, with or without deflection sheave, (Fig. 1.1) and the ground mounted winder, with or without fleet angle (Fig. 1.2).

The Koepe winder can serve one or two shaft compartments and the conveyance can be suspended by more than one "head rope" (Fig. 1.3). "Tail ropes" are used to balance the head ropes and are attached to the bottom of the conveyance, in most cases by means of swivels. The number of tail ropes is the same as the number of head ropes or one larger diameter rope can be used to balance more than one head rope. The tail rope loop is formed freely or by means of tail sheaves.

Although the Koepe winder has been in use in Europe for more than 100 years without any significant problems, the installation of the system in the deeper South African shafts in the late nineteen fifties resulted in severe rope problems. Within a few weeks of installation broken wires started to appear in the Lang's Lay triangular strand head ropes. The lay length pattern along the rope became seriously disturbed and after six months the ropes had to be discarded because of distortion of strands due to spinning and twisting. The rope spin had also an adverse effect on the sheave tread life, the severity of the wear being a function of the winding depth. Tail ropes experienced problems such as the tendency to deform into a figure of eight and birdcaging.

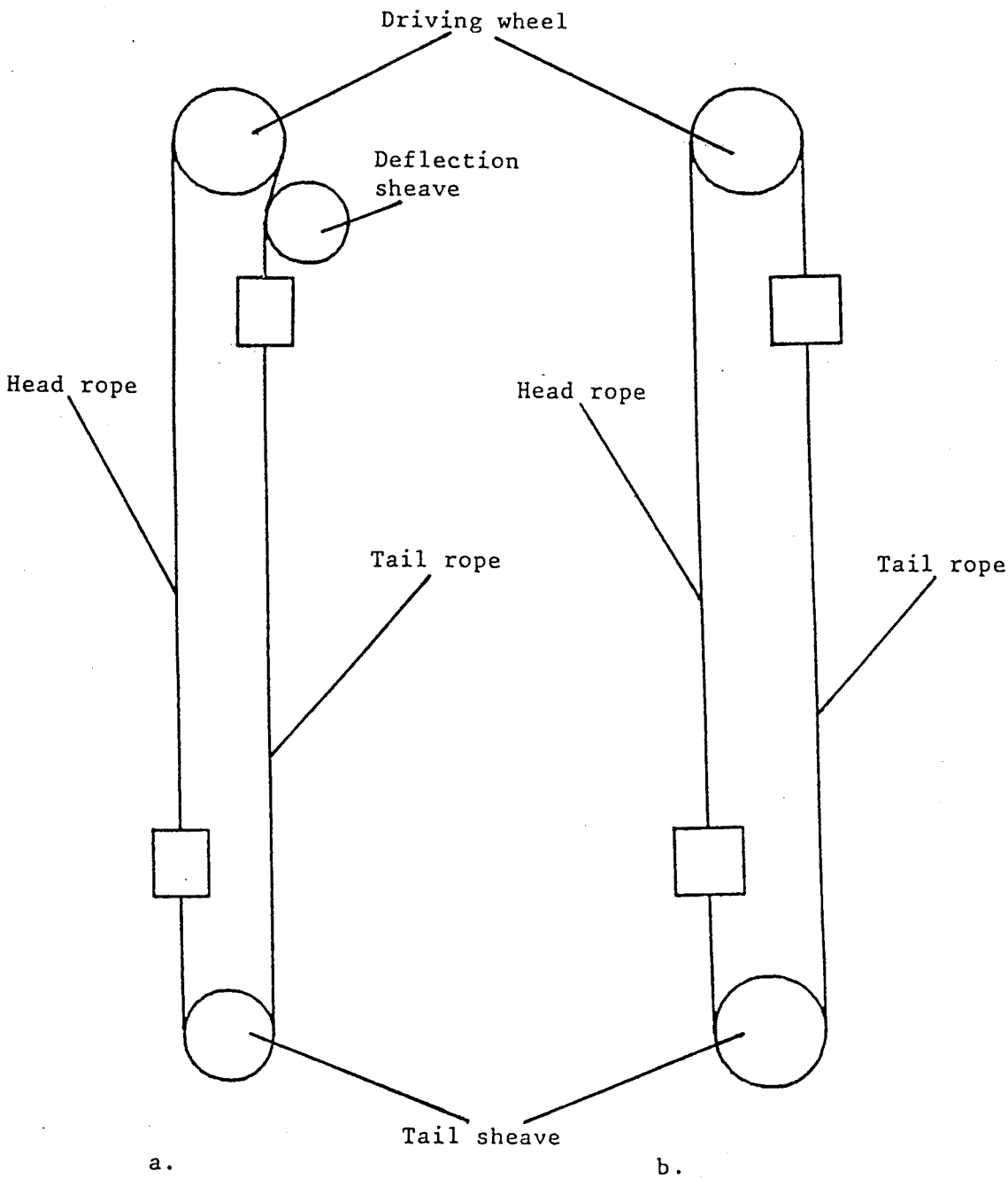

Figure 1.1 Tower mounted Koepe winders

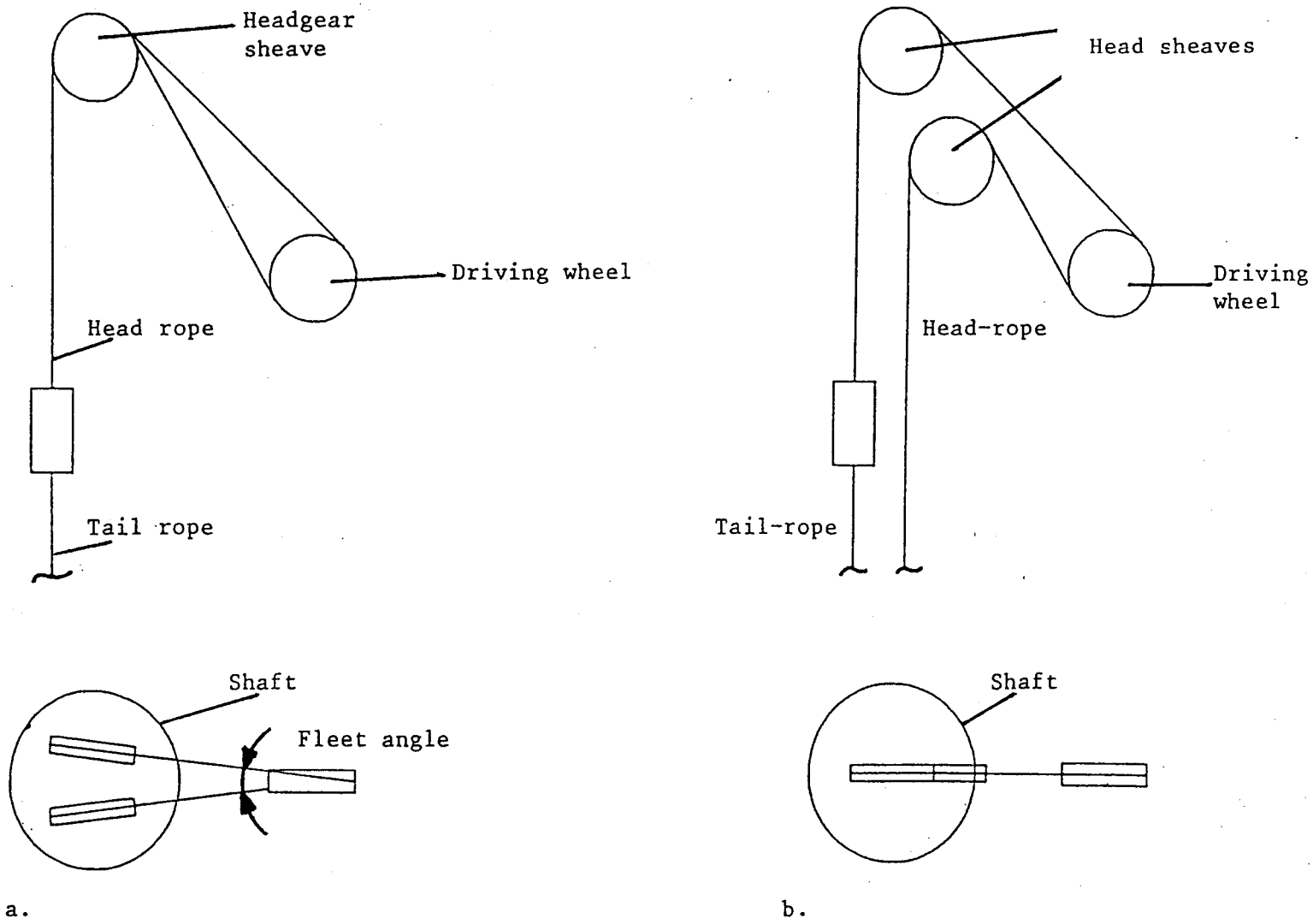

Figure 1.2 Ground mounted Koepe winders

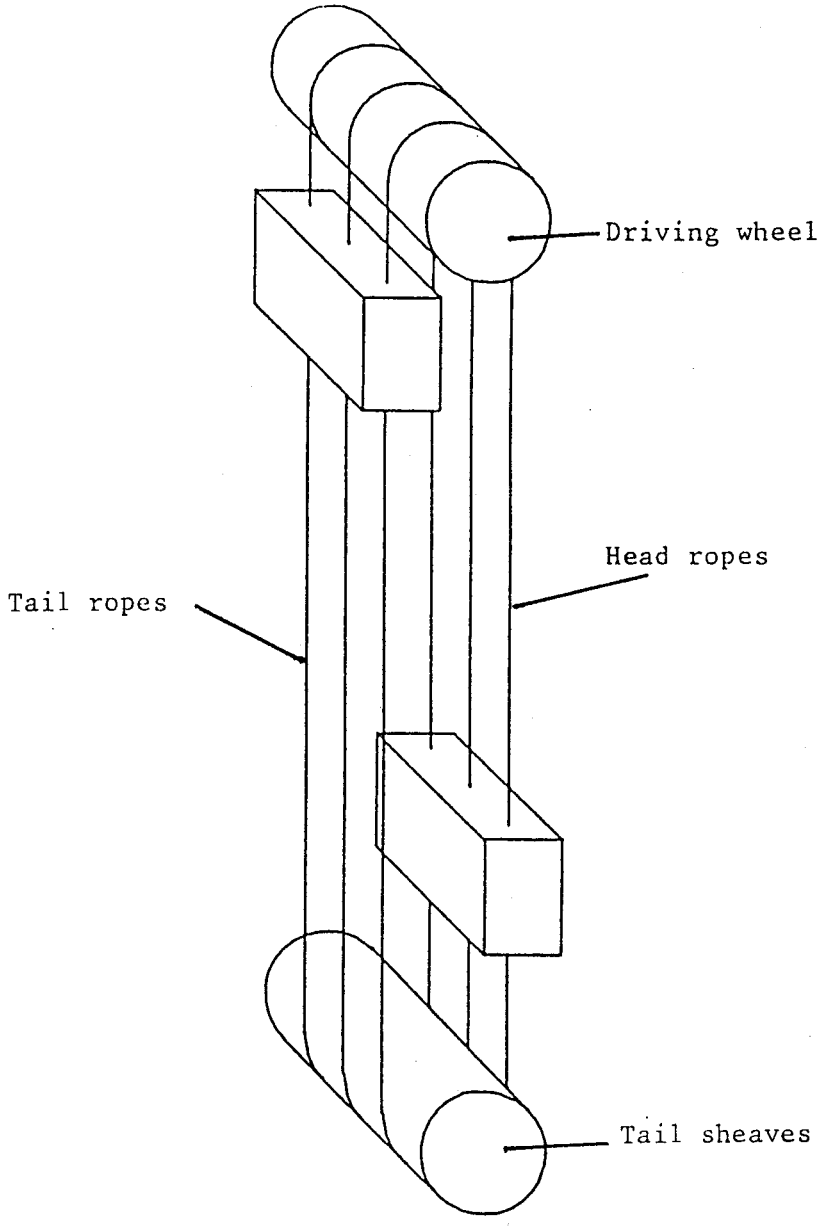

Figure 1.3 Multi-rope Koepe winder

The torsional behaviour of the ropes was identified as the reason for the problems. Mathematical models of the torsional behaviour of Koepe head and tail ropes were proposed but these were based on the incorrect assumption that the torque varies along the length of the rope. The various researchers were led to this assumption by observing the variation of the lay length along the rope. However the only way of varying the torque along a length of vertical rope is by applying a torque externally over that length.

1.2 Definitions

Some technical terms or expressions, which are used repeatedly in this dissertation, are defined below:

Torque factor: If a wire rope is subjected to a tensile load F with its two ends restrained from rotating relative to one another; a torque M=C.F is induced in the rope. The coefficient C is called the torque factor and its units are Nm/N. The torque factor is not necessarily a constant, it can be a function of the applied tension and torque. The torque factor is commonly referred to as C factor.

Torsional stiffness: If the two ends of a length of wire rope, $\triangle z$, are rotated relative to each other by $\triangle\Phi$ degrees while under constant tensile load F a torque $M = T(\triangle\Phi/\triangle z)$ is induced in the rope. The coefficient T is the torsional stiffness and its units are Nm/(deg/m). The torsional stiffness is not necessarily constant, it can be a function of the applied tension and torque. The torsional stiffness is commonly referred to as the T factor.

Low torque or non-spin rope: This is a wire rope constructed from two or more layers of strands helicaly wound around a core in opposite directions. It can also be a single strand rope constructed from multiple layers of wires, helicaly wound around a core wire, with alternating lay directions. Because of the alternate lay directions a non-spin rope under tensile load develops relatively low torque. It has a low torque factor and high torsional stiffness.

High torque rope: This is a wire rope constructed from a single layer of strands helicaly wound around a core. Under tensile load a high torque rope, as its name implies, develops relatively high torque. It has a high torque factor and low torsional stiffness.

Relative rotation: This is the rotation of a rope cross section with respect to another cross section. The relative rotation is positive if it is in the direction of the helix lay, in other words if it causes a shorter lay length. Otherwise, it is negative. Its units are degrees, radian or number of turns. The rate of rotation per unit length between the two cross sections may vary.

Twist : This is the rotation of a rope cross section with respect to another cross section, per unit length. Its units are degrees per meter or radian per meter.

Rotation of a cross section: This is the rotation of a rope cross section while travelling in the shaft, with respect to a position which it previously occupied and which is regarded as zero reference. The rotation is regarded positive if it is in the direction of the helix lay. Otherwise, it is negative. It has units of degrees, radians or number of turns (of 360°).

Lay angle deviation: This is the change of the lay angle β. It is denoted by θ and is positive if it causes shorter lay length. Otherwise, it is negative.

Upgoing head rope: This is the section of the head rope between the upgoing conveyance and the driving wheel.

Downgoing head rope: This is the section of the head rope between the driving wheel and the downgoing conveyance.

Upgoing tail rope: This is the section of the tail rope between the upgoing conveyance and the tail rope loop.

Downgoing tail rope: This is the section of the tail rope between the downgoing conveyance and the tail rope loop.

Single trip or trip: A trip during which the upgoing conveyance is raised from the bottom station to the top station.

Double trip or cycle: A trip during which the upgoing conveyance is raised from the bottom station to the top station and then lowered to the bottom station.

1.3 Review of Literature

The wire rope was introduced as a hoisting rope by Albert in 1834. Although such an old machine element, little theoretical work has been published about its in-service behaviour. Most improvements on wire rope design were rather a result of a trial and error approach than a result of a rigorous understanding of the mechanisms which determine its behaviour and affect its performance.

1.3.1 Literature on head ropes

Hermes and Bruens[1] were the first to attempt to explain the problem of the torsional behaviour of Koepe head ropes. Based on their paper the National Engineering Institute of the CSIR[2] proposed a revised theoretical model for the torsional behaviour of Koepe head ropes. The model incorporates the C and T factors as constants. The torque along the axis of the head rope is assumed to vary, an assumption which is obviously incorrect because there is no external torque applied to the rope between the conveyance and the driving wheel. Dr. J.T.D. Fritz, formerly Head of the Mine Equipment Research Unit of the CSIR drew the writer's attention to this error. Nevertheless, the final recommendation calling for the use of non-spin ropes was implemented and resulted in marked improvements. The problem of the rotation of the downgoing head rope is addressed by Hitchen[3] and a formula is given to calculate the number of turns any section of the head rope exhibits during a trip. The deeper the shaft, the greater the number of turns. The C and T factors are once again treated as constants. The chalk line test to measure the number of turns the head rope rotates during the trip is described. A piece of chalk is held against the downgoing head rope at the level of the driving wheel.

If the rope rotates as it travels downwards the chalk line forms a spiral. During the next trip, when that section of the rope is the upgoing one, the line is monitored at the driving wheel level. Since the upgoing rope does not rotate, the number of turns counted is equal to the number of rotations the rope exhibits.

Ulrich and Fuchs[4] report chalk line test results on Koepe head ropes in Germany. They found that the number of turns a head rope exhibits on a particular winder is a function of the time the rope has been in operation. The number of turns was also found to be directly related to the permanent elongation observed on the head ropes. During the first stages of the ropes' life the number of turns decreased significantly with time. Significant permanent elongation of the head ropes was observed during the same period. As the rope was ageing the number of turns reached a constant value. In the same paper Ulrich and Fuchs suggest that the rotation of the head rope might be responsible for internal damage to the rope.

Since the problems associated with the torsional behaviour of Koepe head ropes were identified only in the early nineteen sixties recommendations on rope constructions before that do not discriminate between high torque and low torque (i.e. non-spin) ropes. Hitchen[5,6,7], in a series of papers between 1948 and 1958, examines the performance of four types of ropes on Koepe installations. These are six-strand round strand ropes, six-strand triangular strand ropes, multi-strand non-spin ropes and single strand locked coil ropes. Advantages and disadvantages of each of the above four types of ropes are discussed but no reference is made to the torsional behaviour of the ropes. The only remark made relating to the torsional properties of the rope is that non-spin and locked coil ropes would impose smaller turning moments on the conveyances. Nevertheless, Hitchen indicates a personal preference for locked coil ropes.

Pitt, Zeppenfeld and Hallet[8] investigated in 1956 the possible application of Koepe winders in South African shafts. Again, the torsional properties of the head ropes are ignored and they recommend both locked coil and triangular strand ropes as suitable constructions for head ropes.

The problems associated with the torsional behaviour of the head ropes were realised only after the installation of the first deep shaft Koepe winder at Stilfontein in 1958.

Berry and Wainwright[8] review the application of Koepe winders in South Africa during the early nineteen sixties. Conventional triangular strand Langs Lay ropes selected as head ropes for the 1 350 meters deep Margaret shaft at Stilfontein gave extremely short lives although, previously, they had performed well at Bancroft (420 m deep) and Libanon (947 m deep). The first as well as the second set of ropes had to be discarded prematurely because of distortion of strands due to spinning. During the same period similar problems were experienced at West Driefontein (1710 m deep). The non-spin ropes installed subsequently eliminated the problem and behaved relatively well. The mechanism of lay length variations for the head rope is described and deviations of up to 15% from the as-manufactured lay length pattern were recorded.

The performance of fourteen types of ropes tried at Western Deep Levels, Western Areas, West Driefontein and Vaal Reefs is analysed by Fuller and Wainwright[10]. The static load variation to which a rope cross section is subjected during a trip is introduced as a variable in the study of the fatigue endurance of Koepe head ropes. In a later paper, Wainwright[11] suggests dynamic loading as one of the factors which influence the fatigue performance of head ropes . He justifies the new factor by the fact that inspection of head ropes pointed to a discrepancy between the sections of the ropes which are subjected to maximum static load variation and the region where fatigue wire failures were found. In the same paper suggestions are made for the design of head ropes

The Technical Services Department of Haggie Rand Ltd[12] reviewed the head rope performance on five surface Koepe winders, namely: Stilfontein Margaret shaft 1 350 metre deep, West Driefontein No. 5 shaft 1 710 metres deep, Western Deep Levels No. 2 and No. 3 shafts both 1 982 metres deep

and Vaal Reefs No. 2 shaft 1 948 metres deep. The 15-strand "fishback" rope had proved to be the most successful head rope. Premature failures of these ropes were attributed to some extent to the release during installation, of torque built up in the ropes. Release of torque would loosen the outer strand and tighten the inner ones. This upsets the stress distribution, and results in premature rope failure. The paper recommends that slackening of the outer strands should be checked periodically by disconnecting the rope at the bottom of the shaft taking care to prevent the rope from spinning. In cases where the spin tends to unlay the outer strands turns must not be released. Where spin tends to tighten the outer strands, turns must be released and then five to six turns must be put into the rope.

Fritz and Annear[13] examined the failure pattern of a 15-strand fishback Koepe head rope discarded from Western Deep Levels No. 3 shaft. The section of the wire rope which was subjected to bending and twist variations by passing over the driving and deflection sheaves exhibited between three and ten times more wire failures per unit length than rope sections which were not subjected to these loads. The majority of failures (85% to 100%) of sections subjected to all load combinations were found in the inner strands.

1.3.2 Literature on tail ropes

The most critical problem of tail ropes on Koepe installations is the tendency to deform into a figure of eight. Once again that problem is a result of the tendency of a rope to rotate when under tensile load. Hitchen[5,6] reports that flat ropes are used in most shafts in Germany but he makes no comment on the reason why flat ropes are used as tail ropes. Flat ropes, which are not in use in South Africa, have a rectangular cross section. The strands or individual ropes of a flat rope are not "closed" into a rope in a helical shape. They are laid in parallel and held together by means of separate soft wires and they do not develop torque when under tension. That eliminates the tendency of a tail rope to deform into a figure of eight. The assembling is made by hand, which makes the final product rather expensive, especially for deep shaft applications.

Pitt, Zeppenfeld and Hallet[8], in their paper about the possible application of Koepe winders in South Africa, recommend the use of non-spin ropes, such as locked-coil, for tail ropes. They suggest that flat ropes might cause problems during handling and transport in the deep South African shafts. Tail sheaves are considered to be unnecessary and the installation of timber baulks to restrain the twisting of the tail ropes is suggested.

Berry and Wainwright[8] in their review of the application of Koepe winders in South Africa state that non-spin ropes used as tail ropes were reasonably successful. The use of swivels is not recommended where tail sheaves are used, but they suggest that turns should be put periodically into the tail ropes to remove any slack in the outer strands. When tail sheaves are not used, free swivels are necessary and baulking arrangements are suggested to prevent the rope from deforming into a figure of eight in case of non-functioning swivels.

A maximum frictional torque for swivels of 35 Nm under 100 kN tensile load is recommended by Wainwright[11] in cases where tail sheaves are not used. No reference is made in the paper as to how this figure was reached, but it was measured at the Stilfontein Koepe winder.

The importance of tail rope maintenance is emphasized in a publication of Haggie Rand Technical Services Department[14]. More production time is lost due to tail rope problems than is lost due to head rope problems. Freely operating swivels are recommended on both ends of the rope when tail sheaves are not used. The free looping of the tail rope is the ideal design but requires enough space to allow for a minimum loop diameter of 45 times the rope diameter. During installation of tail ropes with tail sheaves free swivels are recommended, which must be locked after the first three to four double trips. The swivels should be released every three months and the spin must be let out under controlled conditions.

The National Mechanical Engineering Institute of the CSIR[15] proposed a model for the torsional behaviour of the tail ropes. The C and T factors are treated as constants. As with the head ropes the model is based on the incorrect assumption, that the torque varies along the rope length. The difference in torque between the two sections of the rope at the loop of a freely suspended tail rope is claimed to be a property of the rope. This is incorrect since the torque in the two sections should be the same.

Shelly [16,17,18] re-examines the behaviour of tail ropes, taking into account that the C and T factors are not constant. The research focuses on the use of swivels. The torque along the length of the rope is again regarded as not constant. He recommends use of swivels with low frictional resistance. He concludes that the tendency of the rope to deform into a figure of eight is a function of the sum of the torque at the two ends of the loop. The greater the sum, the greater the tendency to form a figure eight.

The variation of the C and T factors of a 22mm 15-strand non-spin rope and a 23mm 18-strand non-spin rope are determined experimentally by Fritz and Annear[19]. The 22mm rope had a mean C factor $0,147.10^{-3}$ m and a T factor of 185,6 Nm^2/rad. The C factor for the 23mm rope was $1,098.10^{-3}$ m and the T factor 165,7 Nm^2/rad.

1.3.3 Literature involving geometrical analysis

The papers discussed above considered the rope as an entity with inherent properties of its own. In the following the properties of the rope are derived from its geometrical construction.

The first theoretical contribution towards the study of the torsional loads induced in a wire rope under tension was made by Hruska[20]. Using the lay angle of a wire in a rope as a parameter the tangential forces in individual wires of a rope under tension were calculated. A formula to calculate the resulting torque was subsequently derived.

He mentions that a non-rotating rope can be designed but he questions the practical use of such a rope. In two other papers Hruska[21,22] shows how to calculate tensile and radial forces in the individual wires of a rope. He demonstrates that the tensile strain in the straight core wire of a strand under tensile load is greater than the strain in the helicaly wound wires and in fact inner wires break first in a laboratory tensile test on a strand. Hruska explains that in service outer wires instead of inner wires break first because of abrasion and the high pressure to which these wires are subjected on the sheave.

Machida and Duvelli[23] extended Hruska's work using an advanced geometrical approach. They developed explicit formulas for the calculation of the torque, the axial load and bending moments of the wires in a strand. The equations developed are linear. Measurements on specially made epoxy oversized rope specimens show good correlation between theoretical and experimental results. The authors show that the axial load has no influence on the torsional rigidity of the strand.

Gibson, Cress, Kaufman and Gallant[24] following Hruska's approach developed a simplified method of calculating torque induced in a rope under tension. Assuming that the number of wires in the strands becomes very large and their size very small in order to maintain the same metal area, integrals instead of summation can be used to determine the generated torque. Excellent agreement between analytical and experimental results is reported for six strand ropes and good agreement for non-rotating ropes.

Costello[25,26] and his fellow workers dealt with the mathematical modeling of wire ropes in a more fundamental manner than previous investigators. The strand is analysed as a collection of smooth helical wires. These wires under tensile and torsional loads are deformed into a different helix configuration. The system of differential equations which leads from the non-deformed to the deformed condition is solved. The stresses and strains within the strand are calculated. They conclude that strands with ends fixed against rotation are stiffer than strands with ends free to rotate. The stiffness of the strands according to the authors is independent of the applied axial load.

The theory developed for strands is expanded by the Costello team[27,28,29,30,31,32] for wire ropes with complex cross sections. The strands are treated the same way as the individual wires were treated in the previous papers. The modulus of elasticity of different wire rope constructions is calculated and correlates with experimental results.

1.4 Project

The objective of the present project was to model the torsional behaviour of wire ropes used as head and tail ropes on Koepe winders. The study was restricted to the tower mounted Koepe winder without deflection sheave. Two models were developed. The first one incorporates constant C and T factors, while the second incorporates varying C and T factors. The use of constant C and T factors makes the analysis easier and faster. Modelling the behaviour with varying C and T factor made possible a parametric study of the influence of the shape of C and T curves on the torsional behaviour.

The C and T factors were measured experimentally at a specially designed machine at the Mine Hoisting Technology laboratory of the CSIR. (The design and construction of the machine were not part of the present project).

Experiments to verify the theoretical model by measuring torsional and tensile load in Koepe head and tail ropes were done at the West Driefontein No. 5 shaft Koepe main winder.

2. TORQUE TENSION PROPERTIES OF WIRE ROPES

The helicaly formed strands of a wire rope under tensile load tend to unwind. Therefore a rope specimen under tensile load with its two ends restricted from rotating relative to one another develops a torque. The torque induced is a function of the tensile load applied to the rope and the relative rotation introduced between the two ends of the specimen prior to the application of the tensile load. The torque can be calculated by the following relation.

$$M = C.F + T.\triangle\Phi/\triangle z \qquad (2.1)$$

where

M	:	Is the torque developed in the specimen.
F	:	Is the tensile load applied to the specimen.
$\triangle\Phi$	:	Is the relative rotation between the ends of the specimen.
$\triangle z$	:	Is the length of the rope specimen.
C	:	Is the torque factor as defined in Chapter 1.
T	:	Is the torsional stiffness of the rope as defined in Chapter 1.

As was shown by McKenzie[33] the torque M is independent of the path that the tension and twist are applied. It depends only on the final values of F and $\triangle\Phi/\triangle z$.

In order to determine the C and T factors of rope specimens, as was mentioned in Chapter 1, a wire rope torque-tension machine has been designed and constructed at the CSIR. During the course of this project the machine was upgraded from a 500 kN/1500 Nm to 500 kN/3000 Nm. In addition new software packages were developed to control the machine, for the data acquisition and to analyse the test results.

2.1 Wire Rope Torque-Tension Machine

A configuration of the torque-tension machine is given in Fig. 2.1. The machine is divided into three functional systems: the hydraulic system, the machine frame and the control system.

A brief description of the machine is given below, while a more detailed analysis of the capabilities and limitations of the machine are given by McKenzie[33]. In the same reference descriptions of another two torque-tension machines, one in United Kingdom and one in Belgium are also given.

The hydraulic system consists of a tensile load actuator, a hydraulic motor which is used to introduce rotation between the two ends of the rope and the power pack.

The main frame of the machine is made of two horizontal beams bolted to the floor of the laboratory. The rope specimen is accommodated into two conical type grips. The first grip is attached to the output shaft of a reduction gearbox driven by the hydraulic motor. The input shaft of the gearbox can be locked by means of a friction brake. The second grip is bolted to the piston of the actuator. The other end of the piston is connected to a scissors mechanism which allows longitudinal movement of the piston but prevents it from rotating.

The control system is divided into the tensile load control system and the data acquisition system. The tensile load is controlled by regulating the pressure in the actuator through a proportional pressure relief valve.

A configuration of the data acquisition system is given in Fig. 2.2. The torque and tensile load in the rope are measured by a 3 000 Nm/500 kN torque-tension loadcell in line with the rope specimen. The signals from the loadcell are amplified by two Kyowa straingauge amplifiers. The amplified signals are digitized by two HP3478A analog to digital converters and fed in to the HP 87 computer.

An extensometer was designed and built so that the elongation of the rope could be monitored during the torque-tension test. It consists of two spring loaded telescopic tubes and is attached to the two endfittings of the specimen. The elongation is measured by a DC Linear Variable Differential Transformer (LVDT).

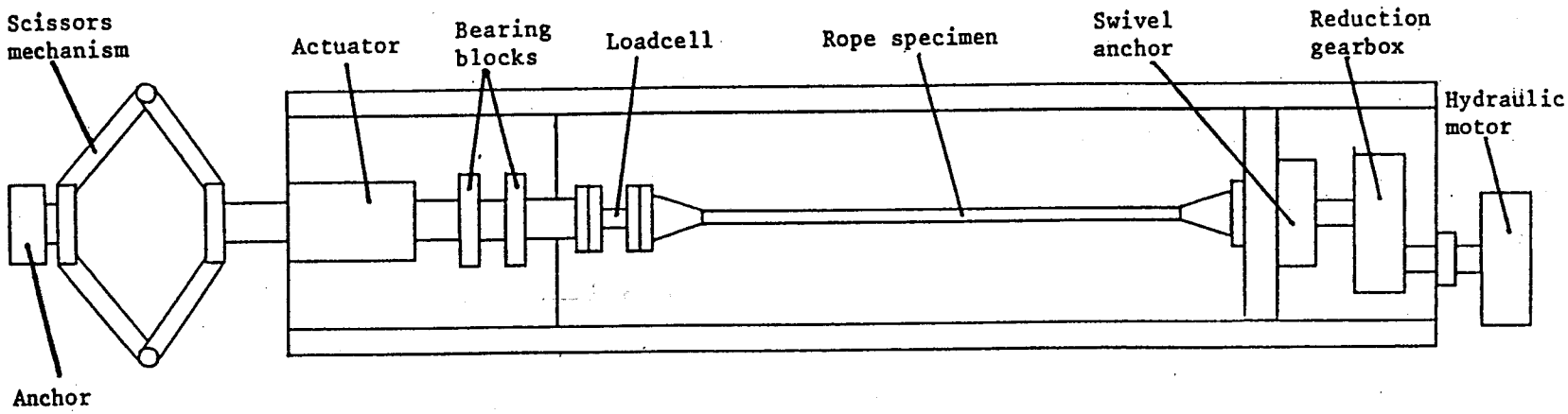

Figure 2.1 Torque-tension machine.

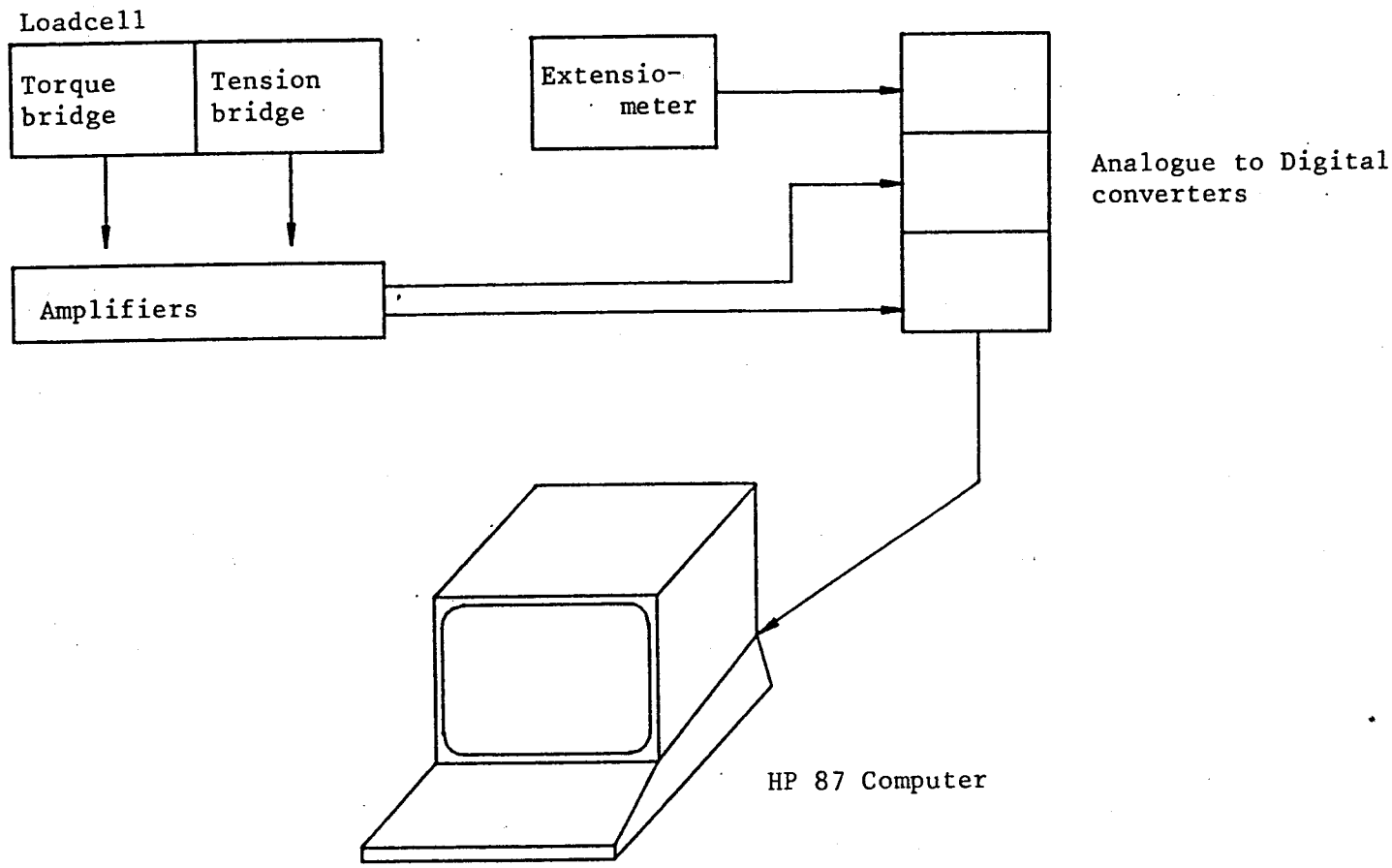

Figure 2.2 Torque-tension machine data acquisition system.

2.2 Specimen Preparation and Test Procedure

From each rope specimen a nominal length of 4 490 mm was cut (dimension A in Fig. 2.3). Two white metal collars were cast on the specimen defining a nominal gauge length of 4 050 mm (dimension B in Fig. 2.3). The two ends of the specimen were subsequently unlaid and cast into white metal conical endcaps. The specimen was then installed in the machine, taking care not to introduce relative rotation between the two ends. The extensometer was then installed. The test procedure was as follows:

(i) With the rope completely slack the zero and calibration values for the torque and tension bridges were recorded. The calibration was achieved by the standard procedure of switching parallel resistors of known resistive value across one arm of each strain gauge bridge.

(ii) A tensile load of approximately 8 kN, enough to keep the rope straight, was applied to the specimen and diameter, lay length and gauge length measurements were taken.

(iii) Maintaining the 8 kN tensile load the zero and calibration values for the elongation were recorded. The elongation calibration was carried out by inserting a 30 mm spacer between the LVDT and the extensometers bracket.

(iv) Three bedding in cycles were run. The maximum tensile load for each cycle being 10% of the ropes' actual breaking force. The actual breaking force was obtained from a tensile test to destruction of a specimen cut from the same rope length.

(v) The test was then performed by progressively increasing the tensile load while recording torque, elongation and tensile load acting on the rope. The maximum tensile load for the test was 30% of the ropes' actual breaking force or 500 kN whichever was smaller. The loading rate was slow (approximately 40 kN per minute) in order to allow the computer to collect sufficient data.

(vi) Different end rotations were applied to the specimen and, for each rotation, steps iv and v were repeated.

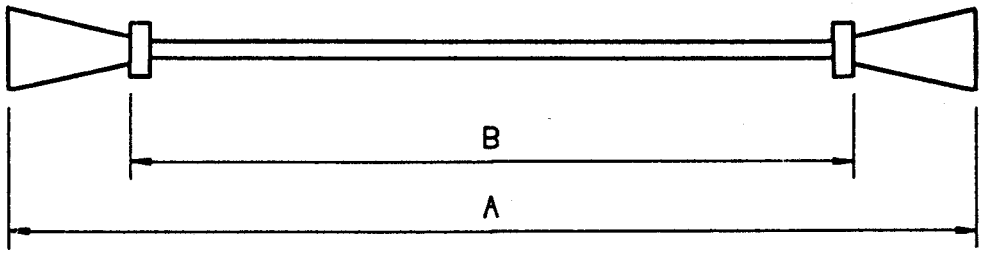

Figure 2.3 Wire rope specimen

2.3 Non-spin and Triangular Strand Ropes

The use of non-spin wire ropes, constructed with more than one layer of strands wound in opposite directions, is the common practice in South African Koepe winders serving shafts deeper than 1 000 m. Triangular strand ropes (one layer of six triangular shape strands) and round strand ordinary lay ropes are used only on Koepe winders serving shallow shafts.

A family of torque-tension curves obtained from a 44 mm triangular strand rope is shown in Fig. 2.4. The torque tension curves of a 44 mm non-spin rope are shown in Fig. 2.5. The torque factor as a function of the tensile load for the two ropes is shown in Figs. 2.6 and 2.7. Figures 2.8 and 2.9 show the torsional stiffness of the two ropes. The elongation of the two ropes for various end rotations is shown in Figs. 2.10 and 2.11. The variation of the modulus of elasticity of the above ropes with tensile load is shown in Fig 2.12 and 2.13. Full construction details of both specimens can be found in Appendix A.

The main differences in the torsional properties of the two ropes are:

- Under the same load and end rotation the triangular strand rope develops higher torque than the non-spin rope.

- The torque-tension curves of the triangular strand rope are almost straight lines. The shape of the torque-tension curves of the non-spin rope depends on the end rotation introduced to the specimen.

- The torque factor of the non-spin rope is much lower than that of the triangular strand rope. The torsional stiffness of the non-spin rope is much higher than that of the triangular strand rope.

From the load elongation curves we can see that the non-spin rope exhibits little elongation as a result of the introduction of end rotation. The triangular strand rope elongated significantly when end rotation was introduced. The modulus of elasticity of the non-spin rope was slightly higher than that of the triangular strand one. This could be due to the different construction but might also be attributed to the fact that the non-spin specimen was cut from a discarded rope after completing about 200.000 trips while the triangular strand specimen was cut from a new rope.

2.4 Load Sharing Mechanism in Multi-layer Non-spin Ropes

The non-linear shape of the torque-tension curves of non-spin ropes is a result of uneven sharing of the tensile load between inner and outer strands. At low loads and negative end rotation the inner strands carry a greater share of the tensile load than the outer strands. The resulting torque is therefore negative as shown in Fig. 2.5. For higher tensile loads and positive end rotation even distribution of stresses between inner and outer strands is achieved and the torque-tension curves become linear.

A method was developed for estimating the load sharing between the inner and outer strands. The rope is subjected to a torque tension elongation test under various end rotations. After the test and with the specimen in the testing machine, the outer strands of the rope are cut out and removed. The inner strands are then subjected to a torque tension elongation test under the same end rotations as the complete rope. The same calibration and zero values are used for both tests.

The load elongation curves obtained from the two series of tests are then compared. For a given end rotation and given strain, the difference in the two tensile loads is assumed to be the tensile load in the outer strands for the same end rotation and strain. This neglects internal friction.

The method was applied to the 44 mm non-spin rope, a discarded head rope from West Driefontein. The percentage load carried by the inner and outer strands as a function of the total tensile load for three end rotations is shown in Fig. 2.14. It is seem that for a negative end rotation of -40° and a tensile load up to 130 kN the outer strands of the rope are under compression. That can be explained by the fact that the outer strands have been unwound. Observation indicates that the outer strands become slack and tend to bulge outwards. This is the first stage of birdcaging.

Using a similar approach the torque contribution of the inner and outer strands could be estimated for various end rotations.

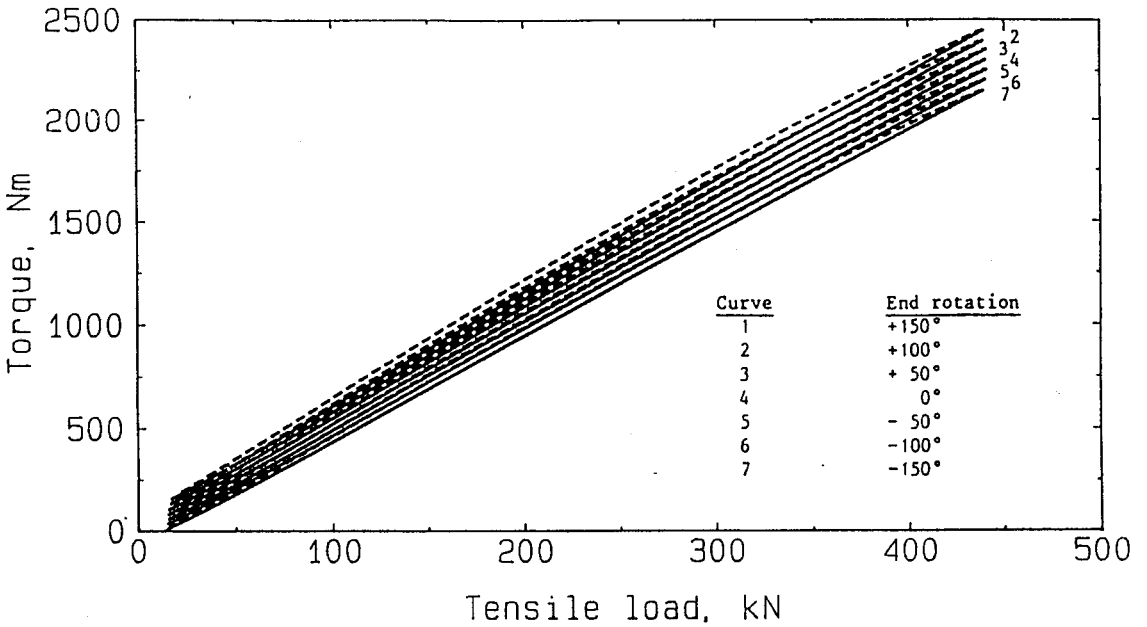

Figure 2.4 Torque-tension curves of a 44 mm triangular strand rope
—— Loading
---- Unloading

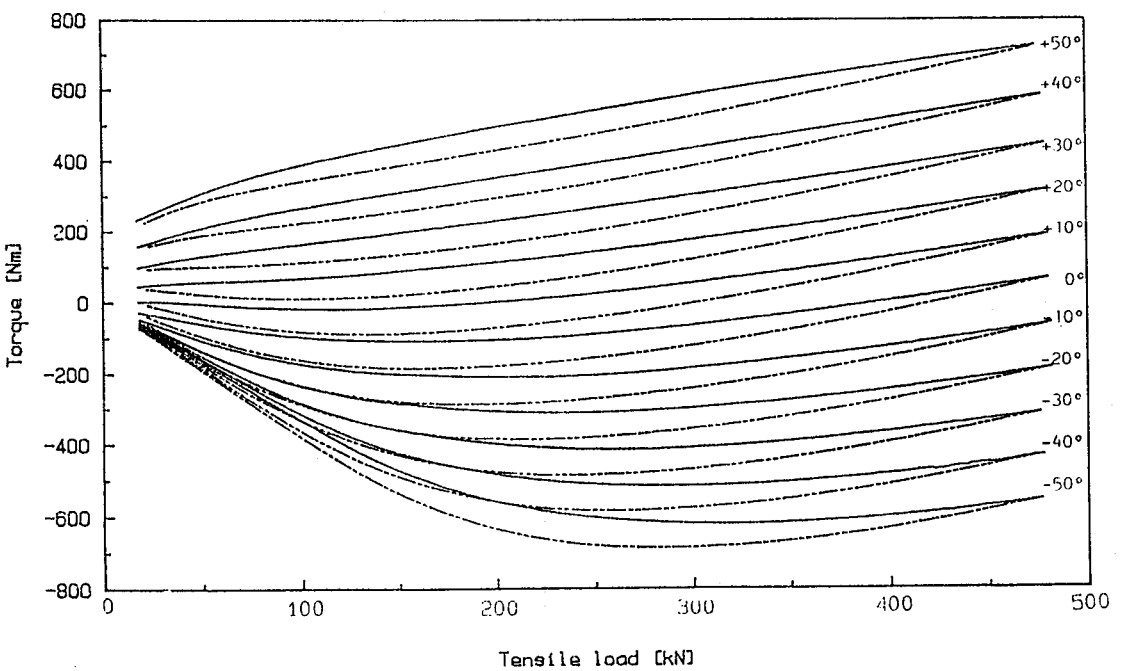

Figure 2.5 Torque-tension curves of a 44 mm non-spin rope
—— Loading
---- Unloading

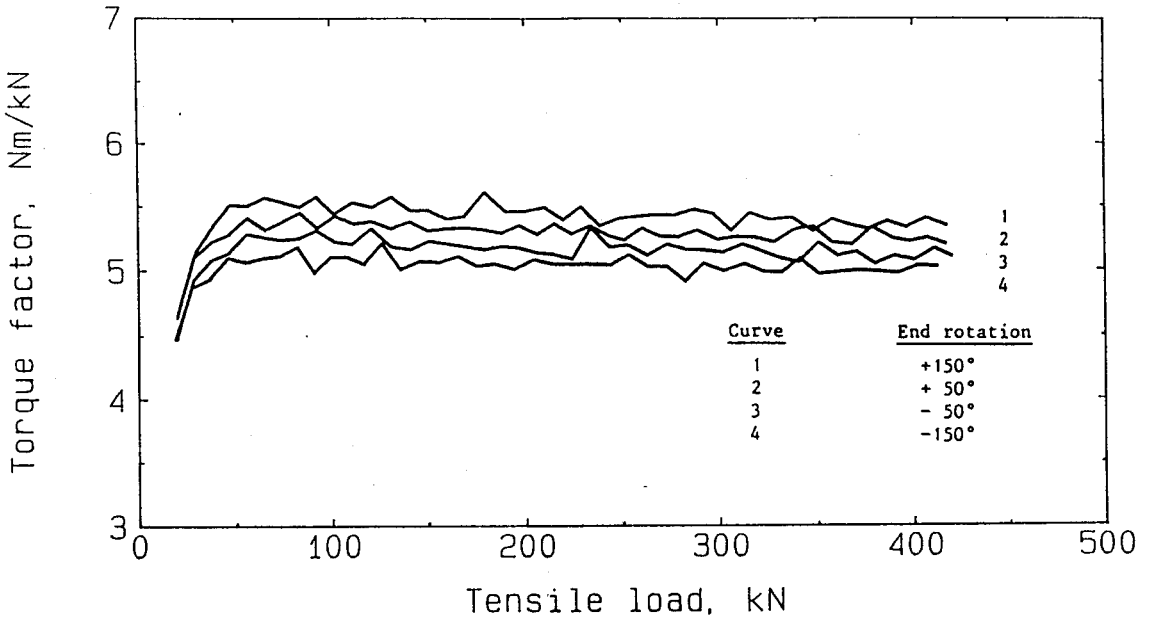

Figure 2.6 Torque factor of a 44 mm triangular strand rope

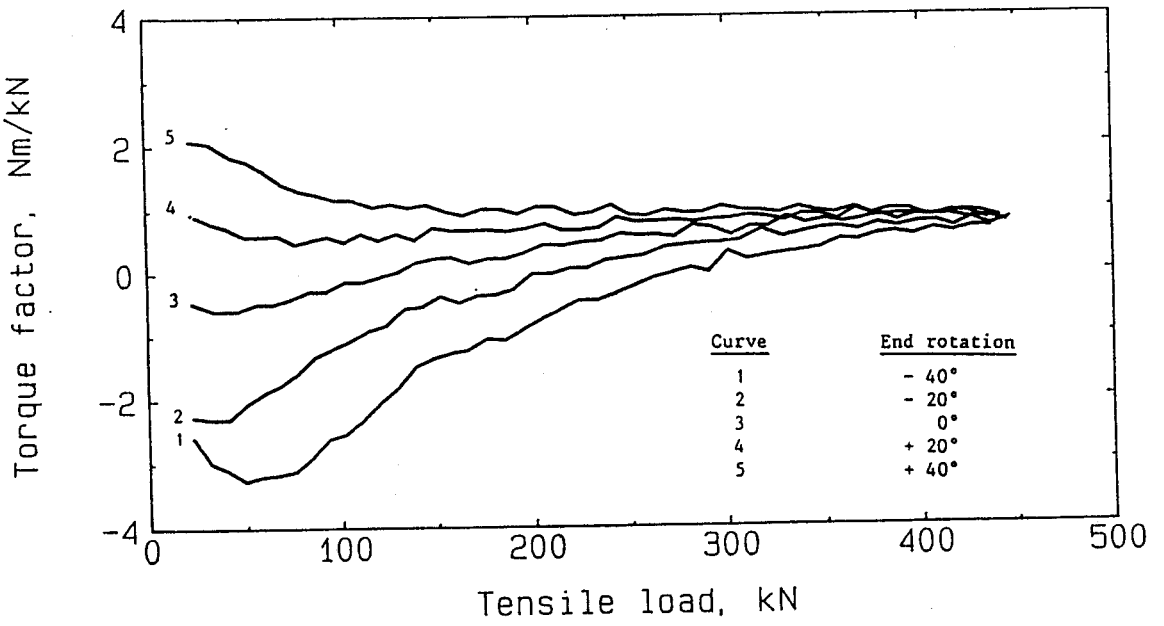

Figure 2.7 Torque factor of a 44 mm non-spin rope

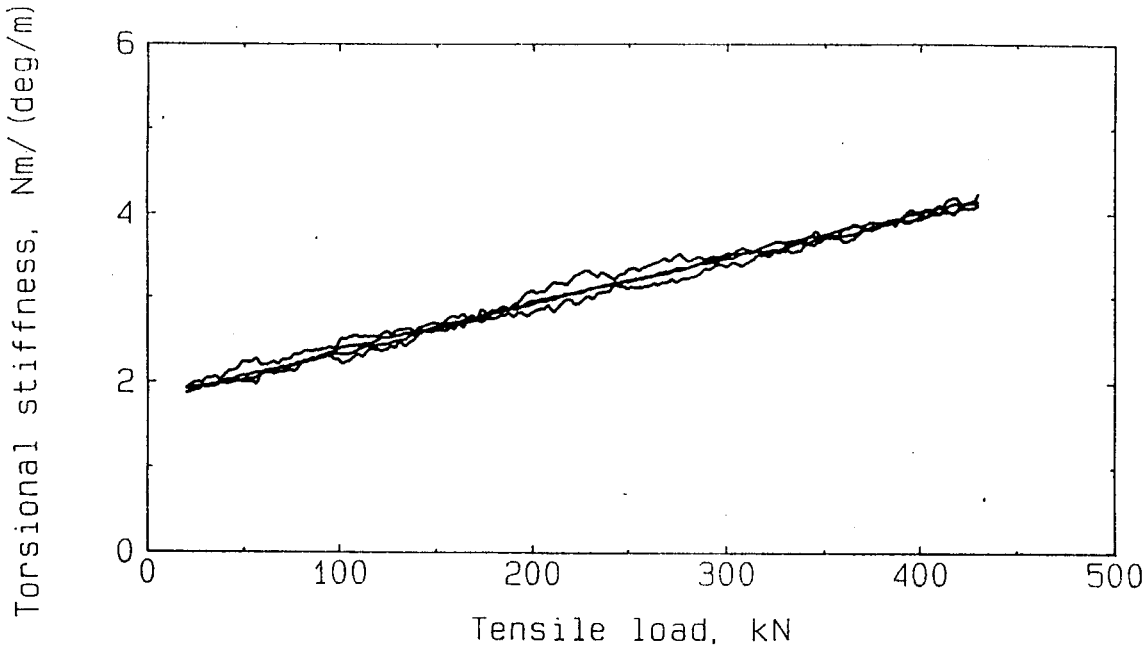

Figure 2.8 Torsional stiffness of a 44 mm triangular strand rope

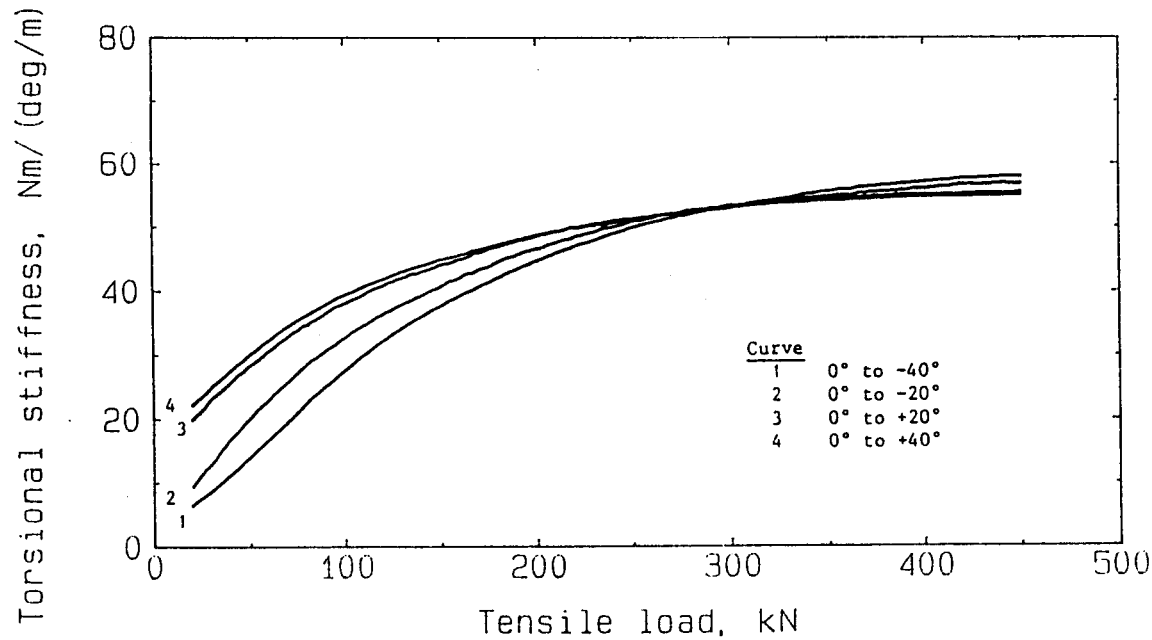

Figure 2.9 Torsional stiffness of a 44 mm non-spin rope

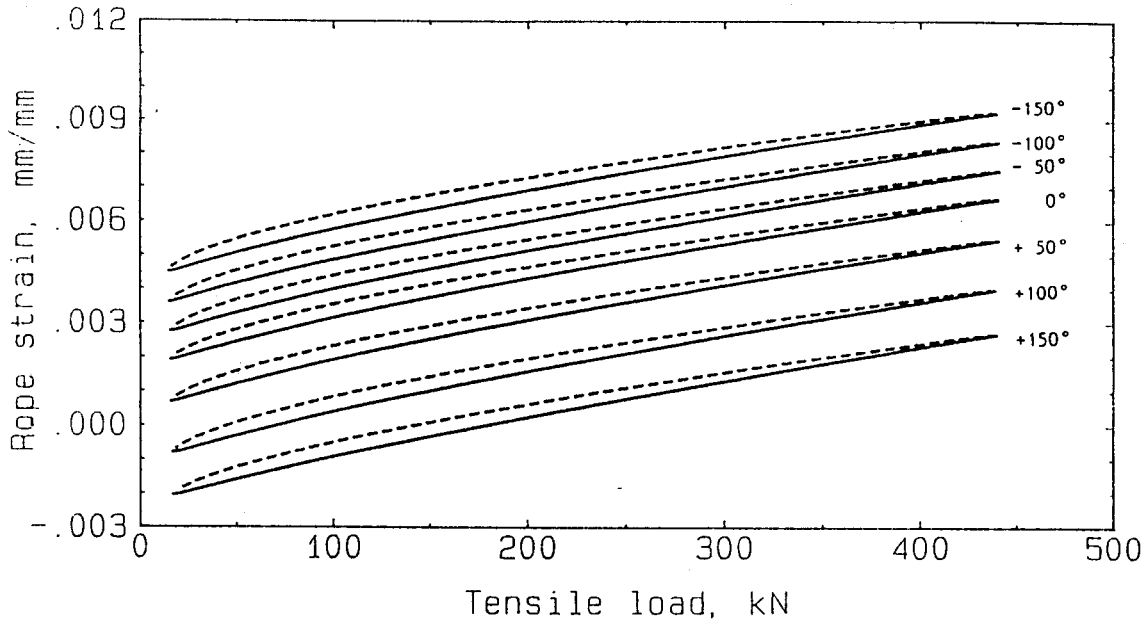

Figure 2.10 Load elongation curves of a 44 mm triangular strand rope
—— Loading
---- Unloading

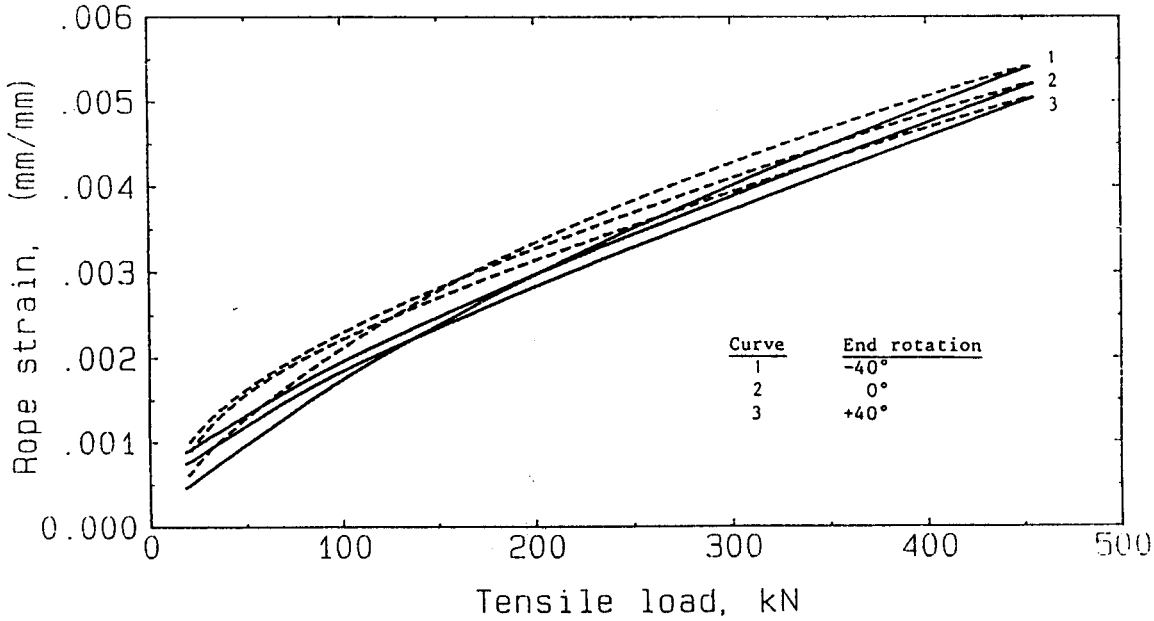

Figure 2.11 Load elongation curves of a 44 mm non-spin rope
—— Loading
---- Unloading

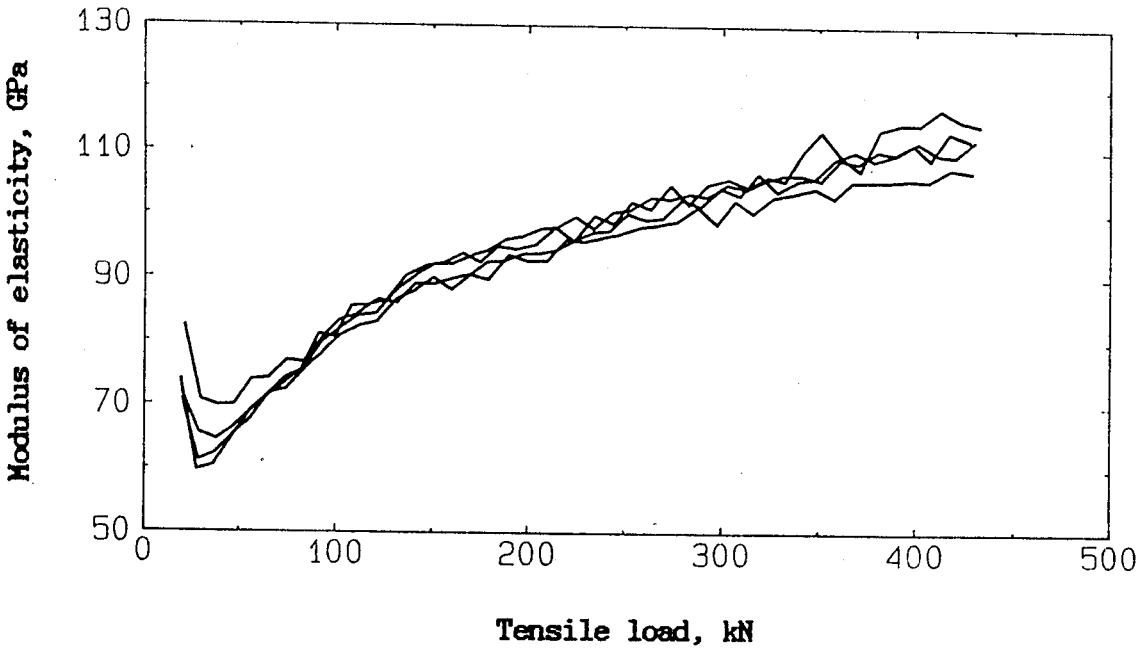

Figure 2.12 Variation of the modulus of elasticity of a 44 mm triangular strand rope

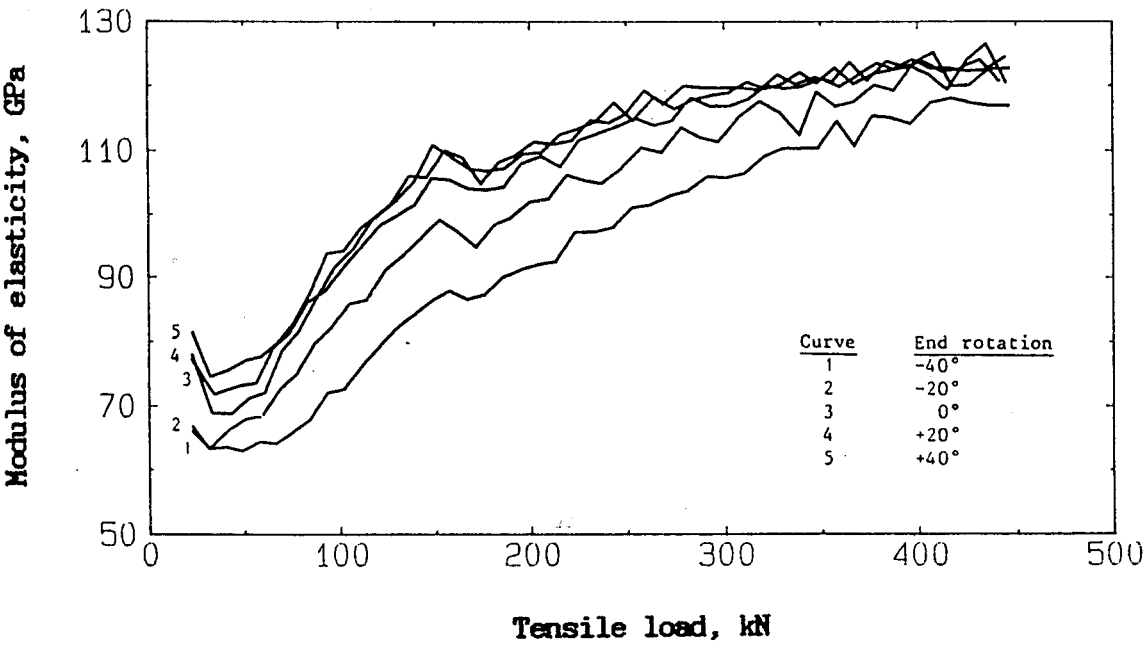

Figure 2.13 Variation of the modulus of elasticity of a 44 mm non-spin rope

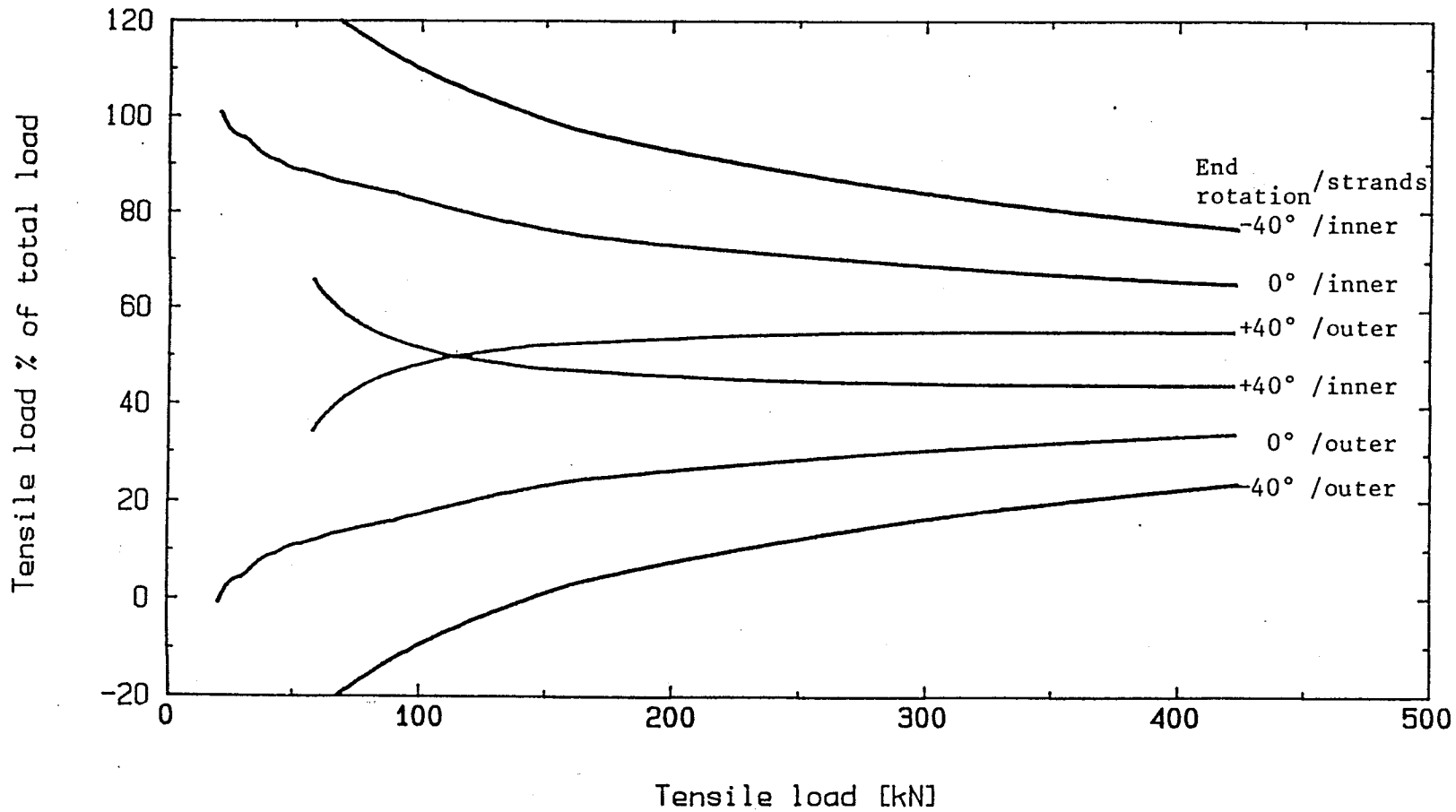

Figure 2.14 Tensile load sharing between inner and outer strands. West Driefontein head rope (44 mm non-spin).

3. THEORETICAL MODEL OF THE HEAD ROPE

The theoretical analysis was restricted to the tower mounted Koepe winder without deflection sheave (Fig. 1.1b). Two models were developed. The first model incorporates the C and T factors as constants. The second model uses the curves obtained from a torque-tension test.

With reference to Fig. 3.1 the following notation was established:

h : Is the hoisting depth [m].
a : Is the overrun distance [m].
u : Is the distance travelled by the conveyances from the stations [m].
z_i: Is the distance of a rope cross section from the i-th conveyance [m]. i = 1 for the upgoing conveyance and i = 2 for the downgoing conveyance. Both z_1 and z_2 relate only to their own compartment and their limits are:

$$0 \leq z_1 \leq h + a - u$$
$$0 \leq z_2 \leq a + u$$

3.1 Assumptions and Boundary Conditions

The following assumptions were made in order to simplify calculations:

a. The length of the rope in contact with the driving wheel is small compared to the overall length of the head rope. It is therefore neglected and the length of the head rope is:

$$L_h = h + 2a \tag{3.1}$$

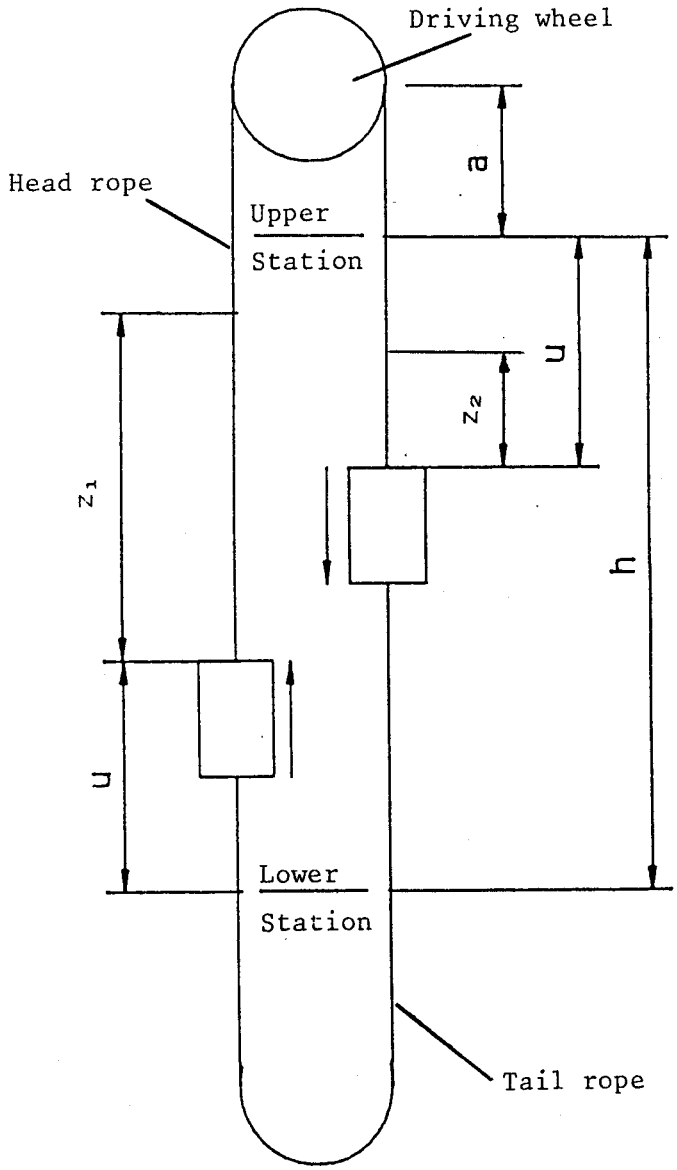

Figure 3.1 Configuration of Koepe winder

b. The gross load of the two conveyances is the same and no loading or unloading takes place.

c. The weight per meter length of the head rope and that of the tail rope are equal.

d. Only static loads are taken into consideration.

The analysis is based on the torque tension relation, equation 2.1, from which an equation is derived for the relative rotation $\triangle\Phi$ over an element of rope of length $\triangle z$. The tension, F, varies linearly with position, z and is expressed accordingly.

In the case of constant C and T factors (details in Appendix B) integration allows for a direct derivation of the relative rotation Φ at any position of the head rope. But in the case where these factors vary and their variation is defined by empirical numerical data, a numerical computerized approach is necessary (details Appendix C).

In both cases, the resulting value of Φ is a function of undetermined torques in the ascending and descending ropes. To determine these torques a number of boundary conditions are used, as follows:

a. The ropes are rigidly fixed to the conveyances i.e. the section attached to the conveyance does not rotate.

b. It follows from the above that the total rotation over the whole head rope is a constant and equal to the initial rotation, Φ_{in}, i.e. the rotation introduced on installation of the rope.

c. While on the driving wheel, the tension in the rope may vary but no rotation occurs.

In addition it is assumed that an element $\triangle z$ about to enter the driving wheel remains unchanged during the subsequent travel $\triangle u$ of the conveyances ($\triangle u = \triangle z$). This assumption is readily acceptable if $\triangle z$ is small enough.

This assumption can not be justified for an element about to leave the driving wheel because, as soon as it is free of the constraint of the supporting material of the wheel, its $\Delta\Phi/\Delta z$ will change to adjust to the new tension.

Finally the two sections of the head rope are assumed to be interchangeable, i.e. at the end of its upwards trip, the upgoing rope becomes the downgoing rope for the start of the next trip (and the downgoing rope becomes the upgoing rope). That is illustrated in Fig. 3.2.

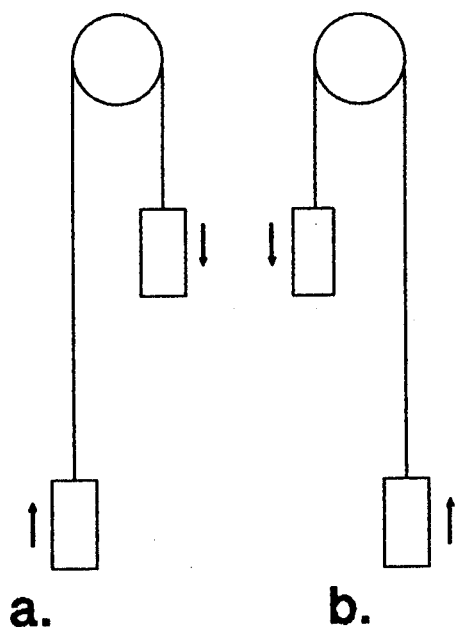

Figure 3.2 Interchangeability of the head rope sections

a. Start of the trip: left section of head rope upgoing and right section downgoing.

b. End of trip, start of next trip: left section downgoing and right section upgoing.

3.2 Theoretical Model of the Head Rope Using Constant C and T Factors

As was mentioned for the case of constant C and T factors, integration allows for a fully analytical solution of the problem. Explicit relations for the torque and the rotation in both the upgoing and downgoing sections of the head rope were derived in Appendix B. The relations are shown in table 3.1 according to the following nomenclature:

$M_{1,u}$: Is the torque in the upgoing rope after a distance u was travelled by the conveyances.

$M_{2,u}$: Is the torque in the downgoing rope after a distance u was travelled by the conveyances.

$\Phi_{1,u,z1}$: Is the relative rotation of a cross section of the upgoing rope at a distance z_1 from the upgoing conveyance. The relative rotation is calculated with respect to the cross section of the rope which is attached to the upgoing conveyance.

$\Phi_{2,u,z2}$: Is the relative rotation of a cross section of the downgoing rope at a distance z_2 from the downgoing conveyance. The relative rotation is calculated with respect to the cross section of the rope which is attached to the downgoing conveyance.

P : Is the gross weight of a conveyance plus 50% of the weight of the tail sheave (if there is one) and 50% of the weight of the rope in the tail rope loop.

q : Is the weight of the ropes in N/m.

k : Is a constant equal to Cq/T.

Table 3.1 Head rope behaviour

Upgoing rope		Eq.
Torque	$M_{1,u} = CP + Cq(h/2 + a^2/L_h + u) + \Phi_{in}T/L_h$	3.2
Relative rotation	$\Phi_{1,u,z1} = k((h/2 + a^2/L_h)z_1 - z_1^2/2) + \Phi_{in}T/L_h$	3.3

Downgoig rope		Eq.
Torque	$M_{2,u} = CP + Cq(h/2 + a^2/L_h + a(h - u)/(a + u)) + \Phi_{in}T/L_h$	3.4
Relative rotation	$\Phi_{2,u,z2} = k((h/2 + a^2/L_h - u(h - u)/(a + u))z_2 - z_2^2/2) + \Phi_{in}z_2/L_h$	3.5

3.2.1 Lay angle variation

Variations in the relative rotation at a rope cross section during a trip result in variations in the lay angle. A wire rope element at its as-manufactured condition is shown in Fig. 3.3a. Figure 3.3b depicts the same element after relative rotation $\Delta\Phi$ was introduced between its two cross sections. The lay angle increased from the as-manufactured value β to $\beta + \theta$.

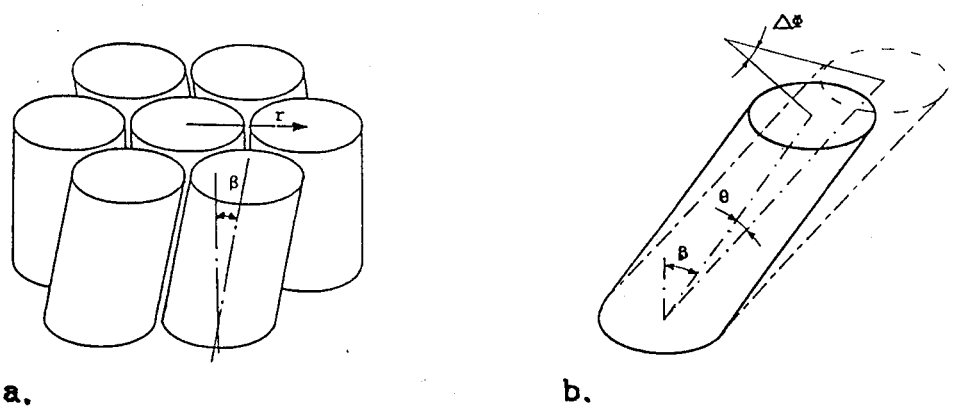

Figure 3.3 Wire rope element

The equations which give the variation of the lay angle during a trip for both the upgoing and the downgoing rope were derived in Appendix B. For the upgoing rope we have:

$$\theta_1 = (k(h/2 + a^2/L_h - z_1) + \Phi_{1n}/L_h).r.\cos^2\beta \qquad (3.6)$$

where r is the distance of the centre of the rope cross section from the centre of the outer strands. The equivalent relation for the downgoing rope is:

$$\theta_2 = (k(h/2 + a^2/L_h - u(h - u)/(a + u) - z_2) + \Phi_{in}/L_h)r.\cos^2\beta \qquad (3.7)$$

The lay angle deviation for the upgoing rope is independent of the travelled distance. This is in accordance with the fact that no rotation occurs in that rope. A rope element in the upgoing rope therefore maintains a constant lay angle value until it enters the downgoing section of the rope. As soon as it enters the downgoing rope its lay angle changes either in a positive direction (causing greater lay angle) or in a negative direction (causing smaller lay angle).

There is only one value of the travelled distance u for which the lay angle of a cross section of the upgoing rope entering the downgoing section remains the same. As shown in Appendix B that is for

$$u' = \sqrt{a^2 + ah} - a \qquad (3.8)$$

For $u < u'$ the lay angle of elements in the upgoing rope entering the downgoing rope is smaller than the lay angle of their adjacent elements in the downgoing rope. Those elements therefore rotate in a positive direction in order to comply with the downgoing rope loading conditions.

For $u > u'$ the lay angle of elements in the upgoing rope entering the downgoing rope is greater than the lay angle of their adjacent elements in the downgoing rope. In this case elements entering the downgoing section of the head rope rotate in the negative direction.

3.2.2 Rotation of the downgoing rope - Chalk test

From equation 3.6 it was shown that the upgoing rope does not rotate during the trip. On the other hand the downgoing rope as can be seen from equation 3.7 rotates continually during the trip. The rotation of the downgoing rope can be determined experimentally by the so-called chalk test described in Chapter 1.

As is shown in Appendix B the number of turns measured at the driving wheel as a function of the travelled distance is given by the following equation

$$N = k.u(h - u)/360° \qquad (3.9)$$

For $u = h$ according to the above equation the rope exhibits zero turns. This means that the rope rotates as many clockwise turns as anticlockwise. The change of direction happens at $u = h/2$ when:

$$N = k.h^2/1440° \qquad (3.10)$$

The line drawn on the downgoing rope is actually a double spiral as is shown in Fig. 3.4. Equation 3.10 shows that the number of turns is proportional to the square of the hoisting depth h. This explains why problems on Koepe winders manifested themselves only at the deep South African shafts.

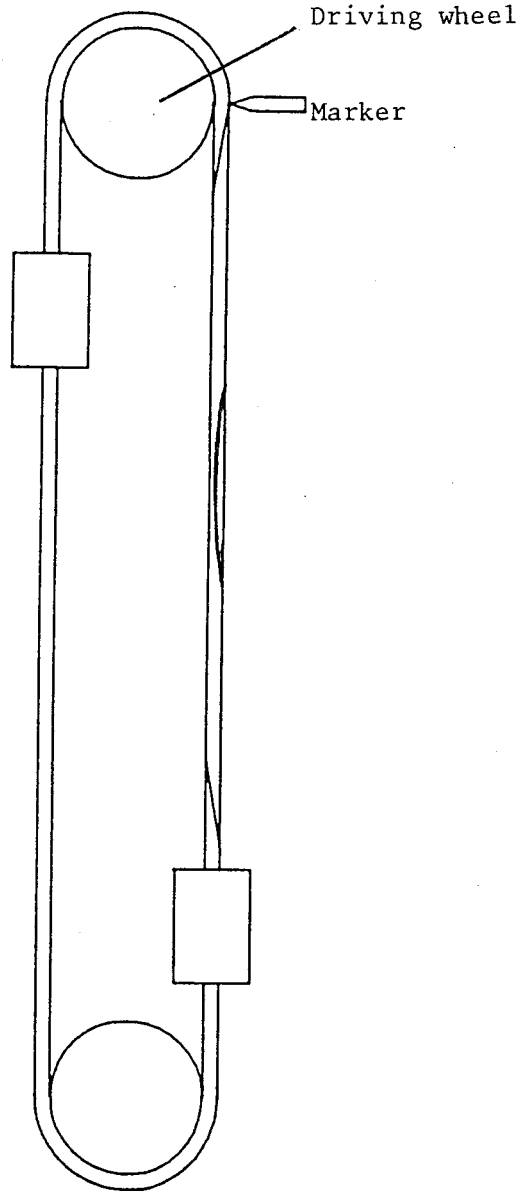

Figure 3.4 Chalk line test

3.2.3 Application of the model to a practical example

The theoretical model of the torsional behaviour of a Koepe head rope was applied to the West Driefontein No. 5 shaft British General Electric (BGE) Koepe winder. The particulars of the winder and the head rope are given in Table 3.2.

The torque in the two sections of the rope during a trip is given in Figure 3.5. The torque in the upgoing rope increases linearly during the trip. Rapid torque changes take place in the downgoing rope during the first few metres of the trip. Figure 3.6 presents the torque difference between the two sections of the head rope

The lay angle variation during a trip for various rope cross sections was plotted in figures 3.7 to 3.10. Figure 3.9 was drawn for the section which undergoes no changes, as it passes through the driving wheel, in accordance with equation 3.8. The minimum and maximum values of the lay angle deviation for each rope cross section were plotted in Figure 3.11. The greater lay angle variations occur in the rope sections closest to the conveyances.

A graphical representation of the chalk test results is given in Figure 3.12. A total of four turns are counted, two clockwise and two anticlockwise.

Table 3.2 Particulars of West Driefontein No. 5 shaft Koepe winder

Hoisting depth	h	1 700 m
Overrun distance	a	25 m
Head rope weight	q	85 N/m
Cross conveyance weight	P	215 kN
Torque factor	C	0,0007 Nm/N
Torsional stiffness	T	50 Nm/de
Rotation during installation	Φ_{in}	0 deg

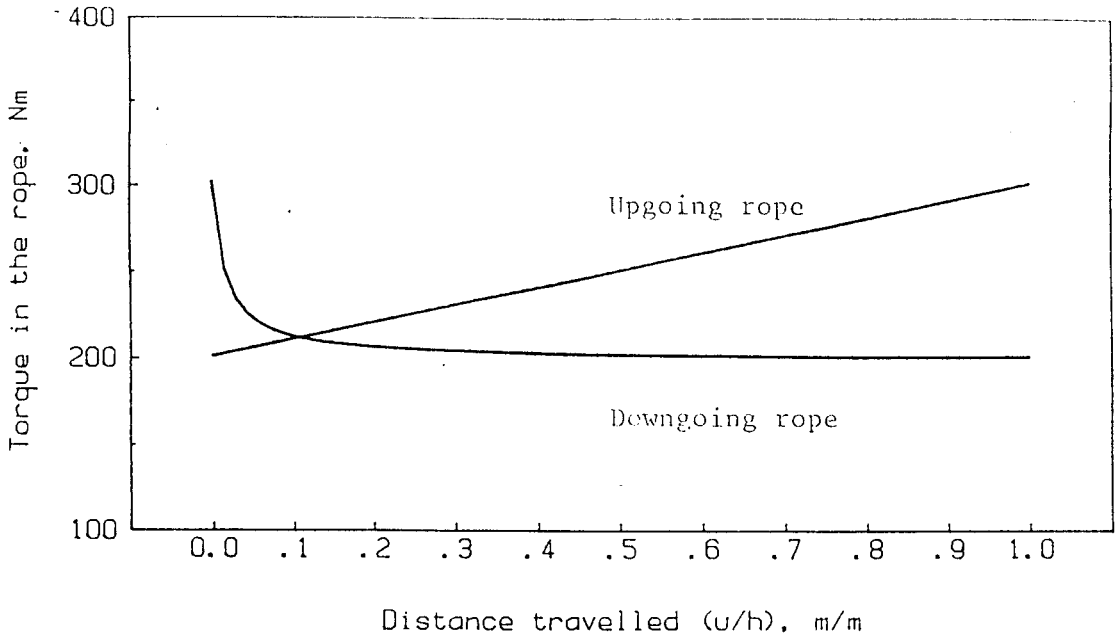

Figure 3.5 Torque in the rope during a trip

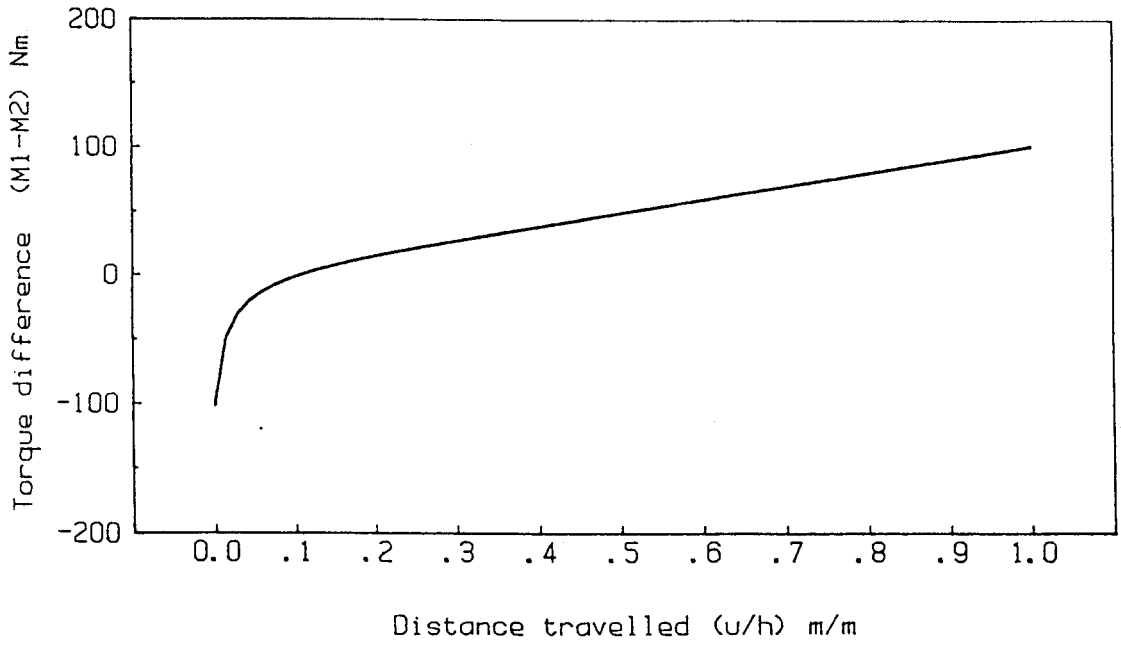

Figure 3.6 Torque difference in the two sections of the rope during a trip

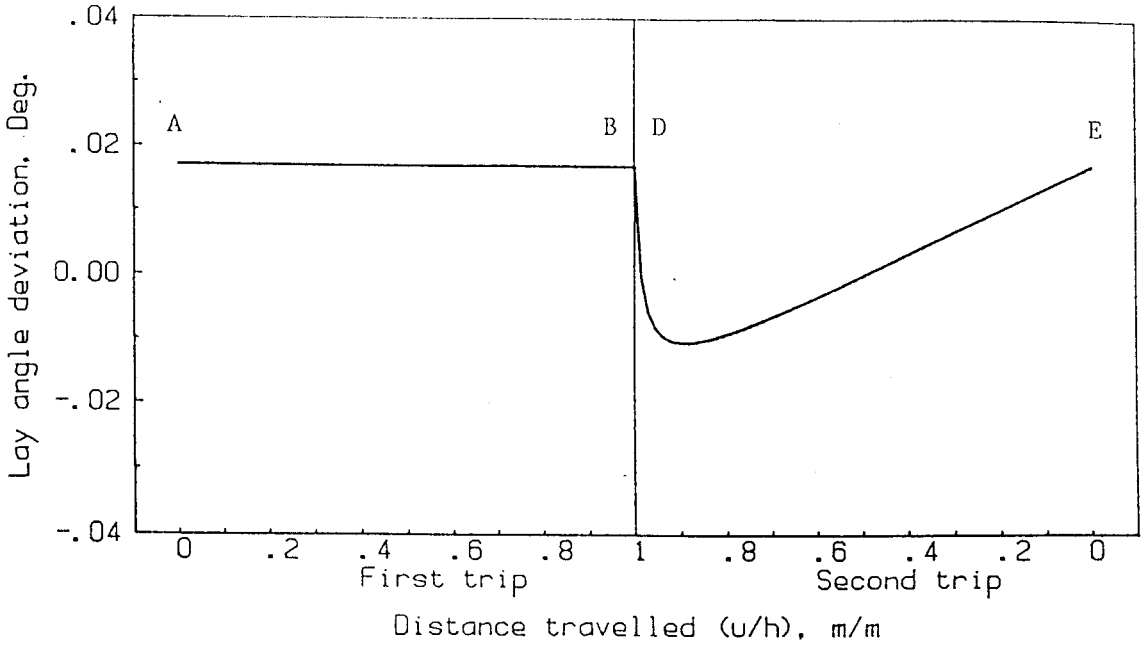

Figure 3.7 Lay angle deviation at cross section during a double trip Distance of cross section from upgoing conveyance z_1=25 m. A to B upgoing, D to E downgoing.

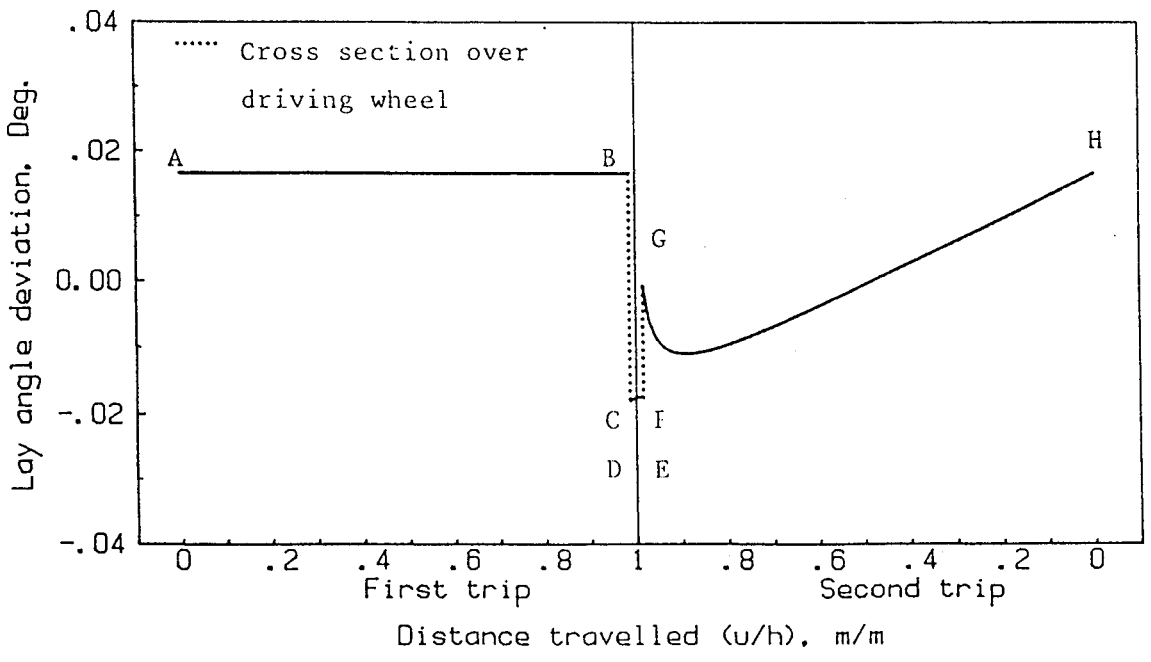

Figure 3.8 Lay angle deviation at cross section during a double trip Distance of cross section from upgoing conveyance z_1=50 m. A to B and E to F upgoing, C to D and G to H downgoing.

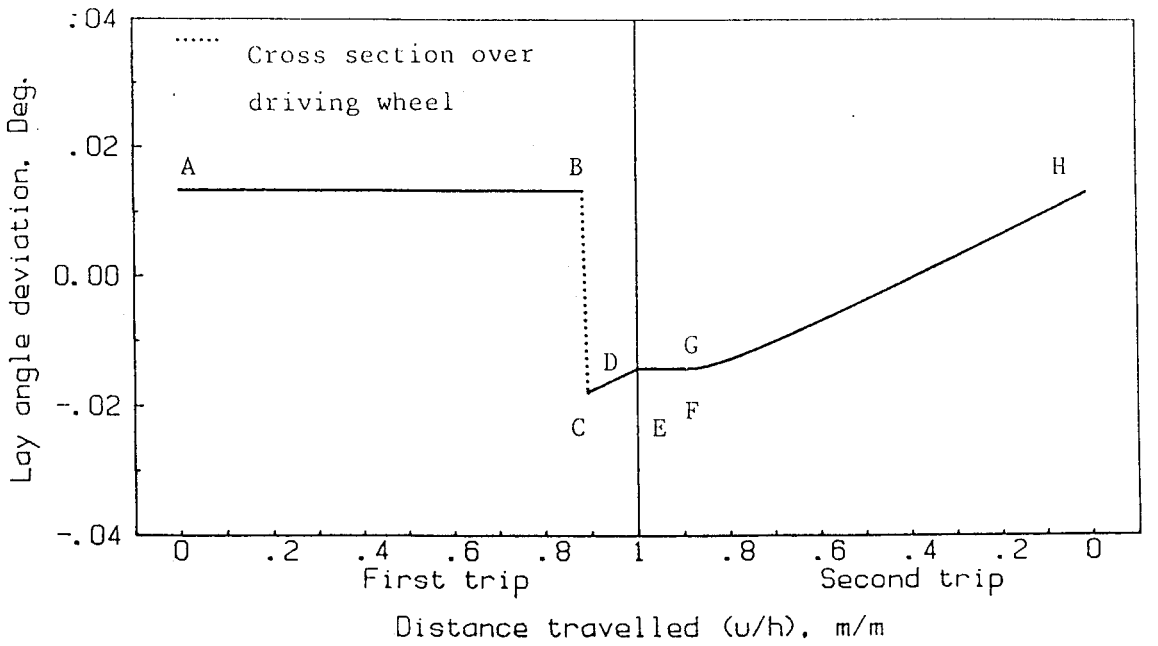

Figure 3.9 Lay angle deviation at cross section during a double trip Distance of cross section from upgoing conveyance z_1=207.6 m A to B and E to F upgoing, C to D and G to H downgoing.

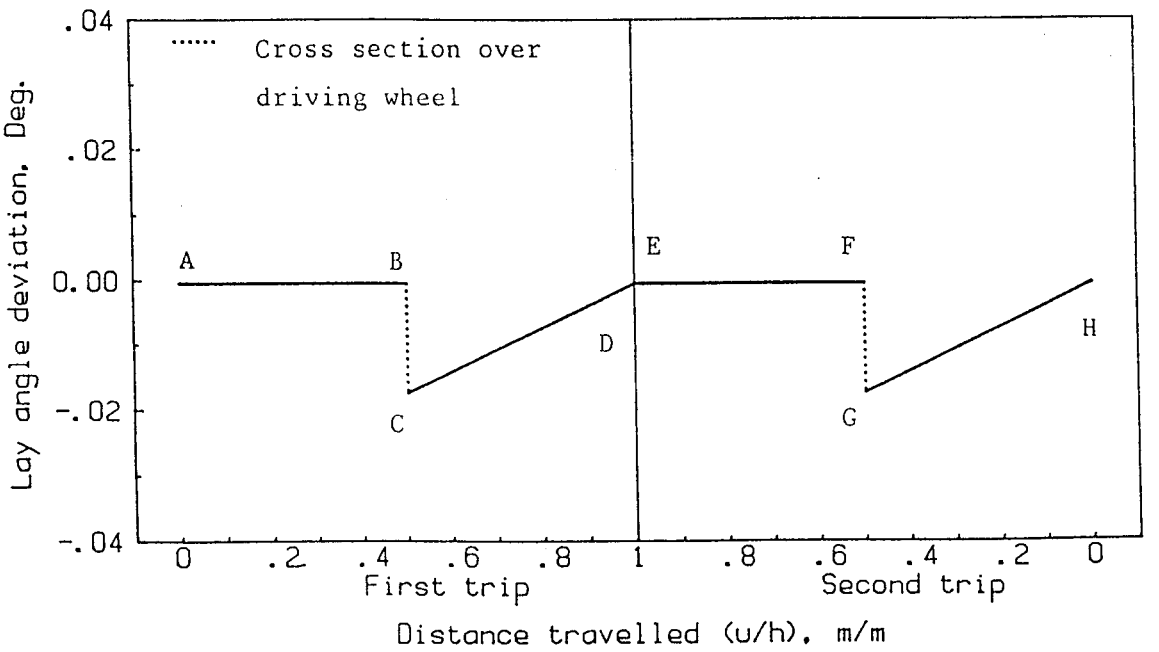

Figure 3.10 Lay angle deviation at cross section during a double trip Distance of cross section from upgoing conveyance z_1=875 m A to B and E to F upgoing. C to D and G to H downgoing.

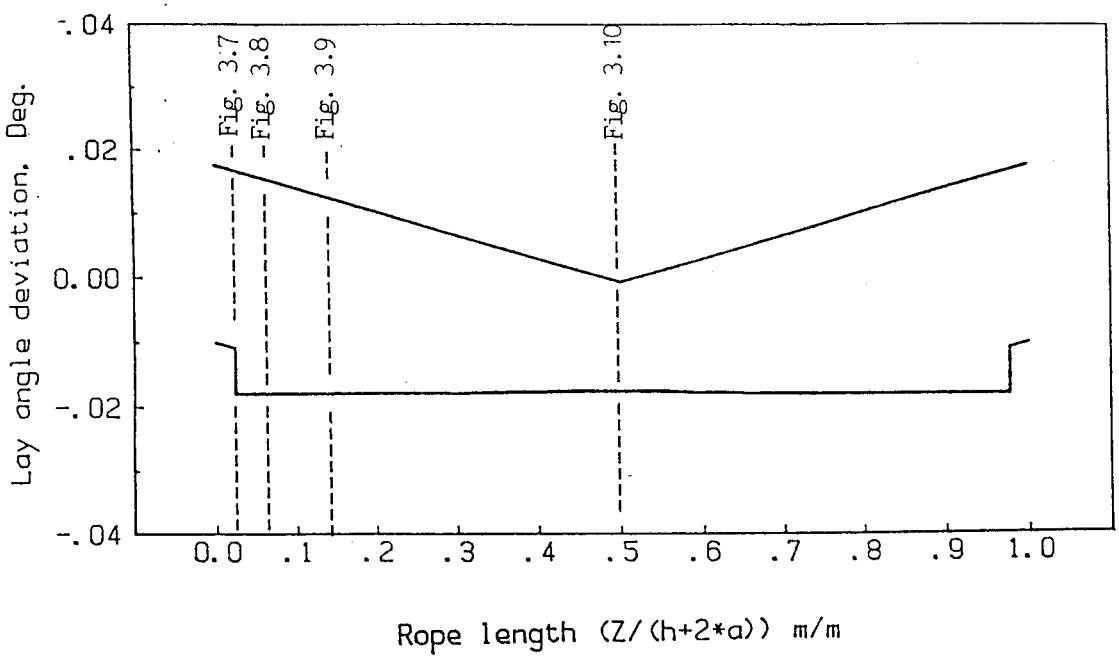

Figure 3.11 Boundary values of lay angle deviation

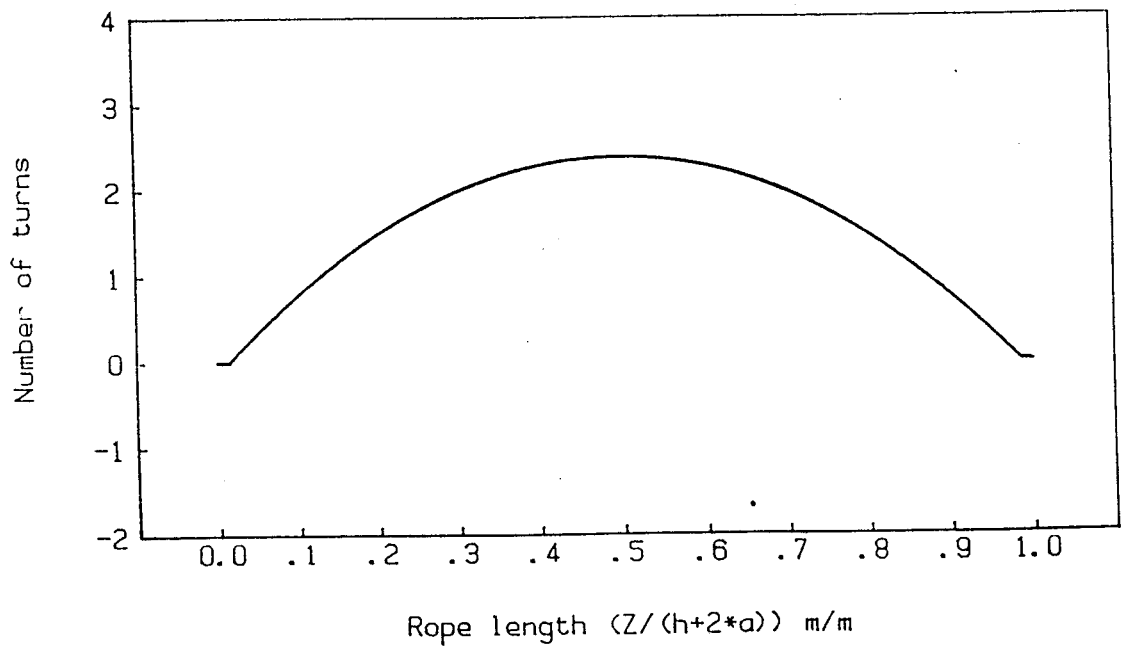

Figure 3.12 Chalk line test

3.3 Theoretical Model of the Head rope Using Variable C and T Factors

The assumption of constant C and T factors made in the previous section, is a good approximation for non-spin ropes for high tensile loads and positive values of end rotation. For low loads the C and T factors vary substantially with the tensile load and the twist introduced in the specimen as illustrated in Figures 2.7 and 2.9.

In order to study the influence of the shape of the torque-tension curves on the torsional behaviour of the head rope, a second model was developed. The new model utilizes the actual shape of the torque-tension curves. The assumption is made nevertheless that the shape of the curves is the same during loading and unloading. Figure 2.5 is reproduced here as Fig. 3.13 showing only the loading curves.

Since the torque along the rope is constant the lay angle varies in order to accommodate the variation of the tensile load due to the rope weight. In order to calculate this lay angle variation the results of Fig. 3.13 had to be modified to obtain values at constant torque. This was achieved by building up a table of twist values for different torques and tensions at intervals of 1 Nm and 1kN respectively. Figure 3.14 illustrates some of the values from that table. This table was used to obtain the twist at each rope element for a constant torque value.

The torque is related to the boundary condition which is the relative rotation between the two ends of the rope. However, whereas in the case of constant C and T factors this relationship is explicit as in equation 3.2, here a numerical algorithm is required to take into account the continuous variation of C and T factors. The torque history during a trip will depend primarily on the initial torque $M_{1,0}$ in the ascending rope.

The algorithm described in the next section was devised to obtain, for a given initial torque $M_{1,0}$, the compatible boundary condition Φ_{1n}. By repeating for different values of $M_{1,0}$ a series of such relations was established as illustrated in Fig. 3.15. The alternative approach would have been to start with a value of Φ_{1n} and obtain the compatible value of $M_{1,0}$, but this was rejected because it would have involved considerable trial and error calculations.

3.3.1 Head rope model algorithm

There are two parts in this algorithm: One for the upgoing rope and one for the downgoing rope. The section for the upgoing rope is completed first and recorded values are input in the calculation for the downgoing rope. Initial input parameters include a rope element of length Δl, small enough to assume that the twist over that element is constant.

Upgoing rope

Step 1: Assume an initial torque value for the upgoing section of the head rope.

Step 2: Utilizing the torque-tension tables of the rope calculate the twist in each element of the upgoing rope.

Step 3: Calculate the relative rotation between the two ends of the upgoing rope, which is equal to the sum of the twist in all elements multiplied by the element length.

Step 4: Decrease the length of the upgoing rope by Δl.

Step 5: Calculate the new value of the relative rotation between the two ends of the upgoing rope.

Step 6: Increase the torque value in the upgoing rope by a small step.

Step 7: Calculate the new twist value for each element.

Step 8: Calculate the new relative rotation value between the two ends of the upgoing rope.

Step 9: If the new relative rotation value is the same as the one calculated in Step 5 go to Step 11.

Step 10: Decrease or increase torque value depending on whether the new relative rotation value is smaller or greater than the old one and go to Step 7.

Step 11: Record torque value and twist distribution in upgoing rope for the travelled distance, u.

Step 12: If the trip has not been completed, go to Step 4. Otherwise go to Step 1 of downgoing rope.

Downgoing rope

Step 1: Assuming that no loading or unloading takes place, the initial torque value in the downgoing rope is the same as the final torque in the upgoing rope (allowance for loading and unloading was included in the algorithm but was not used for this research).

Step 2 to 12: As for upgoing rope, except:

(i) Wherever it states upgoing, read downgoing.

(ii) In step 4 the rope length is increased by $\triangle l$

(iii) At the completion of the trip continue as below.

Step 13: Calculate the relative rotation, Φ_{in} introduced to the head rope on installation.

Step 14: From the recorded values of torque and twist calculate rotation of the rope during the trip (Chalk test).

A computer program was developed to simulate the behaviour of the head rope according to the above algorithm. A listing of the program is given in Appendix C.

3.3.2 Application of the model to a practical example

The theoretical model was once again applied to the West Driefontein No. 5 shaft Koepe winder. The results obtained from the model for the case of no initial end rotation are presented in Figures 3.16 to 3.19. The results are very similar to those obtained for constant C and T factors.

Figure 3.16 shows negative values of the torque for most of the trip. This implies that the contribution of the inner strands towards the total torque in the rope is greater than the contribution of the outer strands and therefore the inner strands carry a higher percentage of the total tensile load in the rope.

The chalk test results are shown in Figure 3.17. Four turns are counted, two clockwise and two anticlockwise.

The variation of the lay angle is shown in Figures 3.18 and 3.19, where a slight variation of the lay angle in the upgoing rope is noticed.

3.3.3 Influence of the shape of the torque-tension curves

Introduction of end rotation causes the winder to operate in a different area of the torque-tension diagram, Figure 3.13. For the case mentioned above, where no end rotation was introduced, the winder operates in area A of the diagram. Introduction of 27 rotations in the positive direction would cause the winder to operate in area B. If 47 rotations in the negative direction are introduced the winder would operate in area C. These particular values of 27 and 47 rotations were obtained from particular runs of the algorithm mentioned earlier. The torque in the rope during the trip and the chalk test results for areas B and C are presented in Figures 3.20 to 3.23.

The difference in the torque between the two sections of the rope (upgoing and downgoing) is shown in Figure 3.24, for various values of the initial rotation, Φ_{in}. Figure 3.25 illustrates the equivalent results of the chalk line test, for the middle cross section of the head rope. Both relations are parabolic, with the slope of the curves decreasing from negative to positive values of initial rotation. This leads to the conclusion that the torsional behaviour is more sensitive to the introduction of negative than positive end rotation.

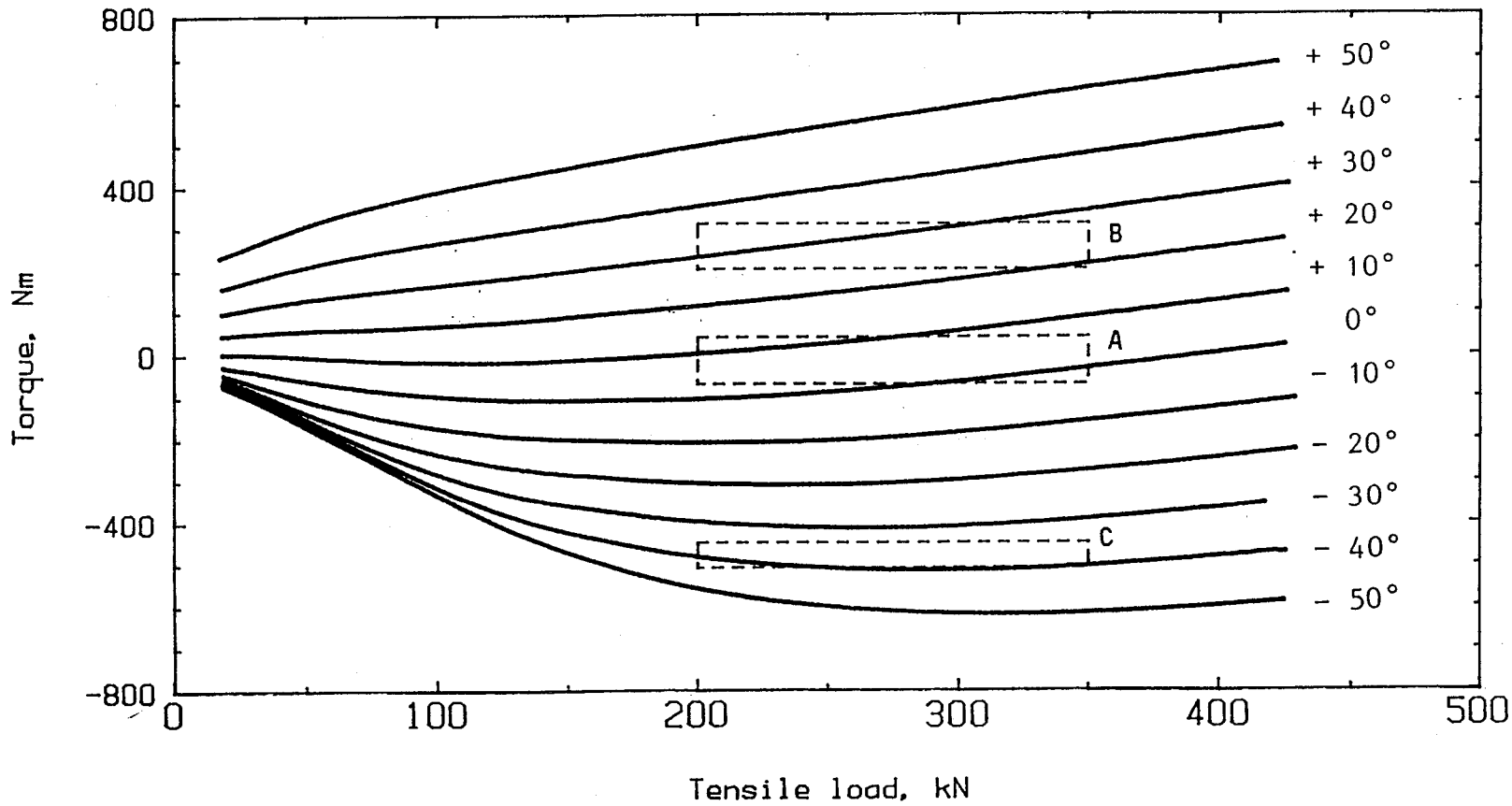

Figure 3.13 Torque tension curves of West Driefontein head rope for various end rotations

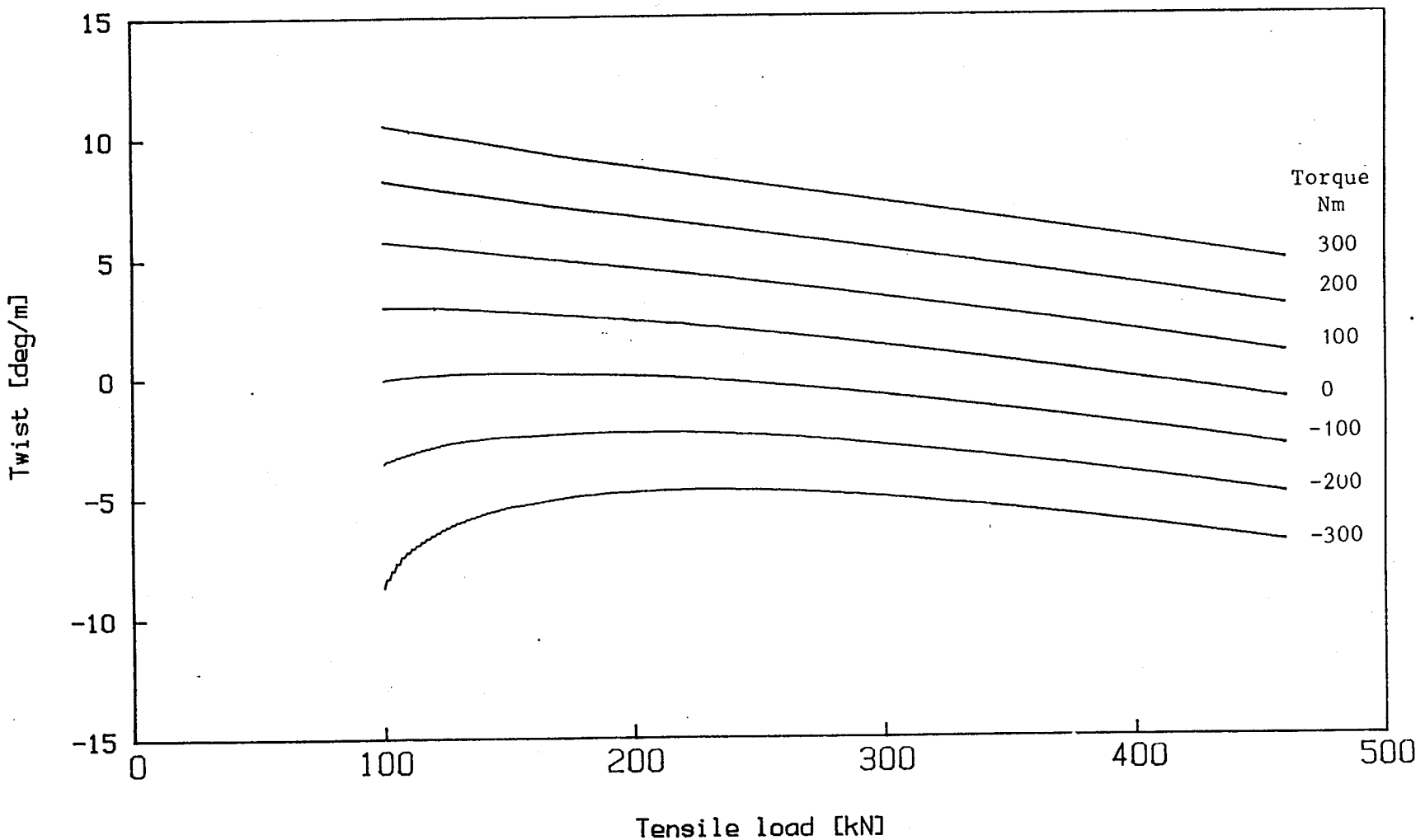

Figure 3.14 Twist curves of West Driefontein head rope for various torque values

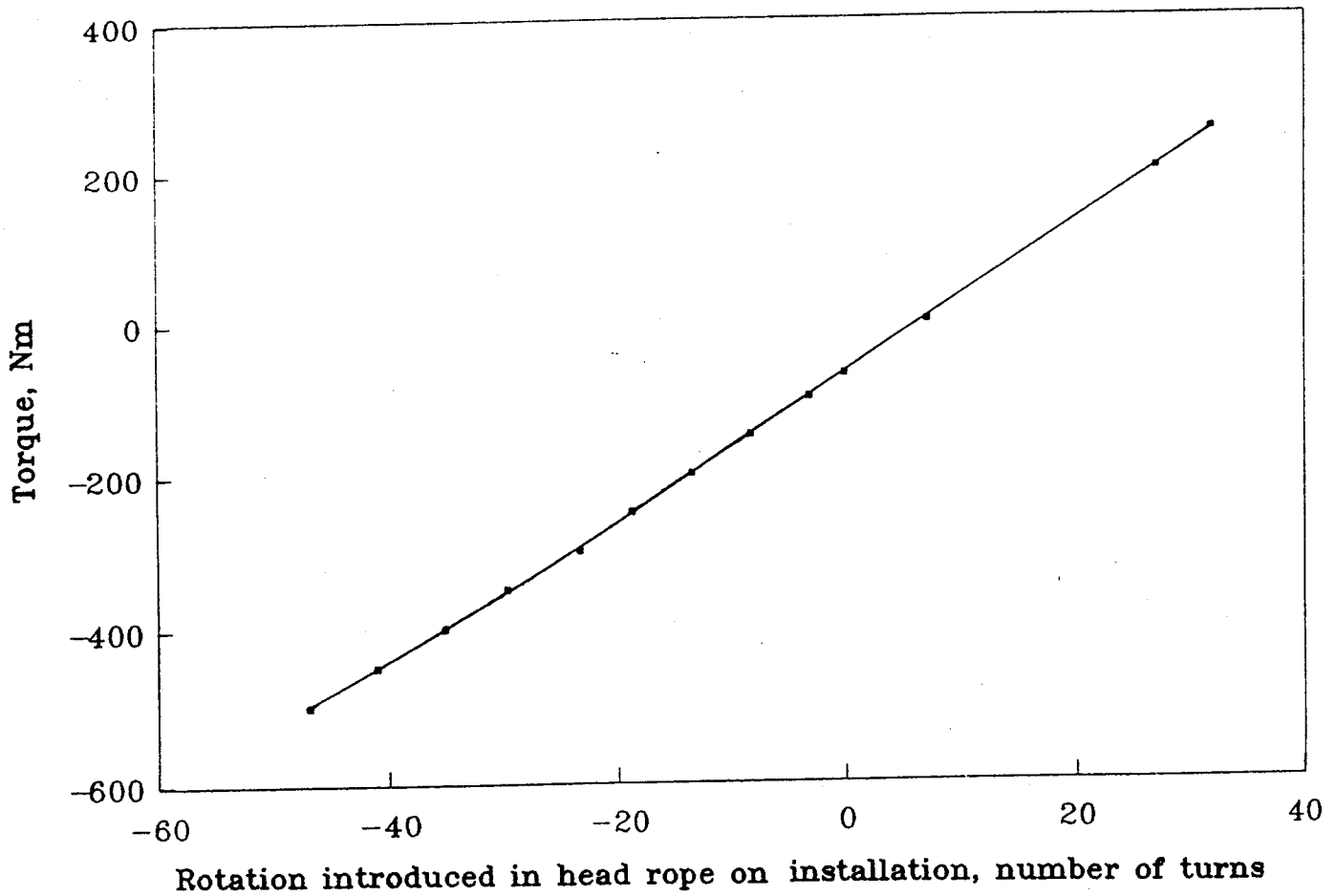

Figure 3.15 Relationship between initial torque and rotation

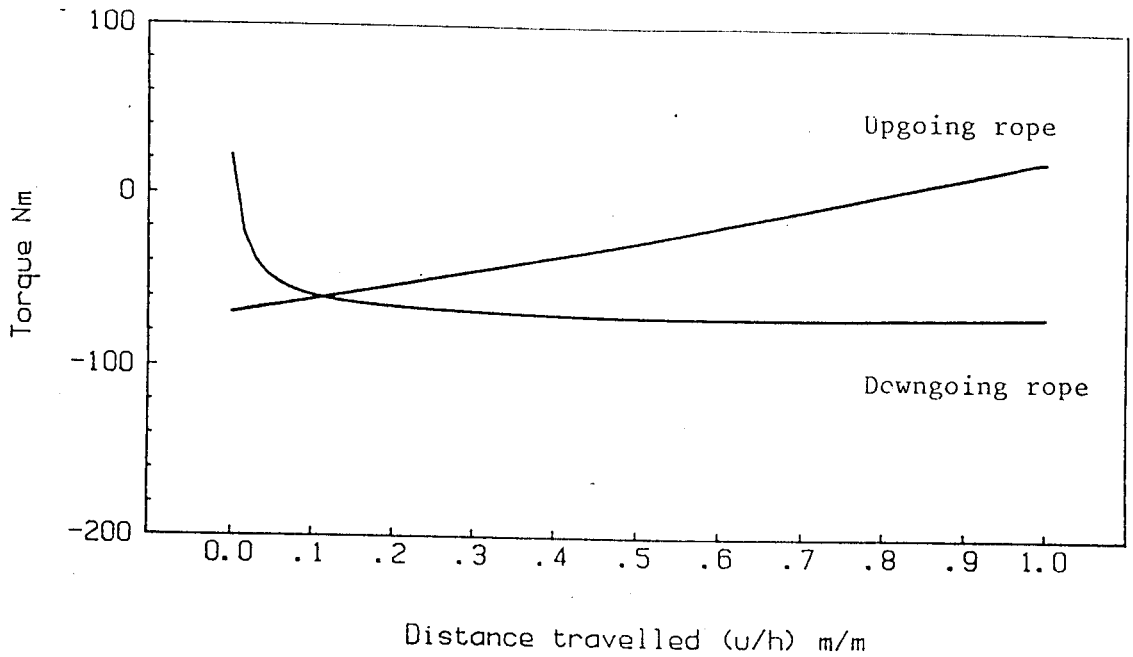

Figure 3.16 Torque in the rope

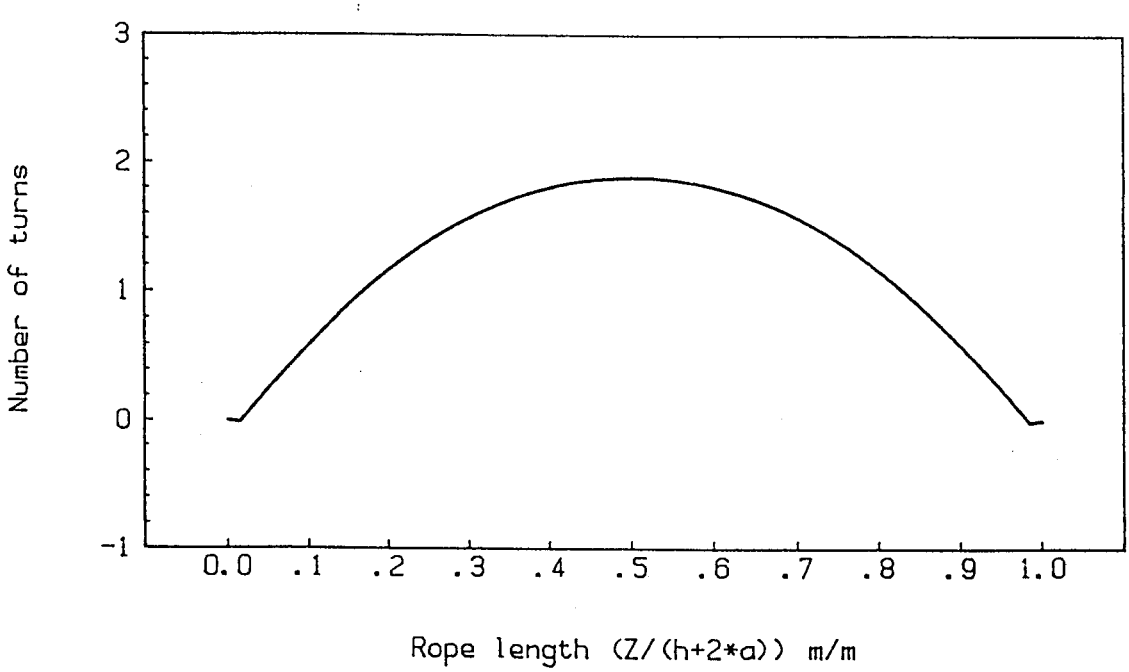

Figure 3.17 Chalk line test

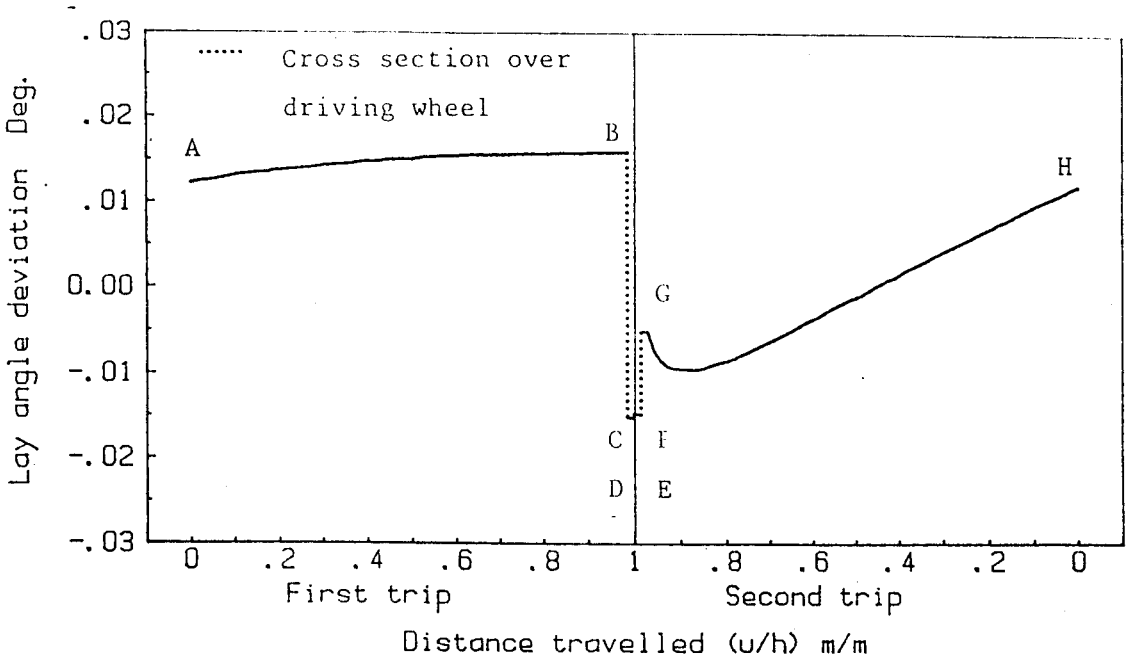

Figure 3.18 Lay angle deviation at a cross section during double trip Distance of cross section from upgoing conveyance z_1=50 m. A to B and E to F upgoing. C to D and G to H downgoing

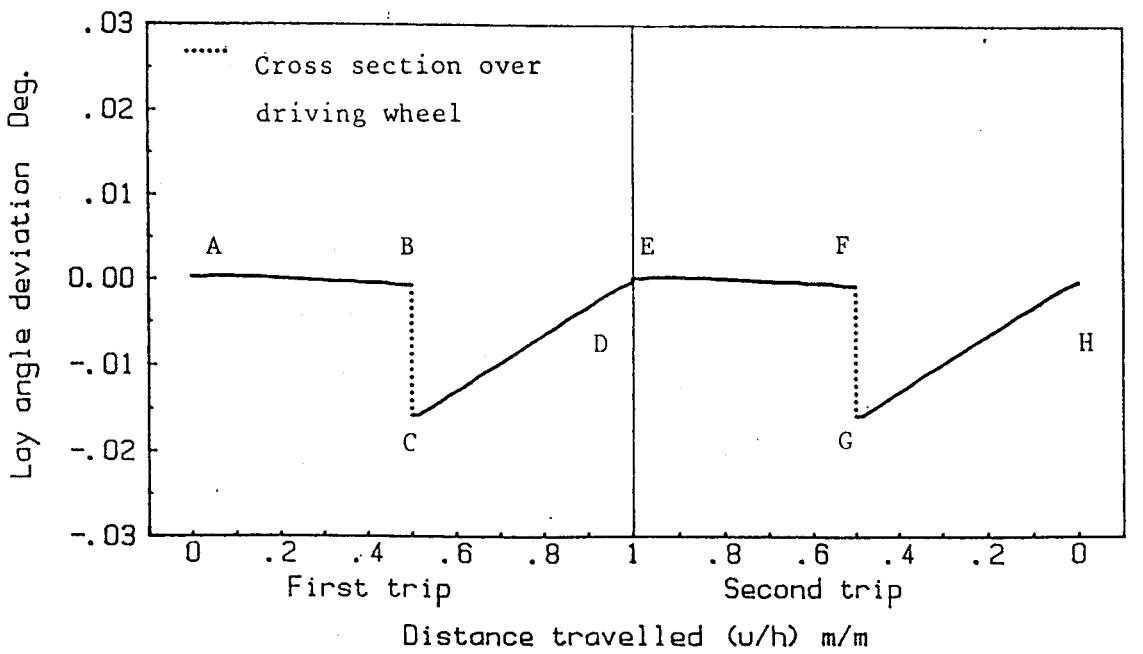

Figure 3.19 Lay angle deviation at a cross section during double trip Distance of cross section from upgoing conveyance z_2=875 m. A to B and E to F upgoing, C to D and G to H downgoing.

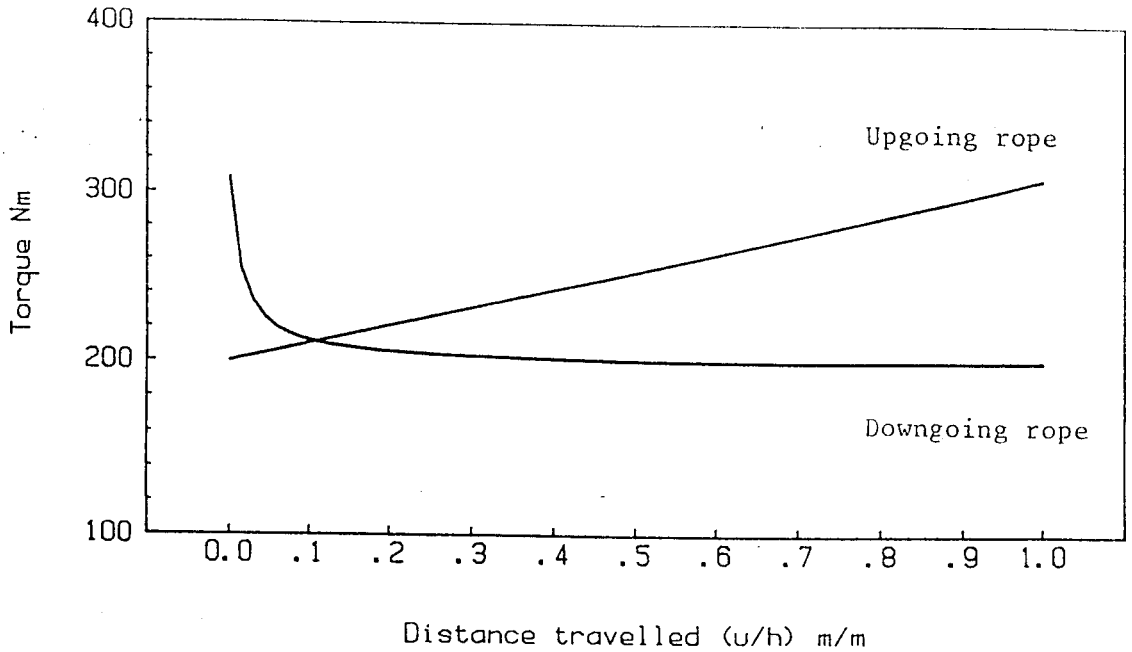

Figure 3.20 Torque in the rope for positive end rotation
Area B, 27 turns

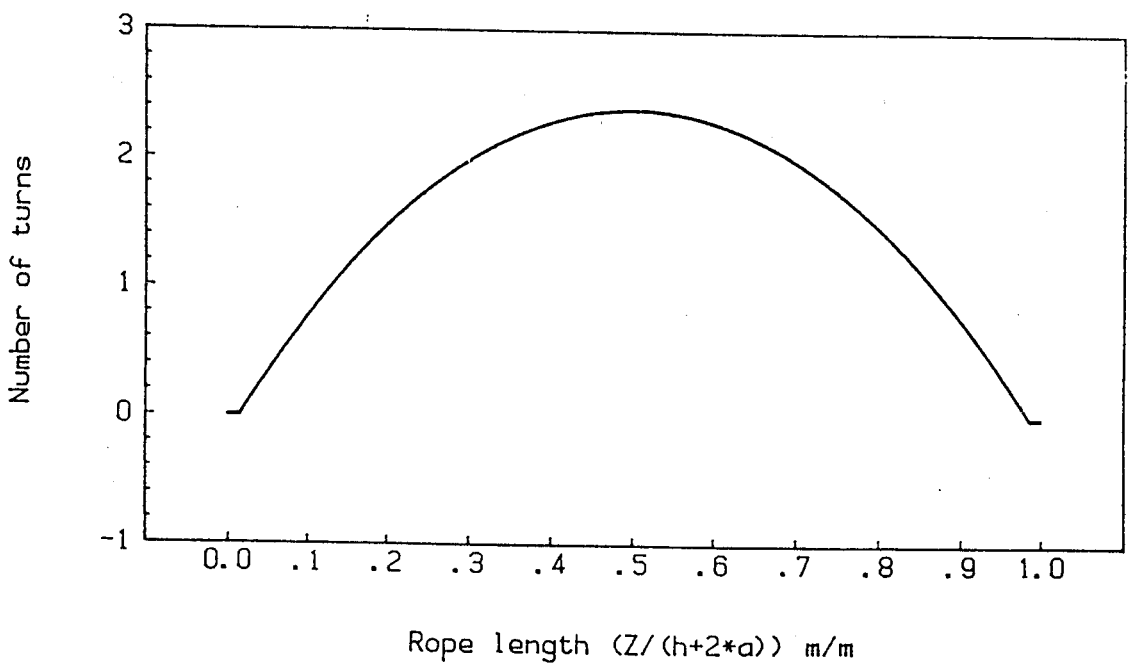

Figure 3.21 Chalk test for positive end rotation
Area B, 27 turns

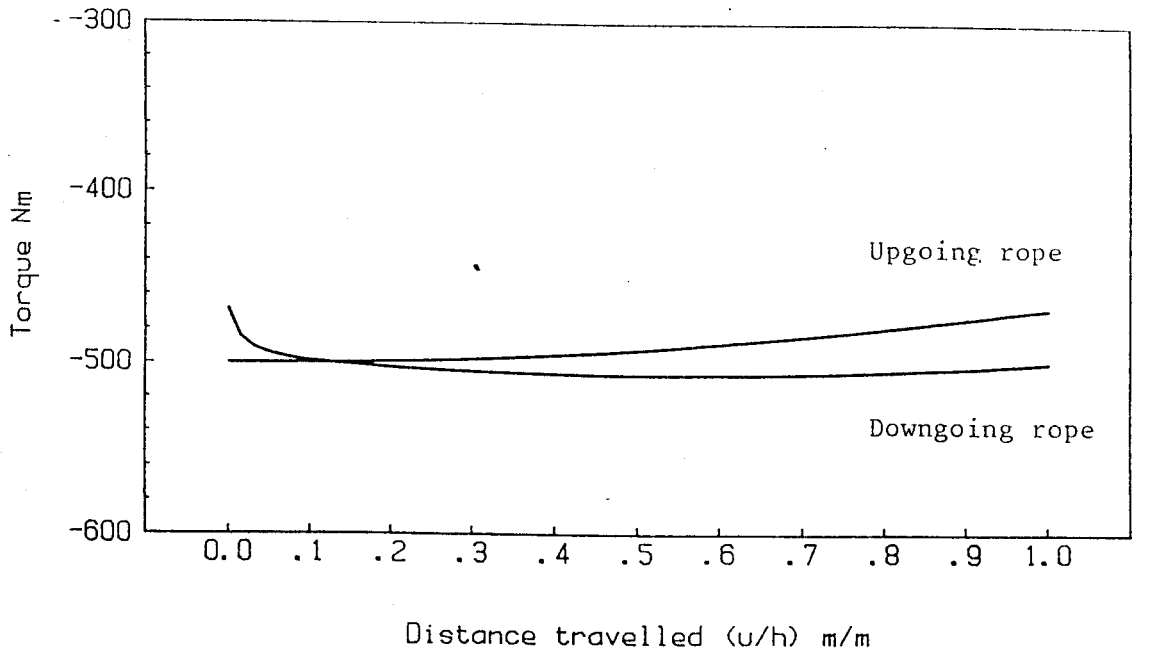

Figure 3.22 Torque in the rope for negative end rotation
Area C, 47 turns

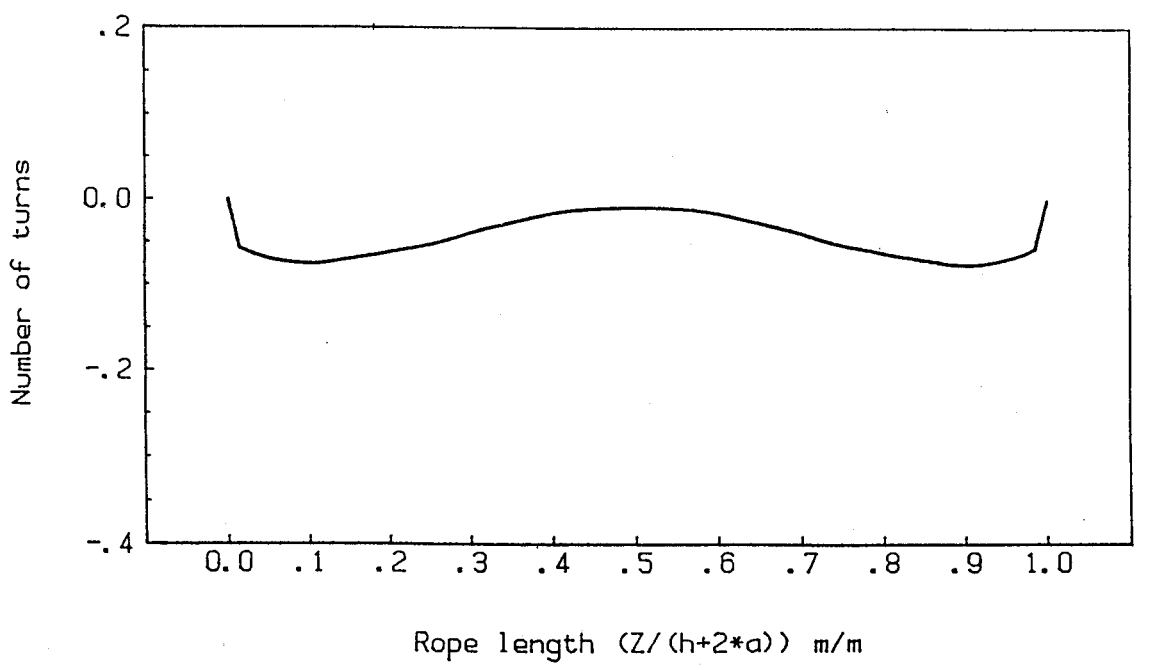

Figure 3.23 Chalk line test for negative end rotation
Area C, 47 turns

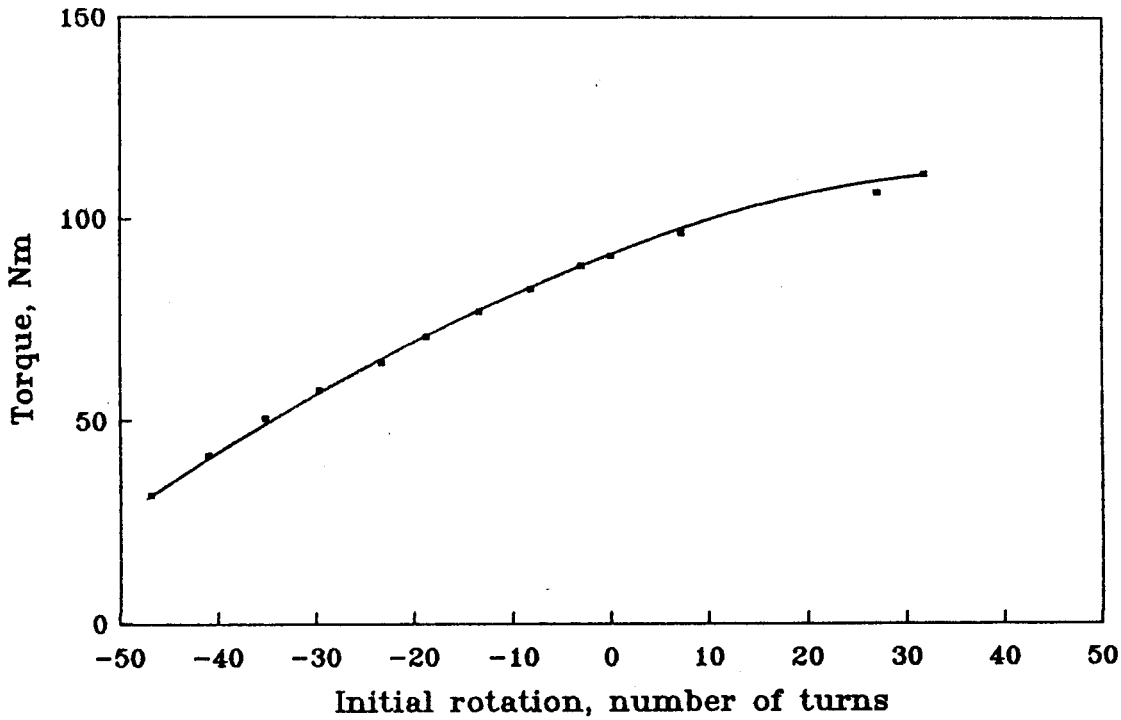

Figure 3.24 Torque difference at the beginning of the trip

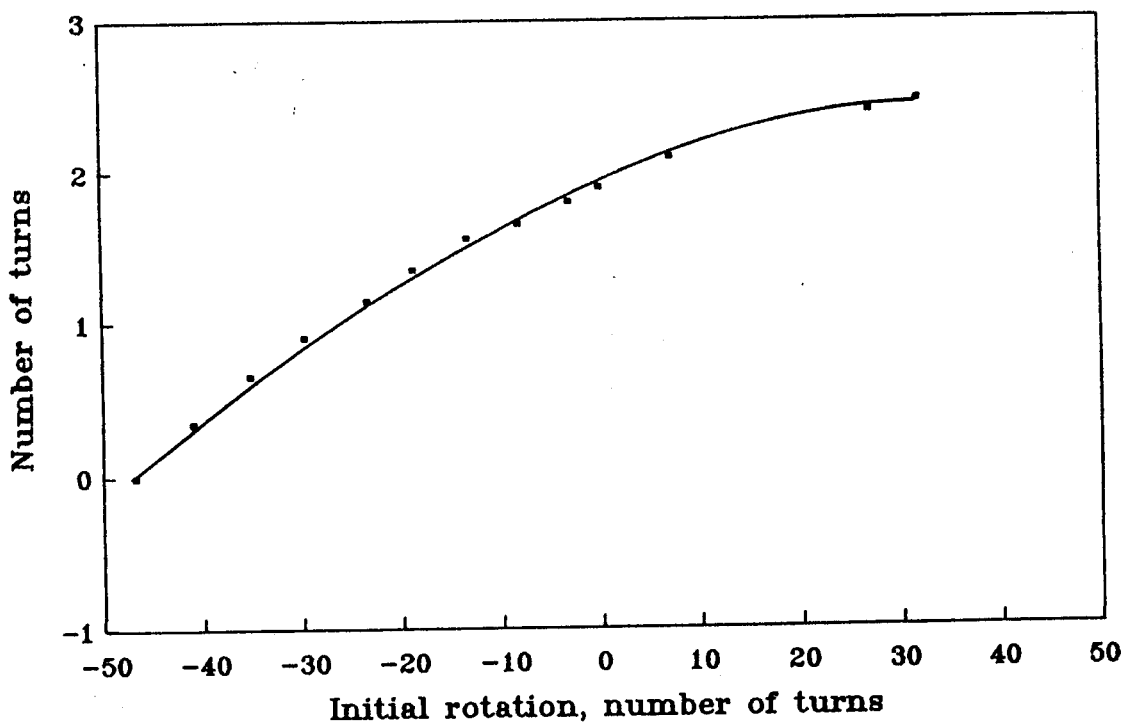

Figure 3.25 Chalk line test results for the middle section of the rope

4. THEORETICAL MODEL OF THE TAIL ROPE

The torsional behaviour of the tail rope was also modelled using both constant and variable C and T factors. As was mentioned in the introduction the tail loop can either be formed freely or by means of tail rope sheaves. Theoretical models for the torsional behaviour of ropes on both systems are given in the following paragraphs.

With reference to Figure 4.1 the following notation was established:

h: Is the hoisting depth [m].

b: Is the distance between lower station and tail rope loop [m].

u: Is the distance travelled by conveyances from stations [m].

z_i: Is the distance of a tail rope cross section from the i-th conveyance [m], i = 1 for the upgoing conveyance and i = 2 for the downgoing one. Both z_1 and z_2 relate only to their own compartment and their limits are:

$$0 \leq z_1 \leq b + u$$
$$0 \leq z_2 \leq h + b - u$$

4.1 Assumptions and Boundary Conditions

In order to simplify calculations the following assumptions were made:

a. The length of the rope in the tail rope loop is small compared to the overall length of the tail rope. It is therefore neglected and the total length of the tail rope is:

$$L_t = h + 2b \tag{4.1}$$

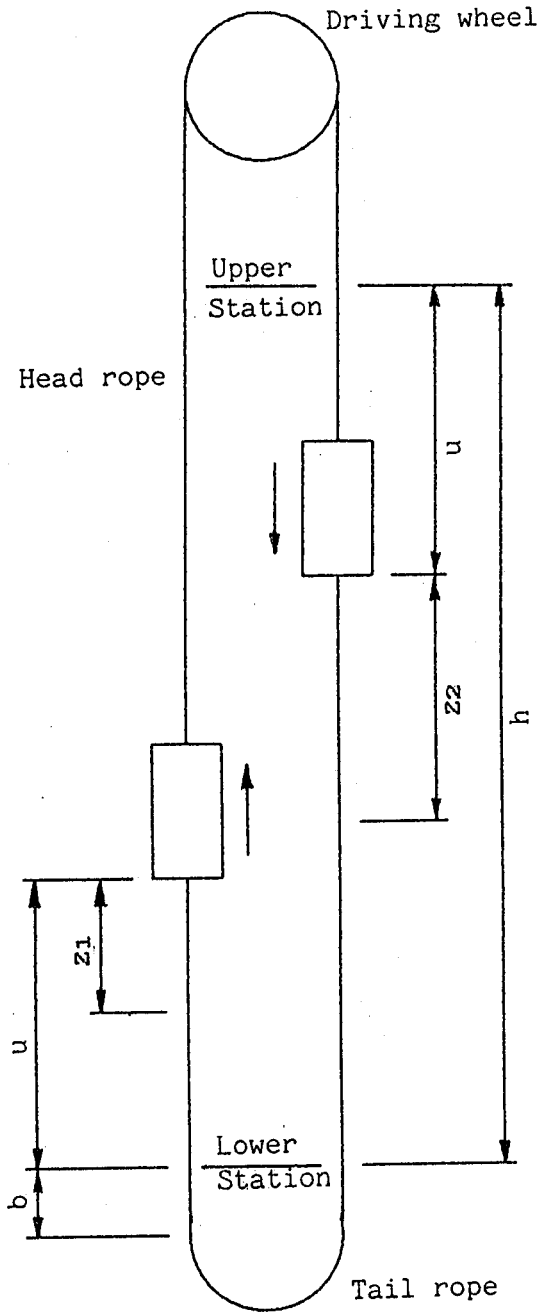

Figure 4.1 Tail rope notation

b. For the calculation of tensile and torsional loads in the tail rope, the two sections of the rope are assumed to be straight lines parallel to each other.

c. Only static loads are taken into consideration.

As was the case with the head rope models, the analysis is based on the torque tension relation 2.1, from which an equation is derived for the relative rotation $\triangle\Phi$ over a rope element $\triangle z$. The tension in the two sections of the rope, varies linearly with position z.

In the case of constant C and T factors, the relative rotation Φ at any position of the head rope is derived directly by integration (details in Appendix D). But in the case where these factors are not constant and their variation is defined by empirical numerical data, a computerized numerical approach is necessary (details in Appendix C).

In both cases, the value of Φ is a function of undetermined torque values, in both the upgoing and downgoing ropes. To determine these torques a number of boundary conditions and additional assumptions are used for each of the two tail rope arrangements.

4.1.1 Tail rope loop formed freely without a tail sheave

On Koepe winder installations where no tail sheave is used and the tail rope is free to deform, it is common practice to employ swivels. Both sections of the rope are attached to the conveyance by means of swivels. The function of the swivel is to release the torque built up in the tail rope and prevent the rope from deforming into a figure of eight. The swivel starts rotating when the torque in the rope exceeds the static frictional torque of the swivel's bearing and stops rotating when the torque in the rope becomes smaller than the dynamic frictional torque of the swivel's bearing.

The assumption is made that the static frictional torque of the swivel is a linear function of the axial load applied to it.

$$M_s = a + b.F \tag{4.2}$$

where

M_s : Is the static frictional torque of the swivel.
F : Is the tensile load applied to the swivel.
a, b : Are constant coefficients.

The dynamic frictional torque of the swivels is assumed to be equal to zero.

$$M_d = 0 \tag{4.3}$$

It is also assumed that the rotation of the swivel takes place in infinitesimal time. This assumption is necessary since we are dealing with static loads. The equilibrium equation for the torque in the rope is not valid during the time that the swivel rotate.

For the case of a freely formed tail loop, the following boundary conditions are used:

a. The total rotation over each section of the tail rope, at any instant, is equal to the algebraic sum of the rotation introduced through rotation of the swivels and through rotation of the tail loop.

b. The rope does not rotate while in the tail loop.

The sign convention implied in these two statements is explained in section D.3 of the Appendix.

4.1.2 Tail rope loop formed by means of a tail sheave

Where Koepe winders are used in deep South African shafts, it is common practice to use tail sheaves. The tail sheaves are guided so as to accommodate vertical movement, but restrict rotational movement of the loop in the horizontal plane. On winders where tail sheaves are employed, the swivels are usually locked a few days after installation. It is nevertheless recommended to free the swivels periodically, to allow excessive spin to untwist.

The following boundary conditions are used in the two sections of the rope;

a. The swivels if used are locked. Therefore the rope cross section attached to the conveyance does not rotate.

b. It follows from the above that the total rotation over the whole length of the tail rope is a constant and equal to the initial rotation, Φ_{in}, i.e. the rotation introduced on installation of the rope.

c. The rope does not rotate while in the tail loop (while in contact with the tail sheave).

In addition it is assumed that the relative rotation of an element $\triangle z$ about to enter the tail loop remains unchanged during the subsequent travel $\triangle u$ ($\triangle u = \triangle z$). This assumption is readily acceptable if $\triangle z$ is small enough.

Finally it is assumed that the two sections of the rope are interchangeable, i.e. at the end of its upwards trip the upgoing rope becomes the downgoing one for the start of the next trip and vice versa.

4.2 Theoretical Model of the Tail Rope Using Constant C and T factors

In the case of constant C and T factors, as was mentioned above, integration allows for an analytical solution of the problem. Explicit equations for the torque and the relative rotation in both sections of the rope were derived in Appendix D.

The equations for the case of a tail rope without tail sheave are shown in table 4.1. The equivalent equations for the case where a tail sheave is used are shown in table 4.2. The following nomenclature is employed:

$\Phi_{1,u,z1}$: Is the relative rotation of a cross section of the upgoing rope at a distance z_1 from the upgoing conveyance. The relative rotation is calculated with respect to the conveyance which, of course, does not rotate.

$\Phi_{2,u,z2}$: Is the relative rotation of a cross section of the downgoing rope at a distance z_2 from the downgoing conveyance. The relative rotation is again calculated with respect to the conveyance.

$M_{1,u}$: Is the torque in the upgoing section of the tail rope during the trip.

$M_{2,u}$: Is the torque in the downgoing section of the tail rope during the trip.

P_t : Is half of the gross weight of the rope in the tail rope loop plus half of the weight of the tail sheave, if there is one

q : Is the weight of the tail rope in N/m

Φ_{s1} : Is the total angle that the upgoing rope swivel rotates.

Φ_{s2} : Is the total angle that the downgoing rope swivel rotates.

Φ_t : Is the rotation of the tail loop in the horizontal plane, when there is no sheave.

θ_1 : Is the lay angle deviation for the upgoing rope.

θ_2 : Is the lay angle deviation for the downgoing rope.

k : Is a constant equal to Cq/T.

In the case where no swivels are employed the equations of tables 4.1 and 4.2 are continuous functions of the travelled distance, u. But in the case where swivels are installed and are free to rotate the relations are not continuous. Whenever a swivel rotates, the torque in the rope becomes zero (equal to the dynamic frictional torque of the swivel). Then the angle that each swivel rotates is calculated from equations 4.4 and 4.7 with $M_{1,u}$ and $M_{2,u}$ equal to zero.

Table 4.1 Freely suspended tail rope without tail sheave

Upgoing rope		Eq.
Torque	$M_{1,u} = CP_t(2u - h)/L_t + Cq(2u - h)/2 + (\Phi_{s1} - \Phi_{s2})T/L_t$	4.4
Relative rotation	$\Phi_{1,u,z1} = ((\Phi_{s1} - \Phi_{s2})/L_t - 2CP_t(h + b - u)/(TL_t) - CqL_t/(2T))z_1 + Cqz_1^2/(2T)$	4.5
Lay angle deviation	$\theta_1 = ((\Phi_{s1} - \Phi_{s2})/L_t - 2CP_t(h + b - u)/(TL_t) - CqL_t/(2T) + Cqz_1/T)r.\cos^2(\beta)$	4.6

Downgoing rope		Eq.
Torque	$M_{2,u} = CP_t(h - 2u)/L_t + Cq(h - 2u)/2 + (\Phi_{s2} - \Phi_{s1})T/L_t$	4.7
Relative rotation	$\Phi_{2,u,z2} = ((\Phi_{s2} - \Phi_{s1})/L_t - 2CP_t(b + u)/(TL_t) - CqL_t/(2T))z_2 + Cqz_2^2/(2T)$	4.8
Lay angle deviation	$\theta_2 = ((\Phi_{s2} - \Phi_{s1})/L_t - 2CP_t(b + u)/(TL_t) - CqL_t/(2T) + Cqz_2/T)r.\cos^2(\beta)$	4.9

Tail loop rotation	$\Phi_t = -(\Phi_{s1}(h + b - u) + \Phi_{s2}(b + u))/L_t - 2CP_t(h + b - u)(b + u)/(TL_t) - Cq(h + b - u)(b + u)/(2T)$	4.10

Table 4.2 Tail rope loop formed by means of a tail sheave

Upgoing rope		Eq.
Torque	$M_{1,u} = CP_t + Cq((2u - h)L_t^2 + (h + b - u)((h + b)^2 + b^2))/(2(b + u)L_t) + \Phi_{in}T/L_t$	4.11
Relative rotation	$\Phi_{1,u,z1} = k((2u - h)L_t^2 + (h + b - u)((h + b)^2 + b^2) - 2(b + u)^2L_t)z_1/(2(b + u)L_t) + kz_1^2/2 + \Phi_{in}z_1/L_t$	4.12
Lay angle deviation	$\theta_1 = (k((2u - h)L_t^2 + (h + b - u)((h + b)^2 + b^2) - 2(b + u)^2L_t)/(2(b + u)L_t) + kz_1 + \Phi_{in}/L_t)r.\cos^2(\beta)$	4.13

Downgoing rope		Eq.
Torque	$M_{2,u} = CP_t + Cq((h - 2u)L_t + 2b(h + b))/(2L_t) + \Phi_{in}T/L_t$	4.14
Relative rotation	$\Phi_{2,u,z2} = - k((h + b)^2 + b^2)z_2/(2L_t) + kz_2^2/2 + \Phi_{in}z_2/L_t$	4.15
Lay angle deviation	$\theta_2 = - (k((h + b)^2 + b^2)/(2L_t) + kz_2 + \Phi_{in}/L_t)r.\cos^2(\beta)$	4.16

4.2.1 Application to a practical example

The theoretical model was applied to the West Driefontein No. 5 shaft BGE Koepe winder. A five meter rope sample from a discarded tail rope was made available by the mine. The specimen was subjected to a torque-tension test, and the torsional properties of the rope were determined. The results of the torque-tension test are presented in Appendix A. The torsional stiffness of the rope was 25 Nm/deg and the torque factor 0,0027 Nm/N.

The results obtained from the theoretical models for both tail rope configurations are summarised in the following paragraphs.

a. Freely suspended tail rope without tail sheave.

The theoretical model was applied to three different study cases:

(i) The swivels are locked.

(ii) The torsional torque of the swivels is constant.

(iii) The torsional torque of the swivels is a linear function of the tensile load.

The results are as follows:

(i) Locked swivels (Figures 4.2).

The torque developed in the rope during the trip is shown in Fig. 4.2a. The continuous line is the torque in the upgoing section of the rope and the dotted line is the torque in the downgoing section of the rope. As was expected, the algebraic sum of the torque in the two sections is equal to zero. The tail loop rotation is shown in Fig. 4.2b. It is obvious that this winder can not operate with locked swivels. The loop rotates up to eleven turns which would cause the two legs of the rope to intertwine for some distance above the loop.

(ii) Swivels with constant frictional torque (Figures 4.3).

The frictional torque of both swivels is assumed constant and equal to 40 Nm. The torque induced in the two sections of the rope is shown in Fig. 4.3a. The initial large drop in torque happens only during the first trip after installation. As can be seen from Fig. 4.3b, the downgoing swivel would rotate approximately 40 rotations during installation in order to reach equilibrium condition. During the trip, torque is built up in the rope and when the 40 Nm value is reached, both swivels rotate. The rotation of the tail loop is shown in Fig. 4.3c. The maximum rotation of the loop is just less than 180° which although would cause the rope to deform into a figure of eight the two legs of the rope would not touch.

The lay angle deviation for two different rope cross sections is shown in Figs. 4.3d and 4.3e. The first cross section which is 50 m away from the conveyance exhibits higher lay angle variations that the second cross section which is 850 m away from the conveyance.

(iii) Frictional torque of the swivel a function of the tensile load (Figures 4.4).

For the last study case we assumed that the swivels have a frictional torque of 20 Nm under zero tensile load. The frictional torque of the swivels increases with tensile loads and reaches the value of 40 Nm at the maximum tensile load i.e. when the conveyance is at the top station.

The torque developed in the two sections of the rope is shown in Fig. 4.4a. The tail loop rotation is presented in Fig. 4.4b and the rotation of the swivels in Fig. 4.4c. Despite the fact that the maximum frictional torque of the swivels was the same as for the second study case, the tail loop rotates up to three rotations. That of course would cause the rope to deform into a figure of eight.

The greater rotation of the tail loop is due to the the fact that the swivels do not rotate at the same time. In order to accommodate the zero torque equilibrium condition in both sections of the rope when only one swivel rotates, the loop is forced to rotate further.

b. Tail loop formed by means of a tail sheave and without swivels (Figures 4.5).

The torque developed in the tail rope for a winder that employs a tail sheave is shown in Fig. 4.5a. The torque in the downgoing section of the rope decreases linearly during the trip. Rapid torque changes take place in the upgoing section of the rope during the first few meters of the trip.

The lay angle deviation for two cross sections of the rope at a distance of 50 m and 850 m from the conveyances is shown in Figs. 4.5b and 4.5c respectively. Cross sections close to the conveyances are subjected to greater lay angle variations than the rest of the rope.

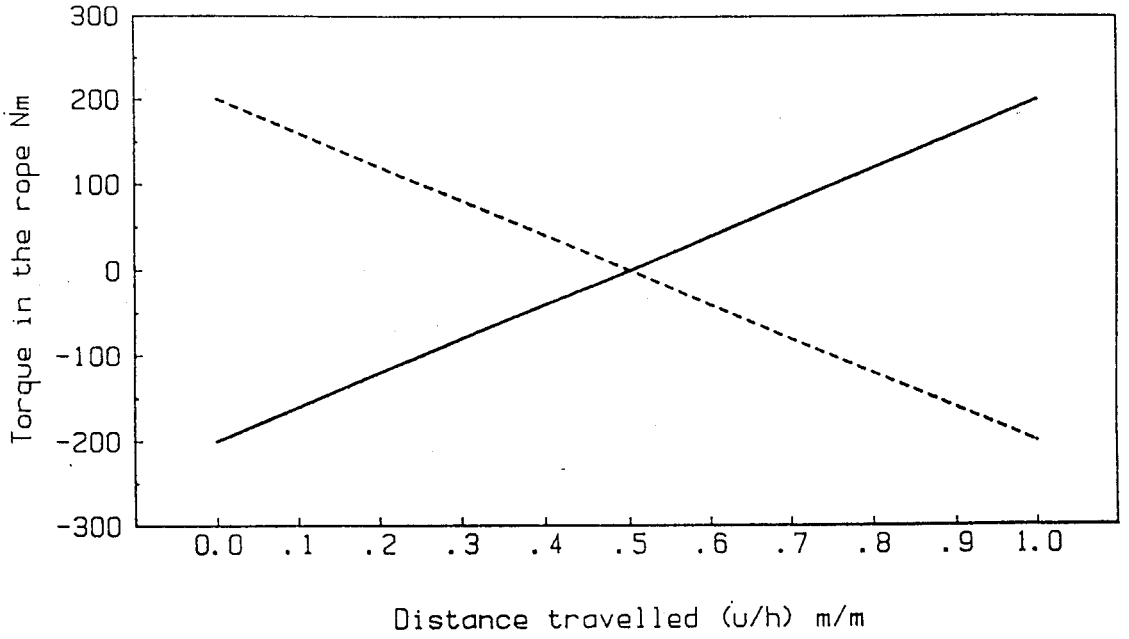

Figure 4.2a Torque in the rope during a trip
—— Upgoing rope
---- Downgoing rope

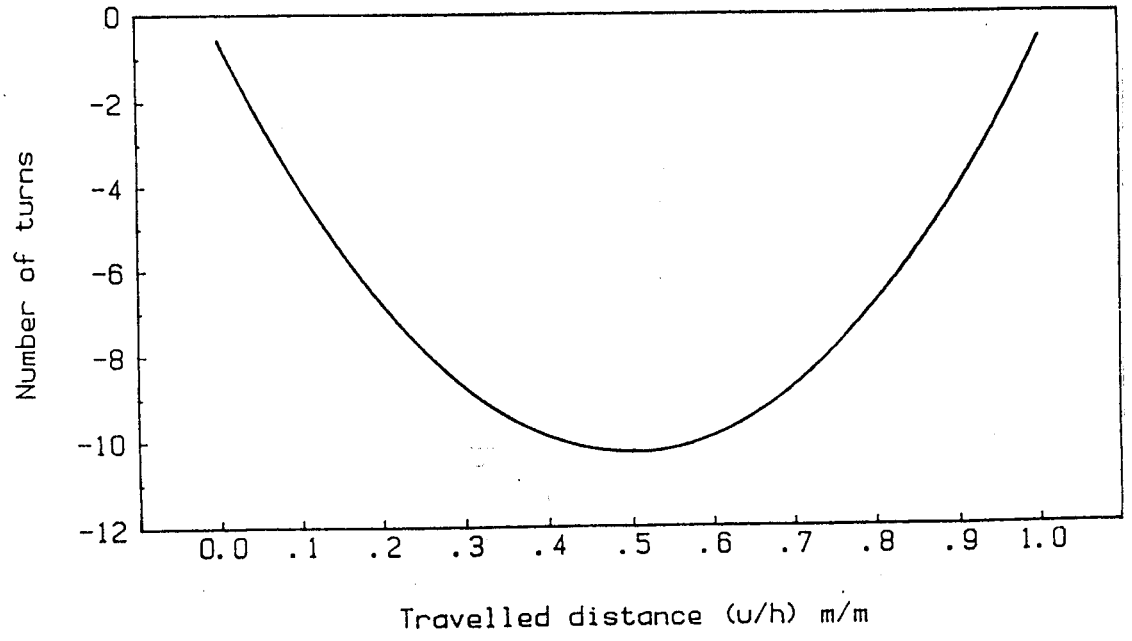

Figure 4.2b Tail loop rotation

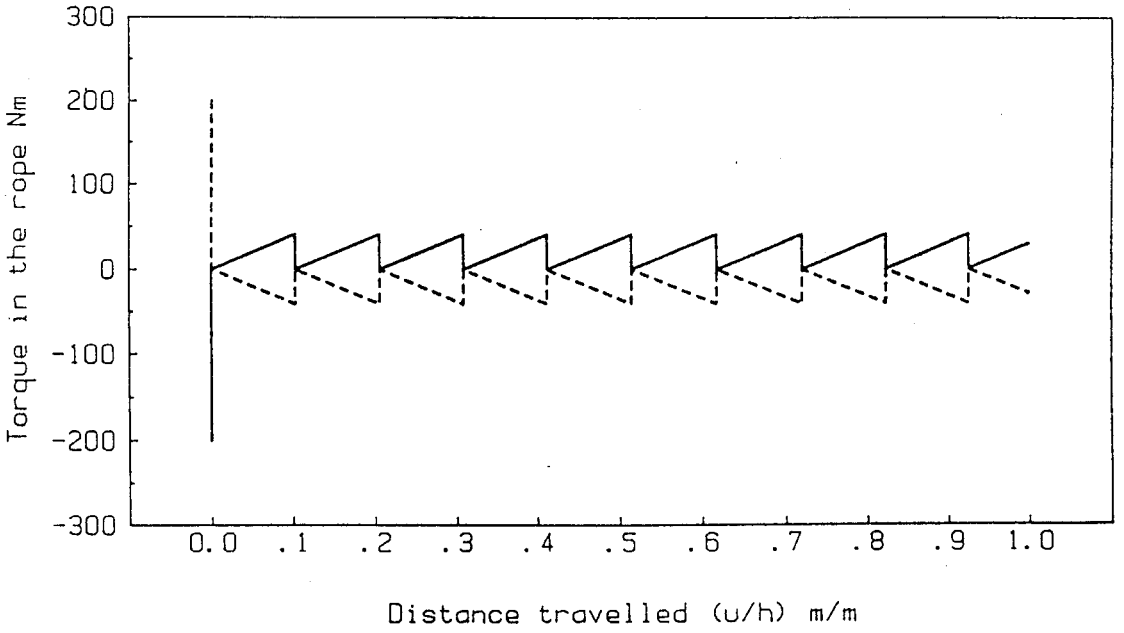

Figure 4.3a Torque in the rope during a trip

—— Upgoing rope

---- Downgoing rope

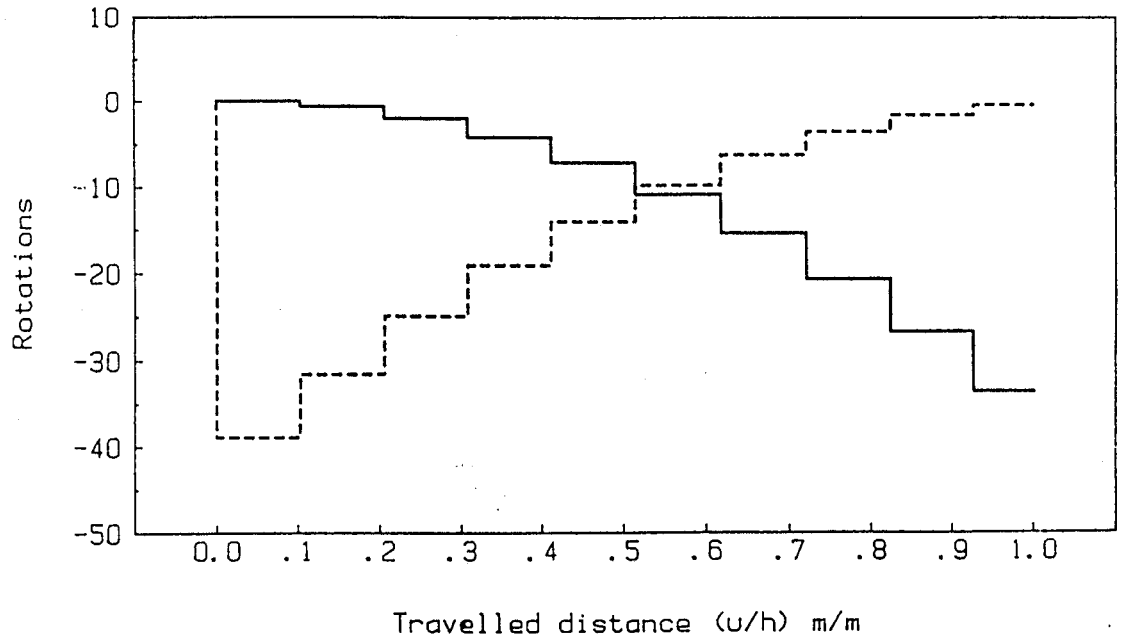

Figure 4.3b Swivel rotation

—— Upgoing swivel

---- Downgoing swivel

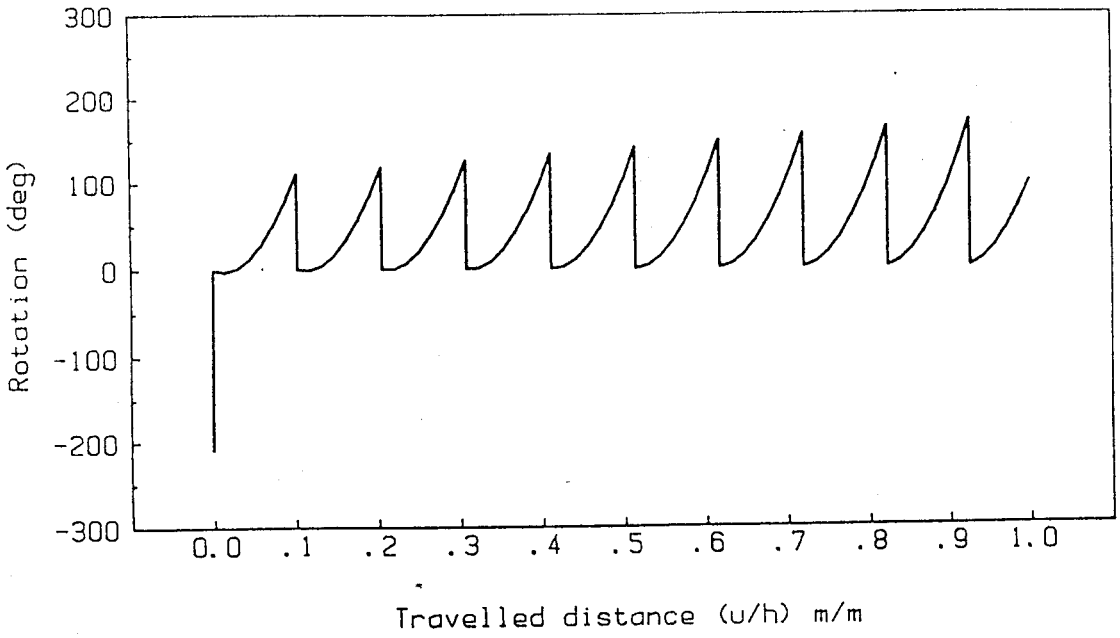

Figure 4.3c Tail loop rotation

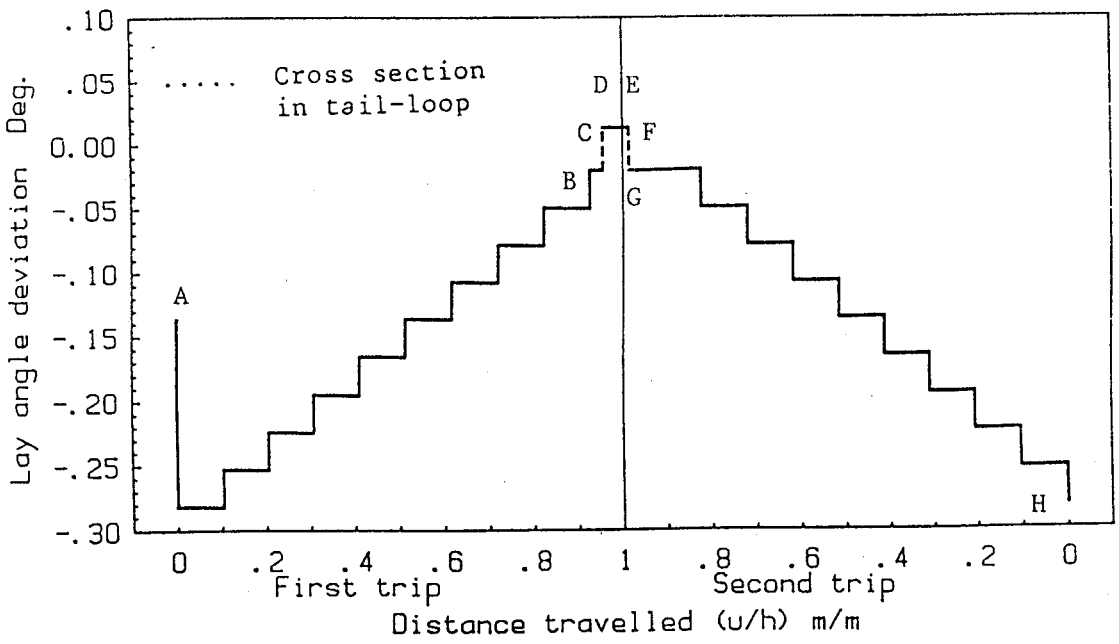

Figure 4.3d Lay angle deviation at a cross section during double trip. Distance of section from downgoing conveyance z_2=50 m. A to B and E to F downgoing. C to D and G to H upgoing.

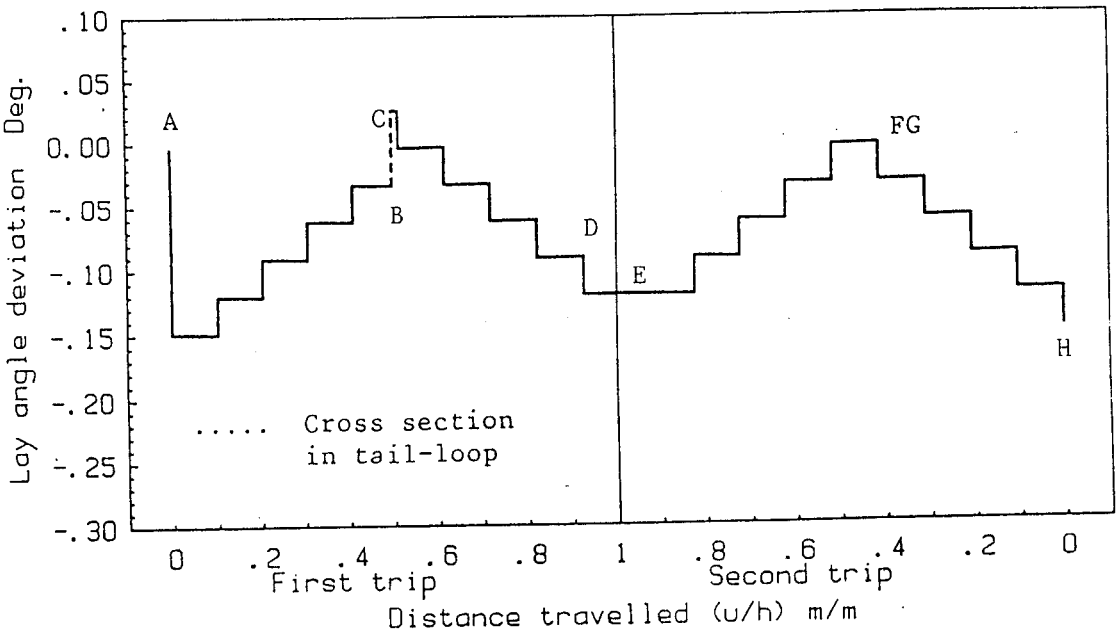

Figure 4.3e Lay angle deviation at a cross section during double trip. Distance of section from downgoing conveyance z_2=850 m. A to B and E to F downgoing. C to D and G to H upgoing.

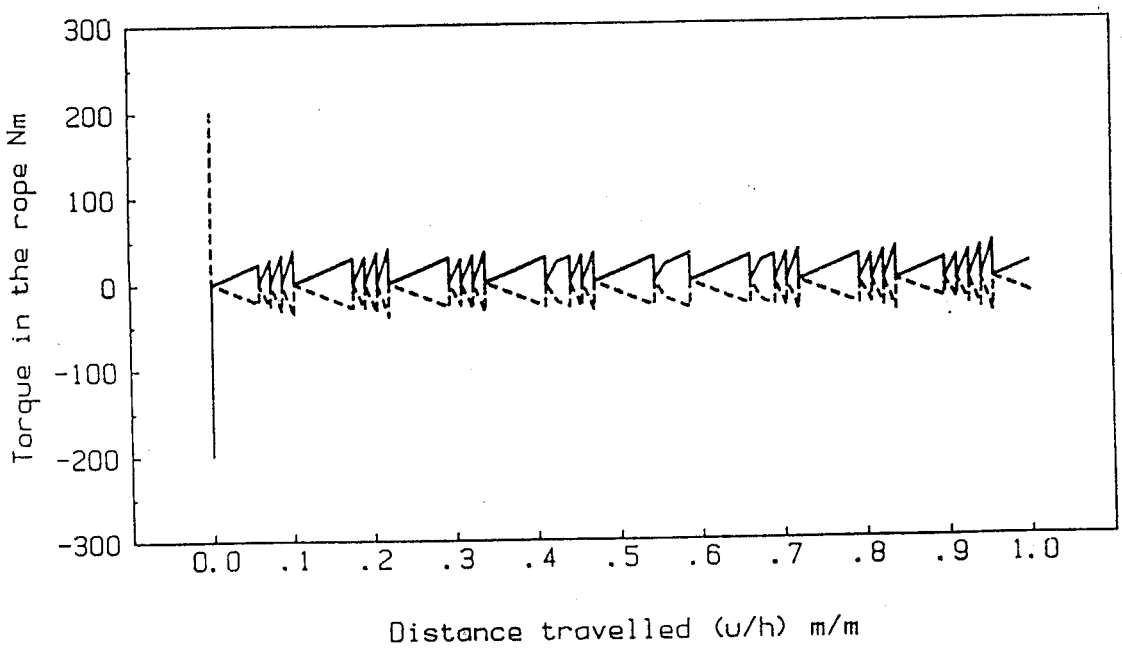

Figure 4.4a Torque in the rope during a trip
—— Upgoing rope
---- Downgoing rope

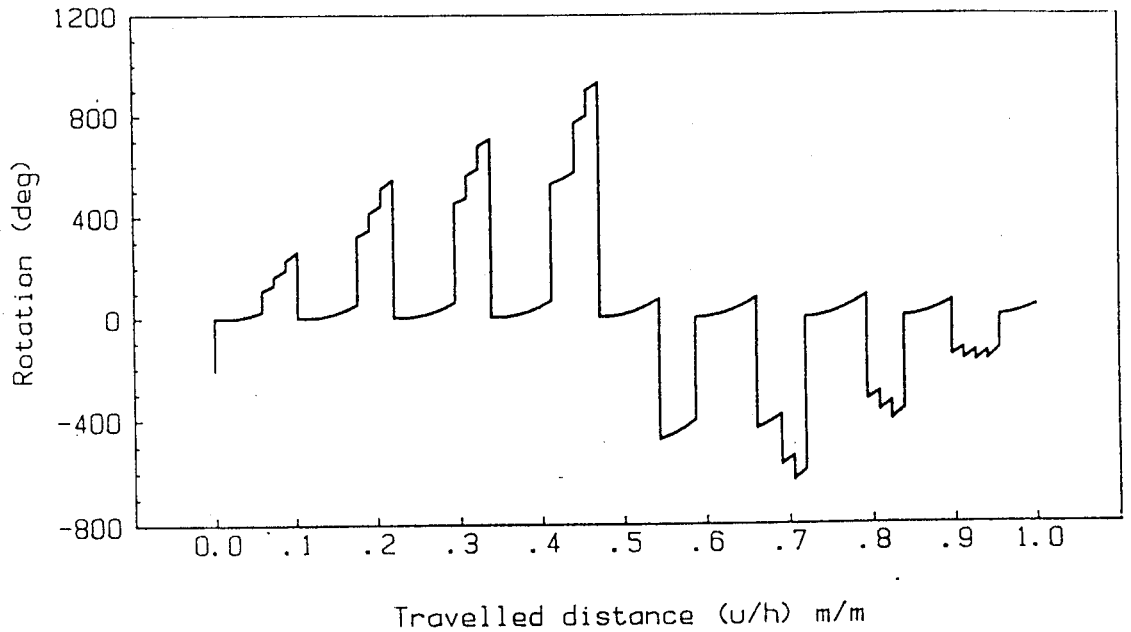

Figure 4.4b Tail loop rotation

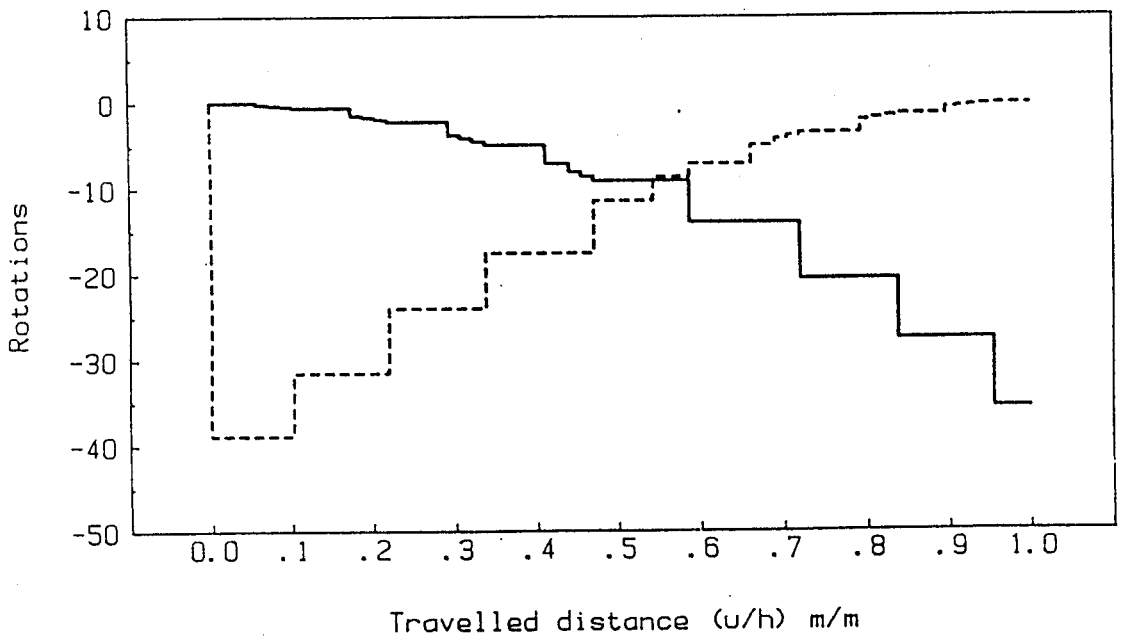

Figure 4.4c Swivel rotation

—— Upgoing rope

---- Downgoing rope

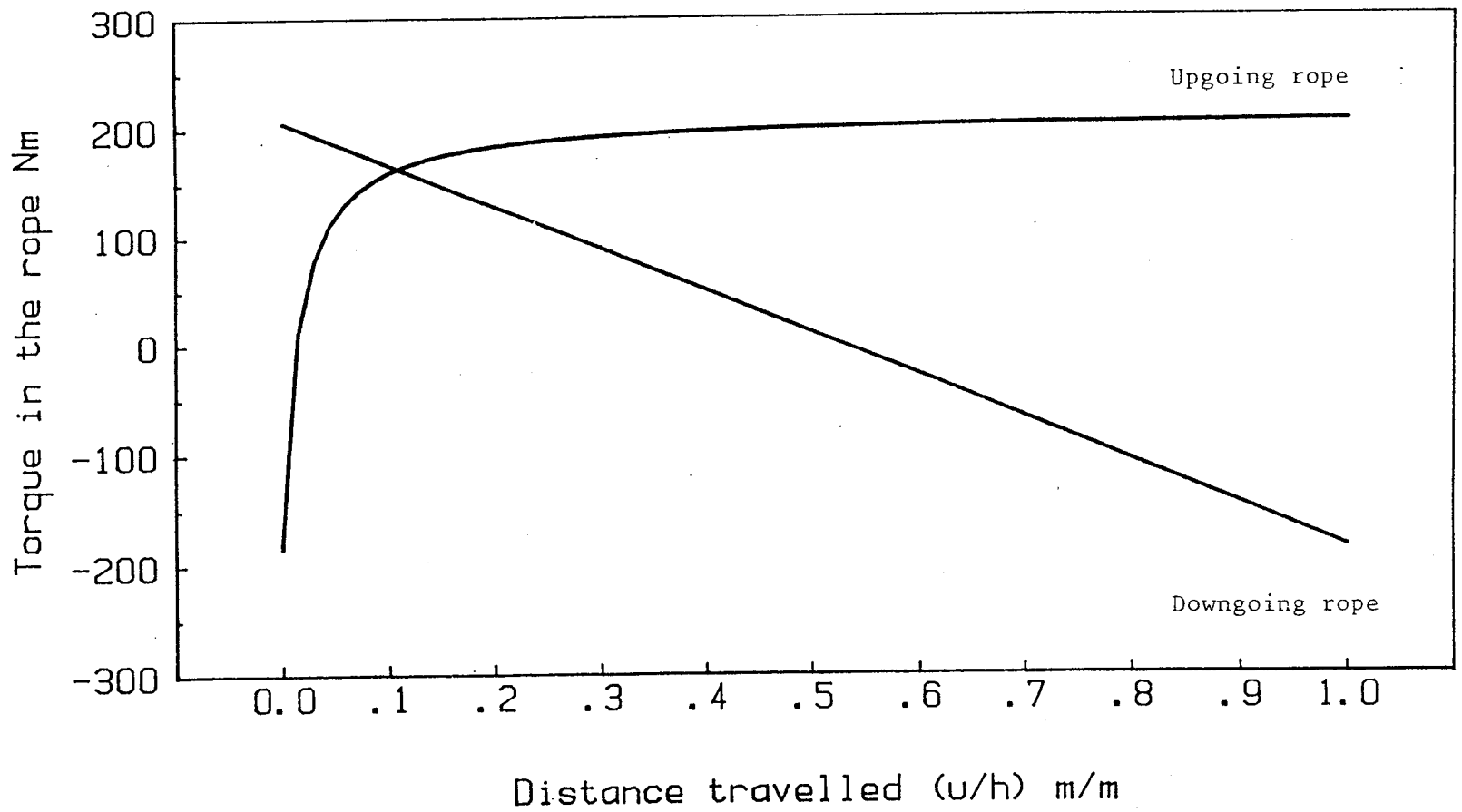

Figure 4.5a Torque in the rope during a trip

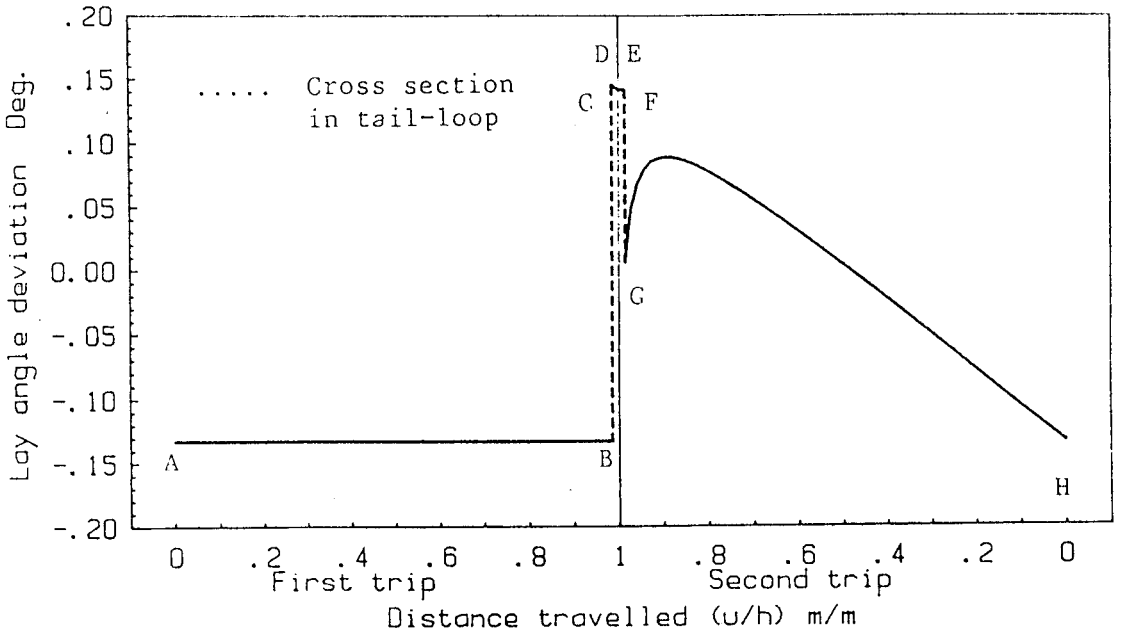

Figure 4.5b Lay angle deviation at a cross section during double trip. Distance of section from downgoing conveyance z_2=50 m. A to B and E to F downgoing. C to D and G to H upgoing.

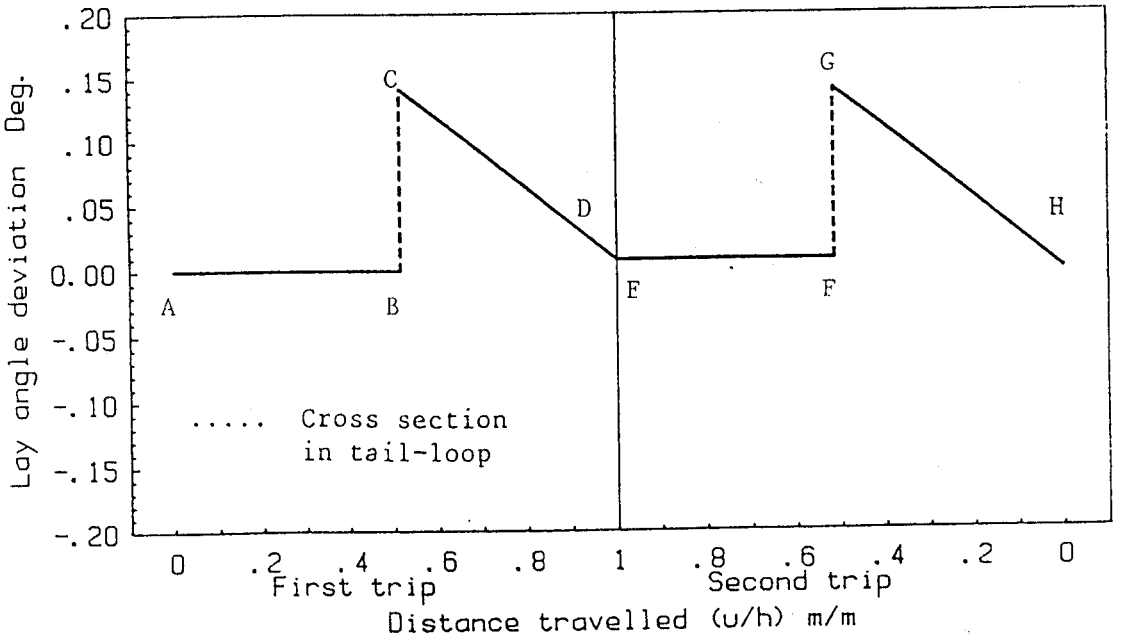

Figure 4.5c Lay angle deviation at a cross section during double trip. Distance of section from downgoing conveyance z_2=850 m. A to B and E to F downgoing. C to D and G to H upgoing.

4.3 Theoretical Model of the Tail rope Using Variable C and T Factors

In paragraph 3.3 the theoretical model of the head rope using variable C and T factors was established. As was mentioned the torque-tension curves are not linear at low values of the tensile load. Since the tail rope operates under very low tensile loads, the variable C and T factors approach is a better model for the torsional behaviour of the tail rope than the constant C and T factors approach.

The theoretical model was developed for a winder which employs a tail sheave and the tail rope is attached to the conveyance without swivels. The logistics of the tail rope theoretical model are the same as those of head rope model. The torque-tension curves of the tail rope are treated the same way as was done in section 3.3 for the head rope.

4.3.1 Tail rope model algorithm

Downgoing rope

As was the case with the head rope,there are two parts in the tail rope algorithm: One for the downgoing and one for the upgoing rope. The downgoing rope calculations are completed first and recorded values are input in the calculation for the upgoing rope. A rope element Δl is again the initial input parameter.

Step 1: Assume an initial torque value for the downgoing section of the tail rope.

Step 2: Utilizing the torque-tension tables of the tail rope calculate the twist in each element of the downgoing rope.

Step 3: Calculate the relative rotation between the two ends of the downgoing rope. which is equal to the sum of the twist in all the elements, multiplied by the element length Δl.

Step 4: Decrease the length of the downgoing rope by $\triangle l$.

Step 5: Calculate the new value for the relative rotation between the two ends of the downgoing rope.

Step 6: Decrease the torque value in the downgoing rope by a small step.

Step 7: Calculate the new twist value for each element.

Step 8: Calculate the new relative rotation value between the two ends of the downgoing rope.

Step 9: If the new relative rotation value is the same as the one calculated in Step 5 go to Step 11.

Step 10: Decrease or increase the torque value, depending on whether the new relative rotation value is smaller or greater than the old one. Go to Step 7.

Step 11: Record torque value and twist distribution in downgoing rope for the travelled distance, u.

Step 12: If the trip has not been completed go to Step 4. Otherwise go to Step 1 of the upgoing rope.

Upgoing rope

Step 1: The initial torque value in the upgoing rope is the same as the final torque value in the downgoing rope.

Steps 2 to 12: As for the downgoing rope.

Step 13: Calculate the relative rotation introduced between the two ends of the tail rope.

A computer program was developed to simulate the tail rope behaviour according to the above algorithm. A listing of the program can be found in Appendix C.

4.3.2 Application to a practical example

The theoretical model of the tail rope with variable C and T factors was also applied to the West Driefontein No. 5 shaft BGE Koepe winder. The tensile load in a rope element of the tail rope about to enter or leave the tail sheave, for the particular winder, is approximately 10 kN, i.e. half the weight of the tail sheave. The available torque-tension data ranged from 25 kN to 500 kN (torque-tension machine range). It was therefore assumed that the weight of the tail sheave was 60 kN.

The torque developed in the two sections of the rope during the trip is shown in Fig. 4.6. The results are very similar to the constant C and T factors model. That is due the linear shape of the torque-tension curves of the particular rope as can be seen in Fig. A.1 of Appendix A. For the same reason introduction of end rotation hardly changes the behaviour.

In order to investigate the influence of varying C and T factors on the tail rope behaviour, the model was run utilizing the head rope torque-tension curves, which are not linear (Fig. 3.13). Two cases were studied:

(i) For the first case, we assume that an initial rotation of ten positive turns were introduced in the rope. The winder operates along the +10 degrees end rotation curve of Fig. 3.13. The torque in the two sections of the tail rope is shown in Fig. 4.7.

(ii) For the second case, we assume that an initial rotation of twelve negative turns was introduced in the tail rope. In that case the winder operates along the -10 degrees end rotation curve of Fig. 3.13. The torque in the two sections of the rope is illustrated in Fig. 4.8.

In both cases the torque in the two sections of the rope is less than the case where the tail rope data were used. The shape of the curves is also different and the torque in the downgoing rope is not a linear function of the travelled distance.

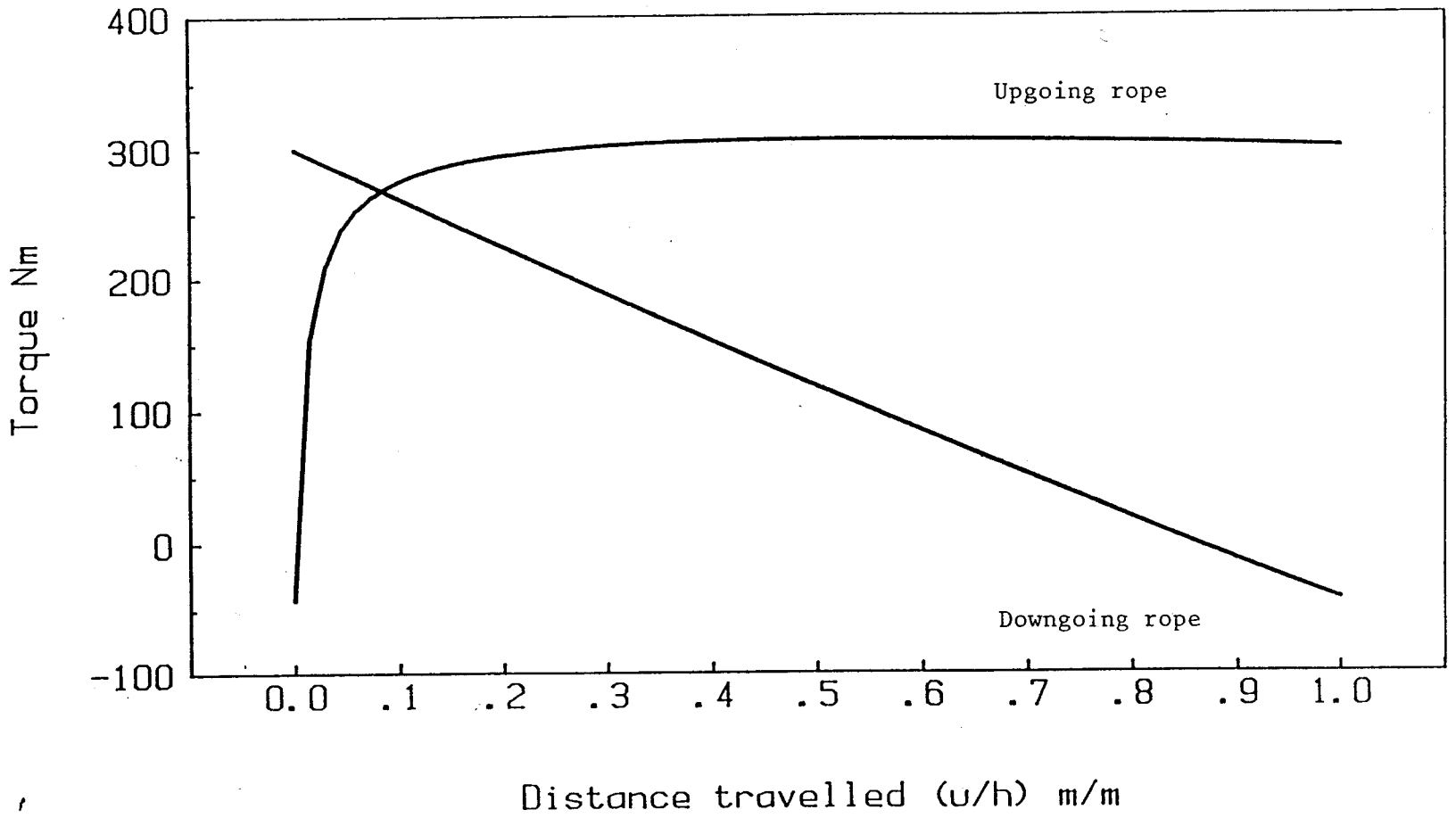

Figure 4.6 Torque in the tail rope for variable C and T factors

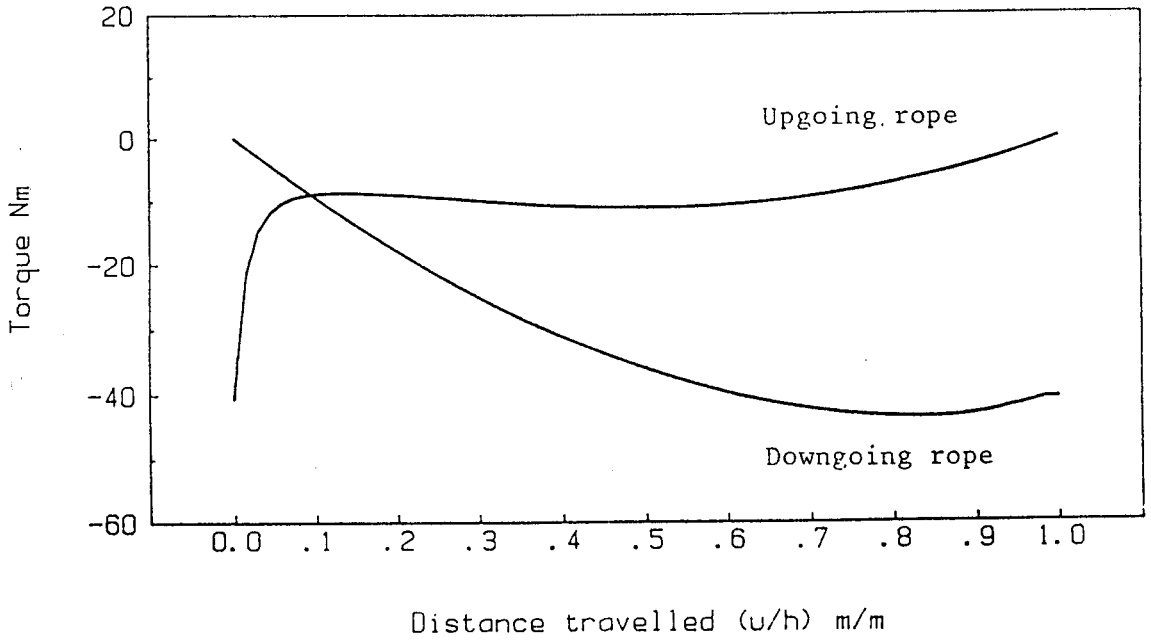

Figure 4.7 Torque in the rope for ten turns positive initial rotation.
Variable C and T factors.

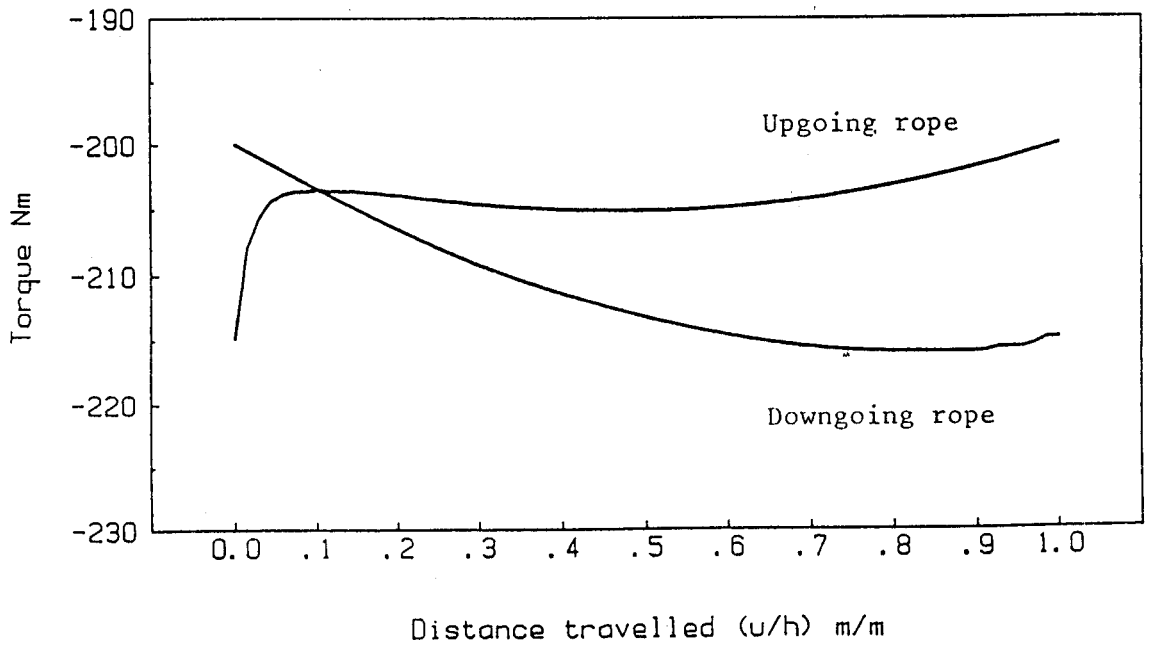

Figure 4.8 Torque in the rope for twelve turns negative initial rotation.
Variable C and T factors.

5. ON-SITE MEASUREMENTS ON A KOEPE WINDER

In order to select a suitable site for experimentation the theoretical model of the head rope with constant C and T factors was applied to the twenty deepest South African Koepe winders. The data for these winders were available from the winder data bank of the Mine Hoisting Technology program of the CSIR. Estimated values for the rope data were obtained from the Haggie Rand Ltd Wire Rope Handbook[34] and from test results availiable at CSIR[33]. In all winder cases the difference between the maximum and the minimum value of the expected torque during the trip was below 200 Nm. Ten winders which gave the highest torque difference were selected and a list was forwarded to the Chamber of Mines Research Organization for assistance to get access to one of these winders to do the experimental work.

The West Driefontein No. 5 shaft British General Electric (BGE) Koepe winder was made available for the on site measurements. The torsional and tensile load in one of the four head ropes of the winder and one of the four tail ropes were measured during two consecutive double trips. The head rope rotation during a trip was determined from a chalk test.

Recording of measurements for further trips was not possible due to the limited time the winder was available.

5.1 Measurement of Torsional and Tensile Loads During a Trip

The objective of the experiments was to measure the variation of the torque in the head and tail rope during a trip. The tensile loads in the ropes at the conveyance were also measured.

Measurement of the loads was done by straingauging certain components in line with the ropes which served as loadcells. The loadcell design and the instrumentation used during the tests are described in the following paragraphs.

5.1.1 Head rope loadcell

A configuration of the head rope attachment of the West Driefontein four-rope Koepe winder is shown in Fig. 5.1. The dynamometer link was chosen as the most suitable component to be straingauged and serve as a loadcell for torque and tension measurements in one of the head-ropes.

The stand-by link, identical to the one on the winder, was brought to the laboratory of the Mine Hoisting Technology programme of the CSIR where an experimental strain analysis study was done. The slotted cross section was identified as the cross section where both tensile and torsional strains were higher. Two full bridges, one for tension and one for torsion (Fig. 5.2) were cemented on the link installed on the winder.

5.1.2 Tail rope loadcell

A configuration of the tail rope suspension gear is shown in Fig. 5.3. The four swivels are usually locked by means of bars 1 and 2. Plates 3 and 4 were straingauged with a full bridge each to serve as a tension loadcell (Fig. 5.4).

In order to measure the torque in the tail rope the bending loadcell illustrated in Fig. 5.5 was manufactured. This loadcell was installed in the position marked by the line aa in Fig. 5.3. The pair of bars 5 and 6 prevented rotation of three of the swivels and the pair 7 and 8 constrained plates 3 and 4 which supported the rope to be measured. The torque in that rope was measured by the bending strain in bar 7 which is prevented from rotating by pins 1 and 2 attached to bar 5.

5.1.3 Calibration of the loadcells

The dynamometer link which served as the head rope loadcell, was removed from the winder for a yearly inspection and service two months after the experiments and was brought to the laboratory of the Mine Hoisting Technology program for calibration. The straingauges were in a good condition and only minor repairs were necessary.

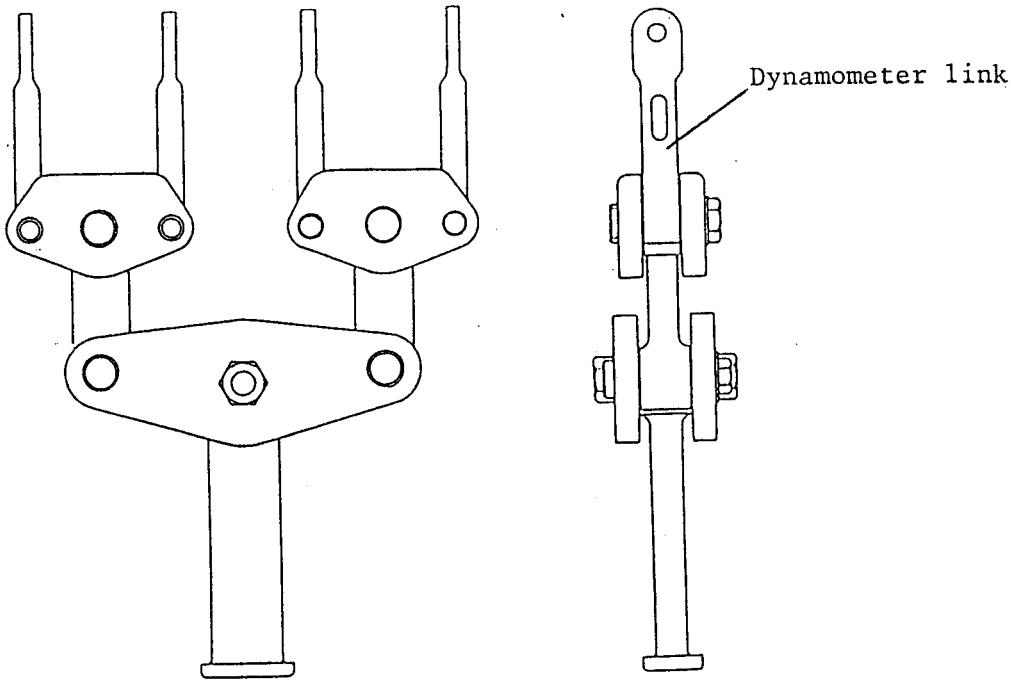

Figure 5.1 Head rope attachment

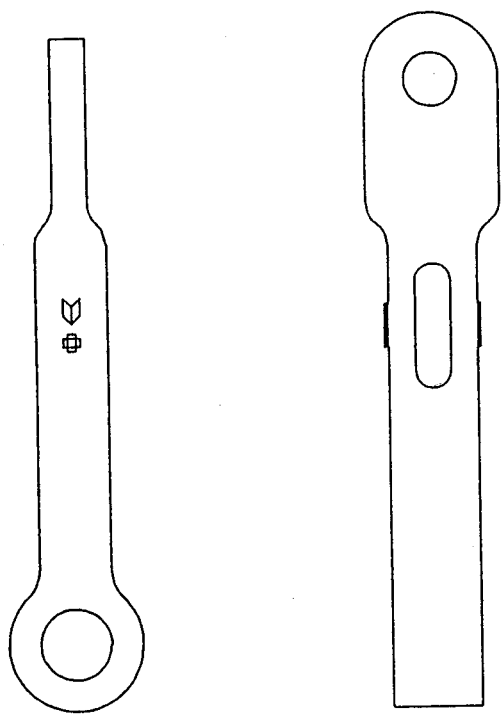

Figure 5.2 Head rope loadcell

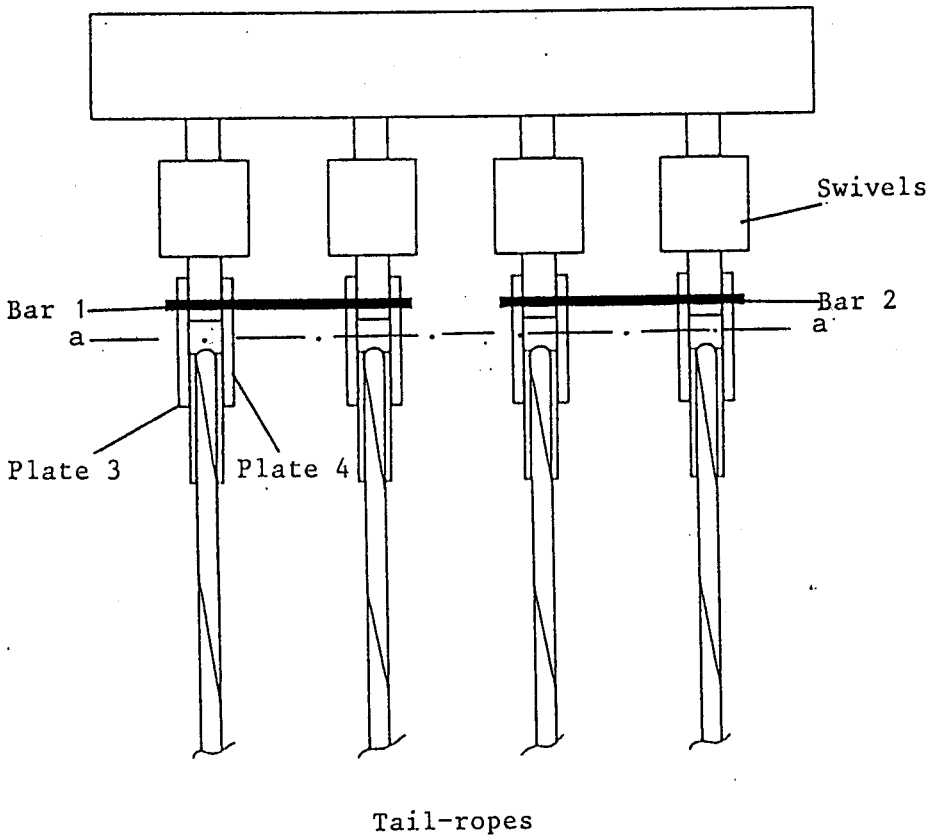

Figure 5.3 Tail rope suspension gear

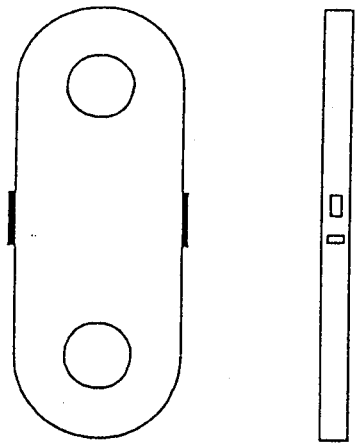

Figure 5.4 Tail rope tensile loadcell

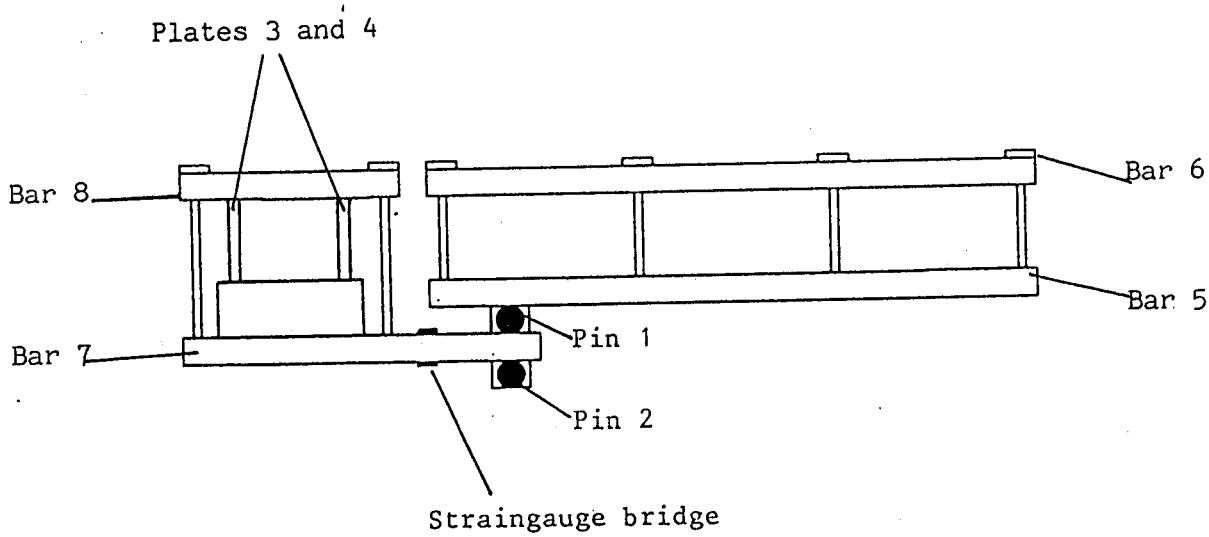

Figure 5.5 Tail rope torsion loadcell

The calibration of the tension bridge was done on a 5 000 kN tensile testing machine. The same instrumentation and wiring that was used for the experimental work at the mine was used for the calibration of all loadcells. The tension bridge sensitivity was 108,3 kN/V.

The torque bridge was calibrated using dead-weights. The conveyance side of the dynamometer link was rigidly held. A lever was fitted in the pin hole on the other end of the link and dead weights of known mass were applied to the lever. Torque was applied in both directions. The torque bridge sensitivity was 641,8 Nm/V.

The plates which serve as the tail rope tension loadcell could not be made available by the mine for calibration. The only availiable alternative was to straingauge and calibrate the stand-by plates which are identical to the plates on the winder. As in the case of the original loadcell, a full bridge was cemented on each plate. The algebraic sum of the two bridges output was used for both the calibration and the analysis of the results. The sensitivity of the loadcell was 24,4 kN/V.

The calibration of the tail rope torque loadcell was done on a 100 kN Universal Amsler testing machine. A force was applied by the machine at the point where the pin was touching on the bar, while the bar was supported at the other end in the same manner as on the winder. The bridge sensitivity was 312,5 Nm/V.

5.1.4 Instrumentation and procedure

A configuration of the data acquisition system used during the measurements is shown in Fig. 5.6. The signals from the five loadcells were amplified and then recorded onto a frequency modulation tape recorder with a built-in calibration facility. In order to be able to correlate the signal from the loadcells with the travelled distance an infra-red bunton detector was used. The detector was giving a pulse each time the cage was passing a bunton. The data recorded onto the tape were plotted onto a chart recorder after each trip.

All instrumentation with the exception of the chart recorder was accommodated in the cage. Power for the amplifiers, tape recorder and bunton detector was supplied by two 12V batteries.

Before each trip calibration signals using both the amplifiers' and the tape recorder's calibration facilities were recorded on the tape. The cage then travelled from the top to the bottom station of the shaft. At the bottom it rested for about three minutes and then it travelled to the top. Two consecutive double trips were run. The travelling speed during the first trip was approximately 11 m/s which is the normal operating speed when men are transported. The speed during the second trip was 5 m/s. This difference in speed was planned in order to investigate the effect of speed. The distance from the top to the bottom stations of the shaft was approximately 1 700 m.

5.2 Analysis of Results

Similar results were obtained during both trips. The analogue signals from the five loadcells and the bunton detector during the second trip are shown in Fig. 5.7. Channel one is the signal from the head rope tension loadcell. Channel two is the signal from the head rope torque loadcell. Channels three and four are the signals from the two tail rope tension loadcells. The signal from the tail rope torque loadcell was recorded on channel 5 and the bunton detector signal on Channel 6.

Figure 5.7 provides an overview by showing all the results together. For the purpose of measurement or detailed analysis outputs from the tape could be either digidized or expanded as in Fig. 6.4 in the next chapter.

High torsional oscillations were experienced in the head rope. The amplitude of the oscillations in some cases was greater than 500 Nm while the difference between the static torsional load at the beginning and end of the trip was only 130 Nm. Using a least square method, second degree polynomials were fitted to more than 25000 points of digitized torque-tension results for the head rope. Assuming a linear relation between rope tension and travelled distance (rope's linear weight), relations were derived for the torque in the head rope during the trip. The results obtained through this approach were confirmed with measurements of the expanded analog signal. The resulting curves which illustrate the torque in the two sections of the rope during the trip are given in Fig. 5.8.

In order to assess the nature of the torsional vibration an analysis of the torsional and tensile vibrations of the head rope is presented in the following chapter.

The torque in the tail rope is shown in Fig. 5.9. For the first 900 m of the trip the torque in the downgoing rope remained constant, while during the last 800 m it decreased by approximately 190 Nm. During the first 100 m of the upgoing trip the torque in the tail rope decreased by another 60 Nm. For the next 1000 m it increased by 250 Nm to the initial value and remained almost constant until the end of the trip.

The torque in the tail rope during the downgoing trip remained constant for the first 900 m. For the last 800 m it decreased linearly by approximately 190 Nm. During the first 100 m of the upgoing trip the torque in the tail rope decreased another 60 Nm. For the next 1000 m it increased linearly to the initial value and remained constant until the end of the trip.

5.3 Chalk Test and Lay Length Measurements

The number of turns that the head rope rotates during a trip was measured by the chalk test. Paint was sprayed on the instrumented downgoing head ropes just below the driving wheel. A thin spiral line was drawn on the rope. The line was observed during the following upgoing trip. The line rotated progressively to a maximum of about 45° at the middle of the trip and then came back to zero degrees.

Lay length measurements at the top and the bottom of the shaft were almost identical. That was nevertheless expected taking into account the small variations predicted from the theoretical model.

As a matter of interest the diameter of the rope was measured at the upper station on portions of the rope which pass over the driving wheel and on portions which do not. For portions of the rope close to the coneyance that do not pass over the driving wheel the mean diameter was 43,5 mm. For portions that pass over the driving wheel the mean diameter was 41,5 mm. The difference in diameter between the two portions can be attributed to wear of the outer wires of the head rope and strands bedding in effects.

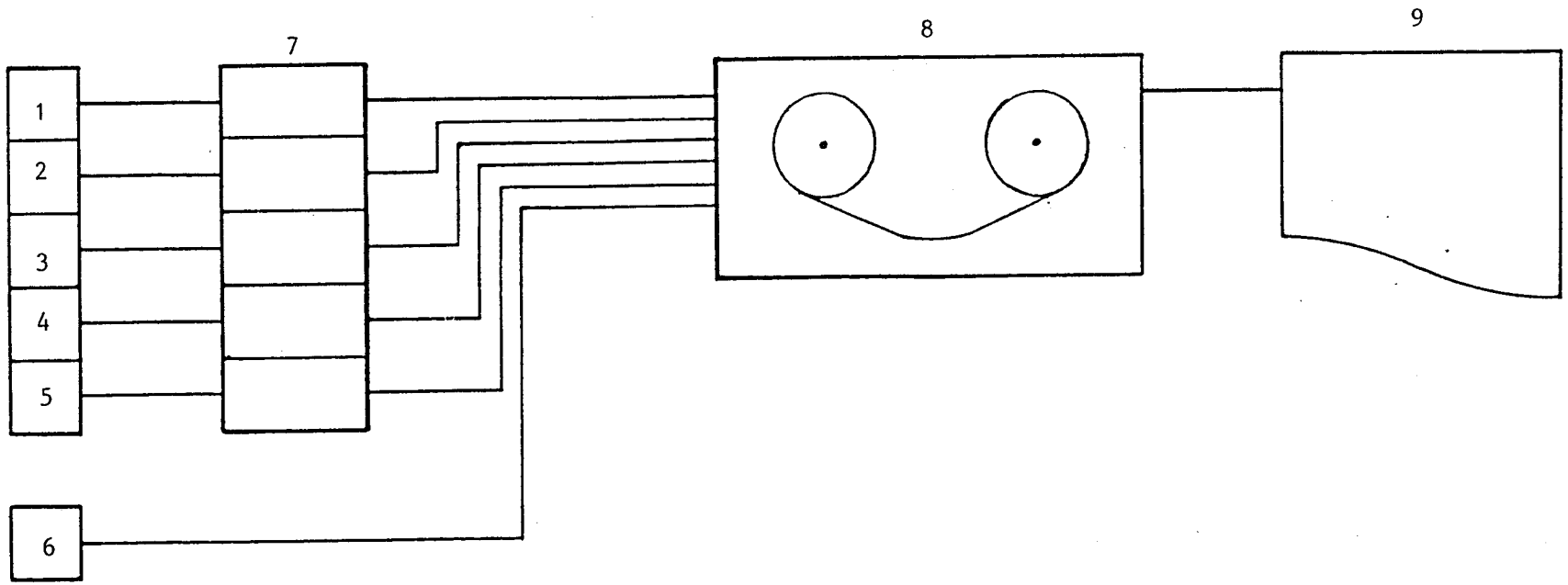

Figure 5.6 Data acquisition system

1 - 5 Loadcells

6 Bunton detector

7 Amplifiers

8 FM Tape recorder

9 Chart recorder

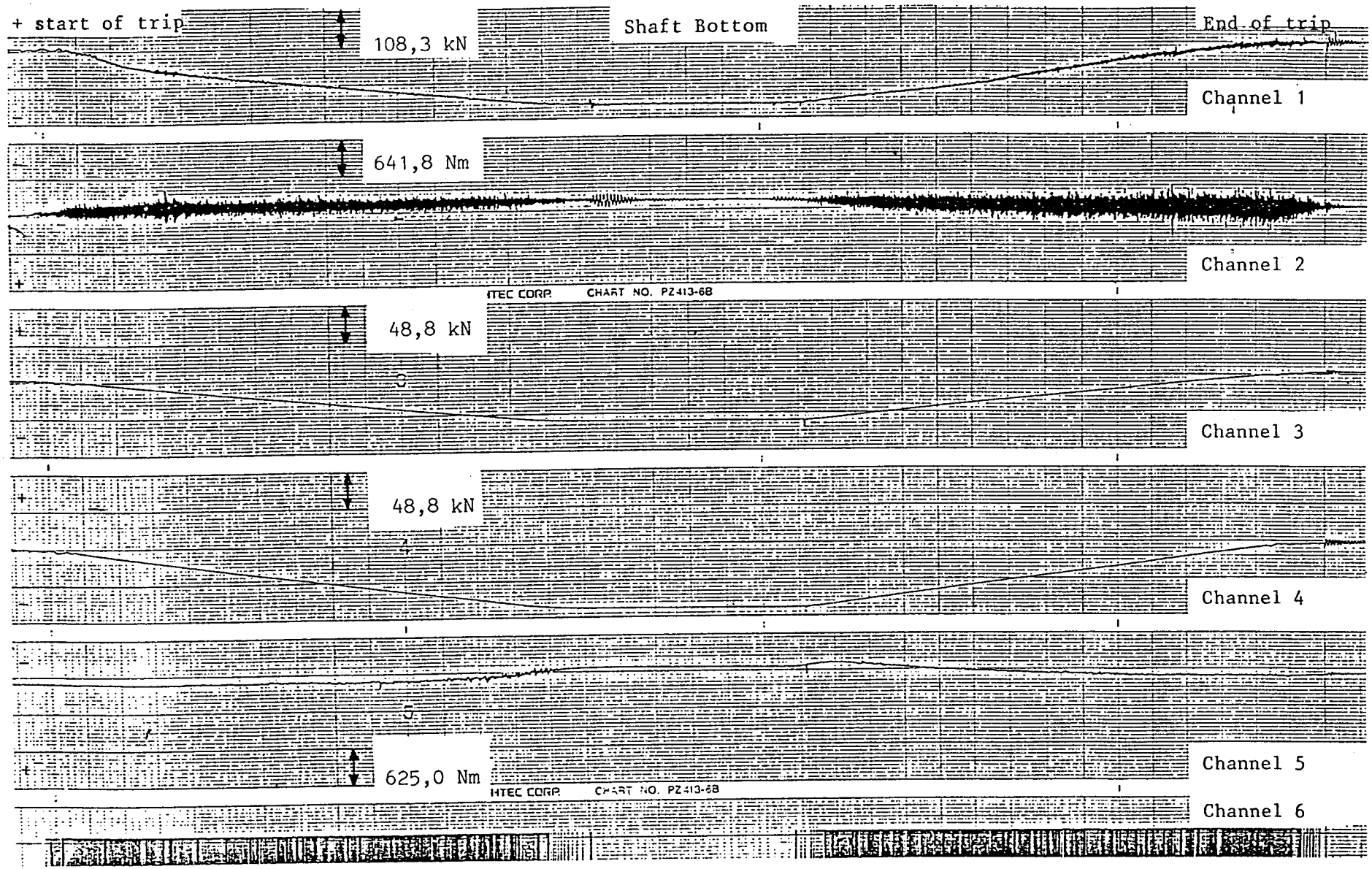

Figure 5.7 Results from the second trip

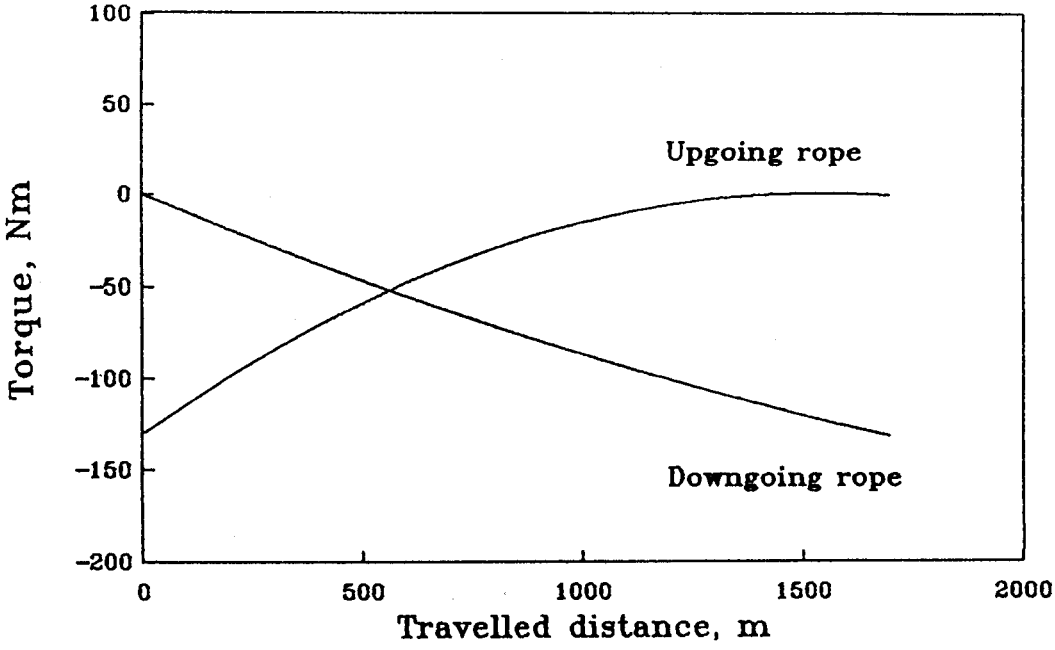

Figure 5.8 Torque in the head rope during the trip

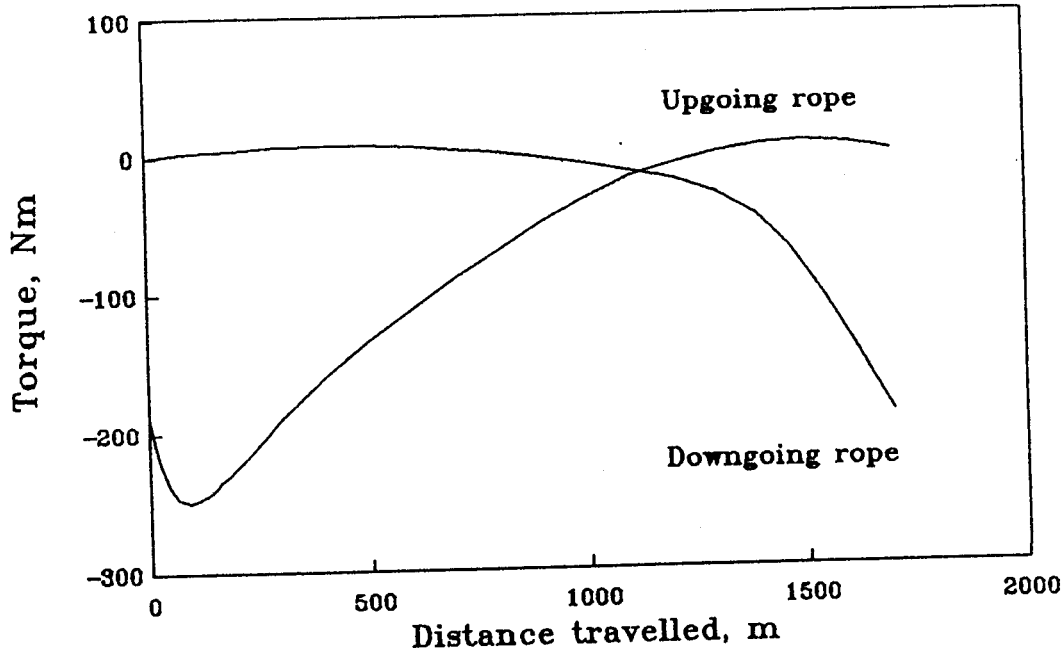

Figure 5.9 Torque in the tail rope during the trip

6. TORSIONAL AND LONGITUDINAL VIBRATIONS OF KOEPE HEAD ROPES

As was mentioned in the previous chapter, due to the high level of torsional oscillation amplitude compared to the static torque values an analysis of the torsional and longitudinal vibrations of a Koepe head rope was done. In the following paragraphs the free torsional and longitudinal vibration of a Koepe head rope are analysed. The derivation of the differential equations of motion for both the torsional and longitudinal vibrations and their solutions can be found in Appendix E. The interaction of the two types of vibration, which involves nonlinear analysis, has not been considered.

6.1 Free Torsional Vibrations of a Koepe Head Rope

The differential equation of the torsional vibration of the head rope is

$$(\partial^2\Phi/\partial t^2) = (G/\rho)(\partial^2\Phi/\partial z^2) \tag{6.1}$$

where

Φ : Is the angle of twist in the rope.
G : Is the effective shear modulus of the head rope.
ρ : Is the density of head rope material.

As was shown in Appendix E the solution of equation 6.1 is

$$\Phi(z,t) = u(z).v(t) \tag{6.2}$$

where

$$u(z) = A_z \cos(\lambda z) + B_z \sin(\lambda z) \tag{6.3}$$

$$v(t) = A_t \cos(\omega t) + B_t \sin(\omega t) \tag{6.4}$$

ω is the angular frequency of the torsional vibration and

$$\lambda = \omega / \sqrt{G/\rho} \tag{6.5}$$

is the eigenvalue of equation 6.3.

A_z and B_z are constants determined by the boundary conditions and A_t and B_t are constants determined by the initial conditions.

Since both ends of the head rope (Fig. 6.1) are restricted from rotating the boundary conditions are:

$$\text{For } z = 0 \qquad \Phi = 0 \tag{6.6}$$
$$\text{For } z = l \qquad \Phi = 0 \tag{6.7}$$

where

z : Is the position on the rope measured from the driving wheel downwards.

l : Is the length of the rope between driving wheel and conveyance.

The first boundary condition after substitution into equation 6.2, taking into account equations 6.3 leads to $A_z = 0$

From the second boundary condition we have that

$$u(l) = B_z \sin(\lambda l) = 0 \tag{6.8}$$

For $B_z \neq 0$ the above equation leads to

$$\lambda l = k\pi \qquad \text{for } k = 1, 2, 3, \ldots \tag{6.9}$$

Substituting λ from the above equation into equation 6.5, and rearranging the terms the angular frequency of torsional vibrations becomes

$$\omega = k\pi\sqrt{G/\rho}\ /l \qquad \text{for } k = 1, 2, 3, \ldots \tag{6.10}$$

Taking into account that $f = \omega/2\pi$ where f is the frequency of the torsional vibration leads to

$$f = k\sqrt{G/\rho}/(2l) \qquad \text{for } k = 1, 2, 3, \ldots \tag{6.11}$$

The effective shear modulus of the head rope was calculated in Appendix F and was found equal to 12 GPa. Taking the density of the rope material equal to 7800 kg/m³ the frequencies of the first four modes of torsional vibration of the head rope were calculated and plotted in Fig. 6.2.

6.2 Free Longitudinal Vibrations of a Koepe Head Rope

The differential equation of the free longitudinal vibration of the head rope is

$$(\partial^2 u/\partial t^2) = (E/\rho)(\partial^2 u/\partial z^2) \tag{6.12}$$

where

u: Is the displacement in the rope.
E: Is the effective modulus of elasticity of the head rope which is assumed constant.

The solution of the differential equation as was shown in Appendix D is

$$u(z,t) = u(z).v(t) \tag{6.13}$$

where

$$u(z) = A_z \cos(\lambda z) + B_z \sin(\lambda z) \tag{6.14}$$

$$v(t) = A_t \cos(\omega t) + B_t \sin(\omega t) \tag{6.15}$$

ω is the frequency of the longitudinal vibrations and

$$\lambda = \omega/\sqrt{E/\rho} \tag{6.16}$$

is the eigenvalue of equation 6.14.

A_z, B_z are constants determined by the boundary conditions and A_t and B_t constants determined by the initial conditions.

Since the rope is fixed at its top end, the first boundary condition is

$$\text{for } z = 0 \qquad u = 0 \tag{6.17}$$

which leads to $A_z = 0$

The tensile force at the bottom end of the head rope must be equal to the inertia force of the attached mass. So the second boundary condition is

$$\text{for } z = l \qquad AE(\partial u/\partial z) + m_t(\partial^2 u/\partial t^2) = 0 \tag{6.18}$$

where

A : Is the metallic area of the rope's cross section.
m_t : Is the attached mass.

$$m_t = m_c + m_p + m_s/2 + q_t(h + a + b - l) \tag{6.19}$$

where

m_c : Is the mass of the conveyance.
m_p : Is the mass of the payload.
m_s : Is the mass of the tail sheave.
q_t : Is the mass of the tail rope per unit length.
h, a, b and l as shown in Fig. 6.1.

The first two components, m_c and m_p, in equation 6.19 can be treated as a rigid body mass. However, the other two components may not be vibrating in unison with the conveyance. Trerefore their inclusion in equation 6.19 implies an approximation which may be justified in view of the low level of vibrations experienced in the measurement of tension in the tail rope (Fig. 5.7, channels 3 and 4).

Substituting u from equation 6.14 into equation 6.18 yields.

$$AE\ v(t)(\partial u/\partial z) + m_t u(z)(\partial^2 v(t)/\partial t^2) = 0 \qquad (6.20)$$

Differentiation of u from equation 6.14 leads to

$$(\partial u/\partial z) = \lambda B_z \cos(\lambda l) \qquad (6.21)$$

From equation 6.15 with double differentiation we get

$$\partial^2 v(t)/\partial t^2 = -\omega^2 A_t \cos(\omega t) - \omega^2 B_t \sin(\omega t) \qquad (6.22)$$

or

$$\partial^2 v(t)/\partial t^2 = -\omega^2 v(t) \qquad (6.23)$$

Substituting the values of u, $\partial u/\partial z$ and $\partial^2 v/\partial t^2$ from equations 6.8, 6.21 and 6.23 respectively into equations 6.20 yields

$$AE\lambda \cos(\lambda l) - m_t\omega^2 \sin(\lambda l) = 0 \qquad (6.24)$$

which taking into account that $\lambda = \omega/\sqrt{E/\rho}$ can be written as

$$\theta \tan\theta = e \qquad (6.25)$$

where

$$\theta = \omega l/\sqrt{E/\rho} \qquad (6.26)$$

$$e = Al\rho/m_t \qquad (6.27)$$

Equation 6.26 was solved numerically. A graphical representation of the solution is shown in Fig. 6.3. The effective modulus of elasticity of the rope was calculated in Chapter 2 and was found equal to 116 GPa Taking into account that $\omega = 2\pi f$ the frequencies of the free longitudinal vibration are given by the relation

$$f = \theta\sqrt{E/\rho}\ /(2\pi l) \qquad (6.28)$$

The frequencies of the first four modes of the longitudinal vibration of the head rope were calculated and plotted in Fig. 6.2 as well.

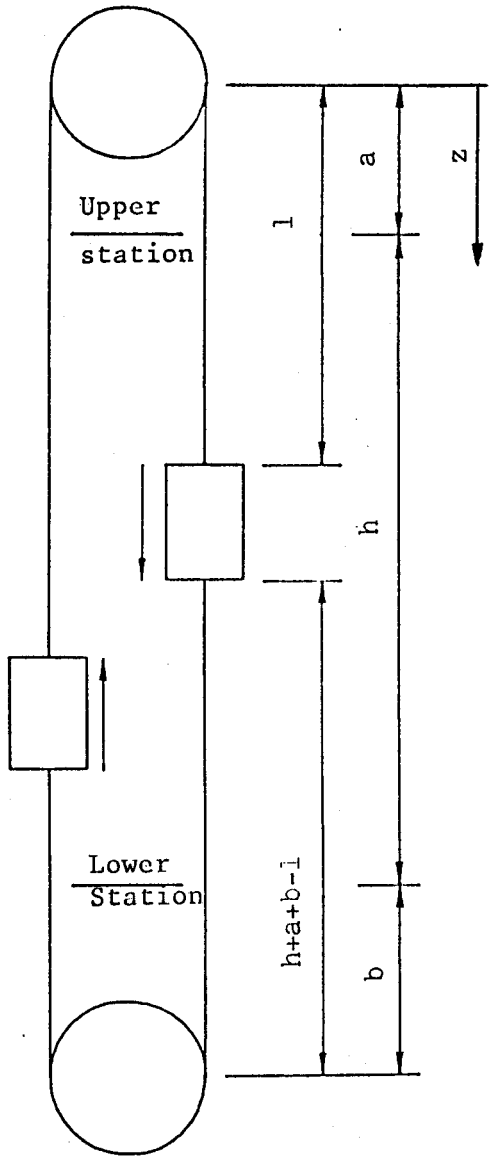

Figure 6.1 Notation for vibration analysis

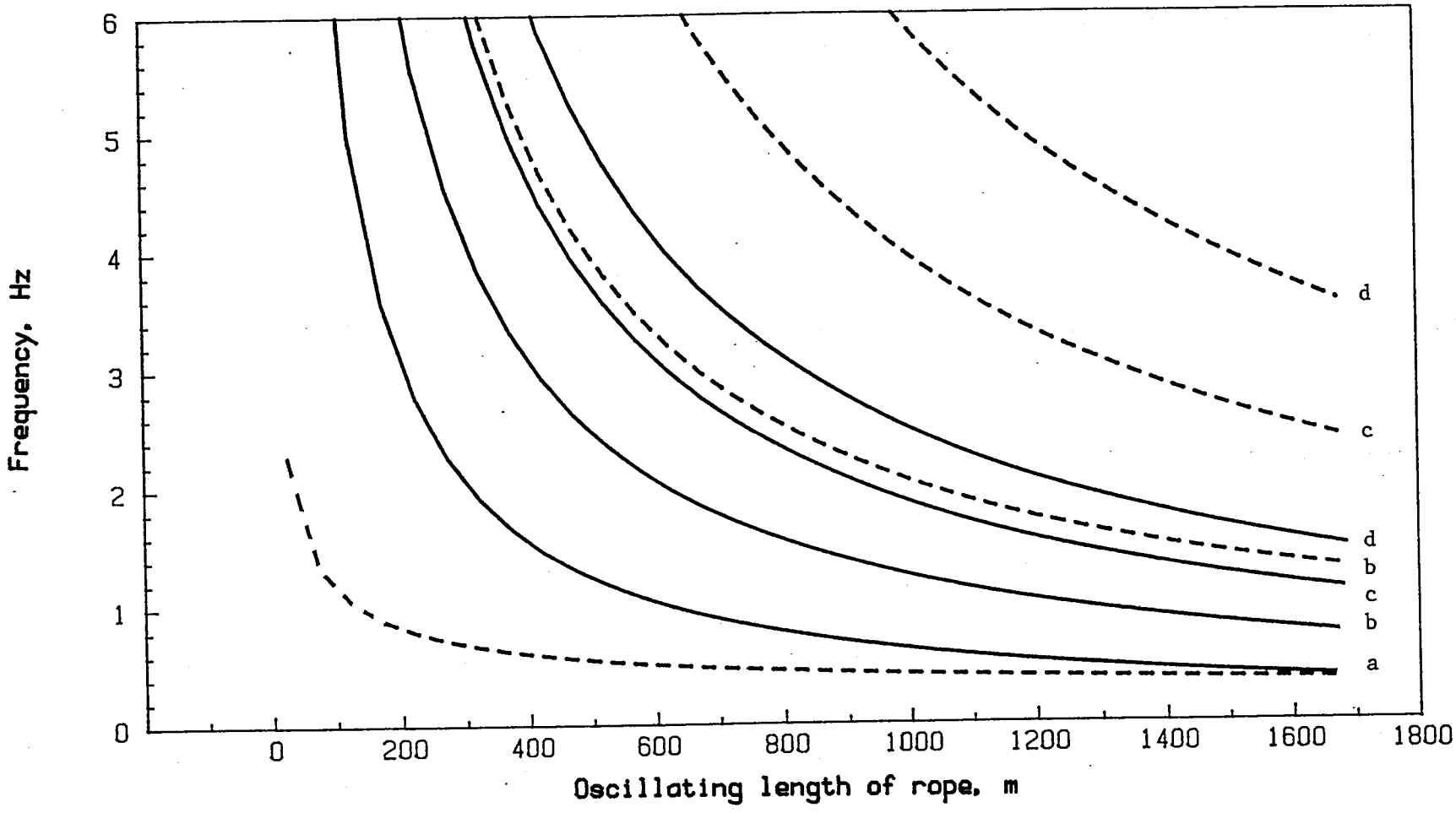

Figure 6.2 Natural frequency of torsional and longitudinal vibration

—— Torsional

---- Longitudinal

a First mode

b Second mode

c Third mode

d Fourth mode

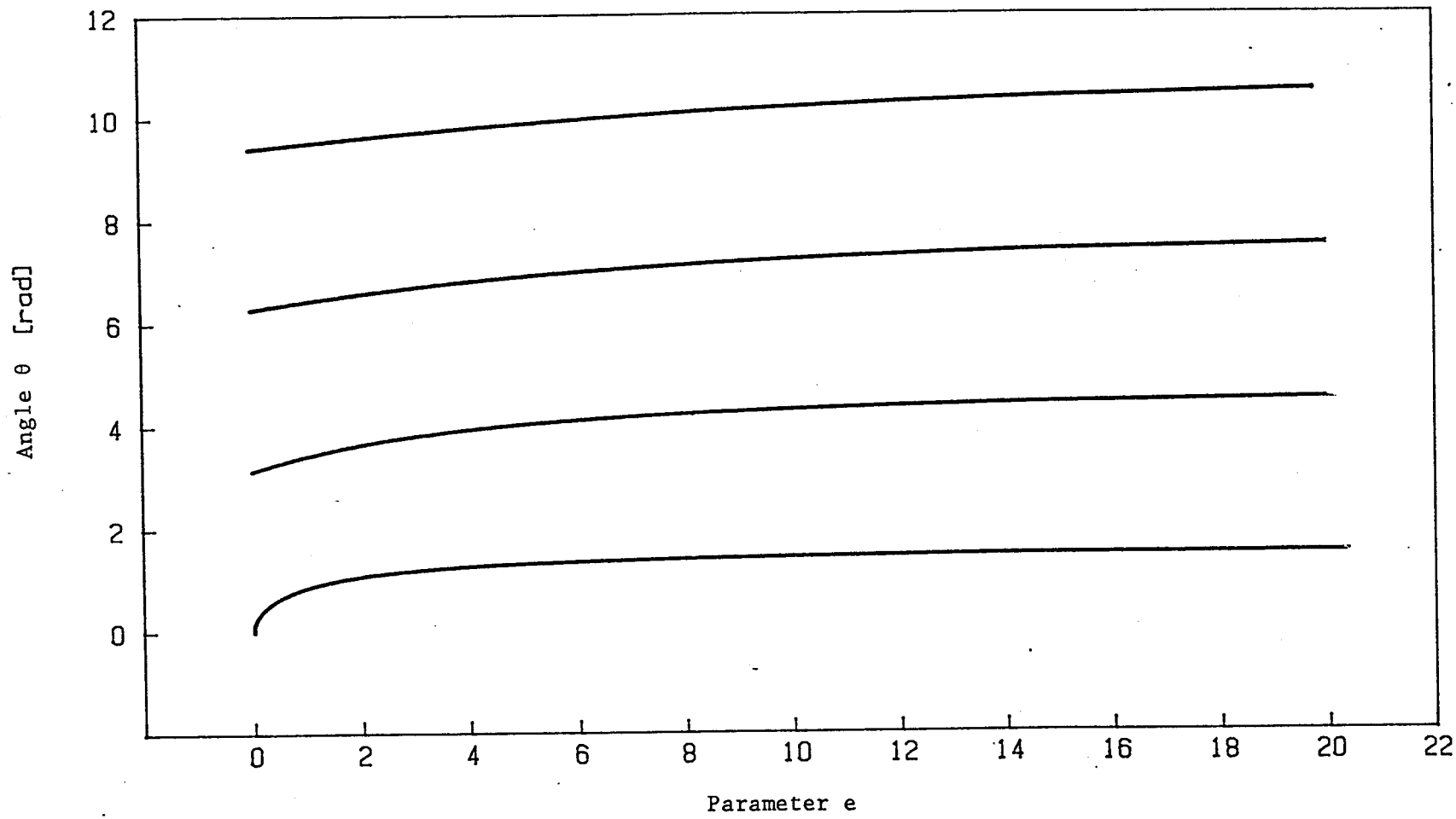

Figure 6.3 Solution of equation θ*TANθ=e

6.3 Comparison Between Experimental and Theoretical Results of the Vibration Analysis

The measured tensile and torsional loads in the head rope for four different values of the travelled distance are shown in Fig. 6.4.

Perusal of Fig. 6.2 and 6.4d reveals that the head rope is vibrating according to its natural frequency at the end of the trip. Both the measured and the calculated frequencies are 0,4 Hz.

It is possible that at the beginning of the trip the rope vibrates according to its natural frequency as well. However this is not certain since an excitation frequency of 4,7 Hz is evident throughout the trip.

Beating and high amplitude values for the torsional oscillations were experienced at 450 m below the sheave. A possible explanation for the resonance is that the 4,7 Hz excitation frequency is very close to the frequency of the third mode of torsional oscillations for that position in the shaft.

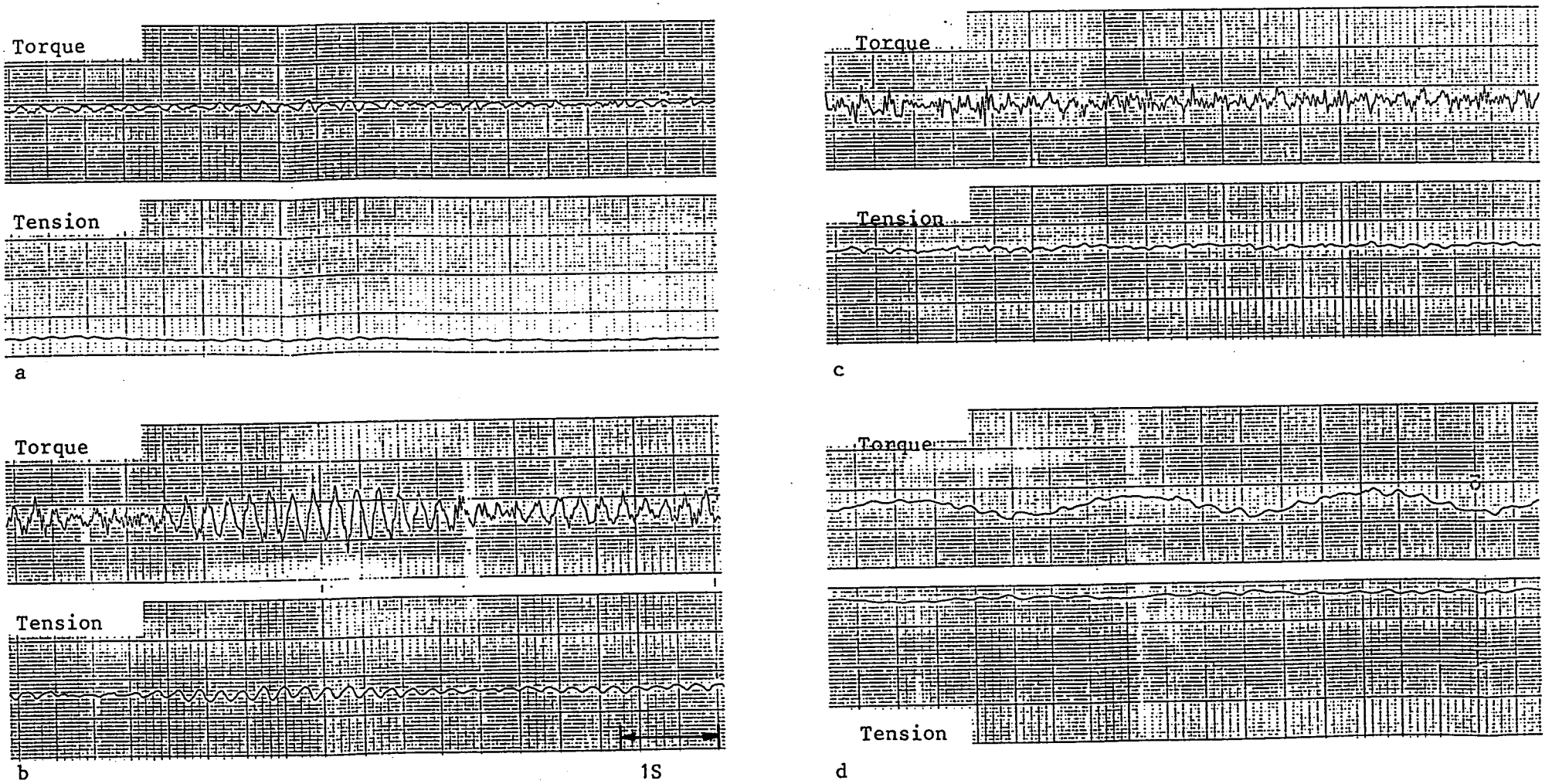

Figure 6.4 Recorded vibration frequencies

a. Travelled distance 30 m: Torque 4,4 Hz Tension 4,7 Hz

b. Travelled distance 450 m: Torque 4,6 Hz Tension 4,9 Hz

c. Travelled distance 950 m: Torque 4,7 Hz Tension 4,7 Hz

d. Travelled distance 1 700 m: Torque 0,4 Hz Tension 3,3 Hz

7 DISCUSSION

7.1 Comparison Between Theoretical and Experimental Results: Head Rope

Discrepancies were found between the results of the theoretical model and the results of the experiments at the West Driefontein Koepe winder.

The torque measured in the two sections of the head rope during a trip at the West Driefontein winder and the values predicted by the theoretical model (constant C and T factors) were plotted in Fig. 7.1. Three main differences were identified between the theoretical and experimental results and are discussed below.

a. The experimentally measured torque difference between the two sections of the head rope at the start of the trip was 130 Nm. The torque difference predicted by the theoretical model was only 105 Nm. This represents a difference of 20%. From Fig. 3.24, reproduced here as Fig. 7.2, the torque difference calculated by the variable C and T factors model, assuming zero initial rotation in the the rope, is even lower at 92 Nm. Figure 7.2 shows that in order for the theoretical model to calculate the same result as the measured value we must assume that an initial rotation in excess of 50 positive turns was introduced in the rope.

b. The measured rope rotation (chalk test) was only 45° while the value predicted by the constant C and T factors theoretical model was approximately two and a half turns. From Fig. 3.25, reproduced here as Fig. 7.3, the rope rotation calculated by the theoretical model with variable C and T factors, for zero initial rotation, was slightly less than two full rotations. Figure 7.3 shows that the theoretical model would have calculated the same rotation as the measured one if we had assumed that an initial rotation of 45 negative turns was introduced in the head rope.

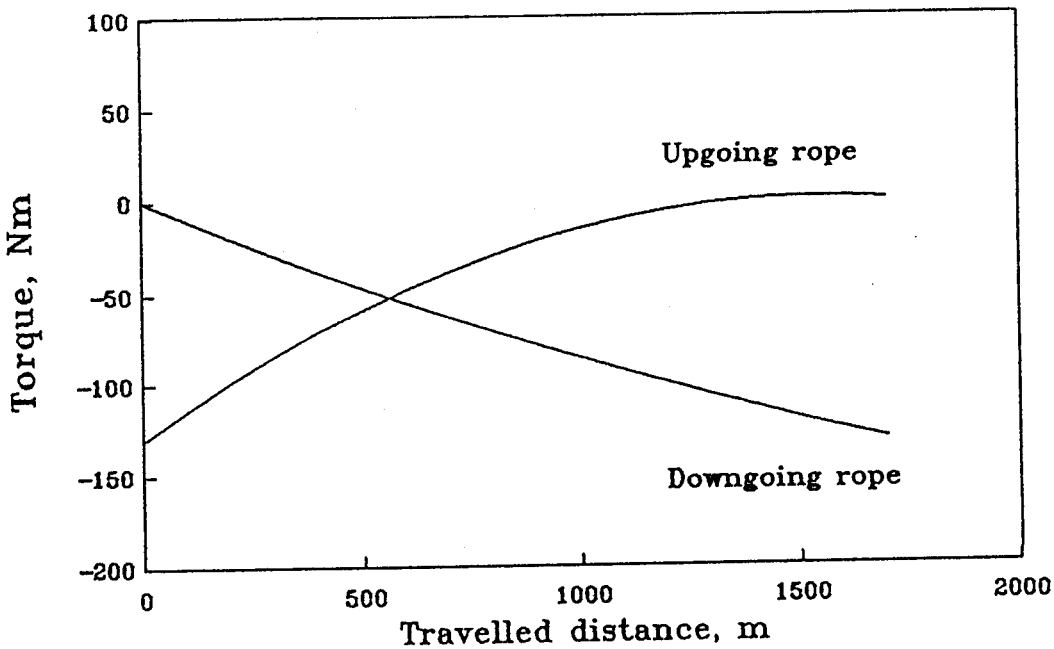

a. Experimental

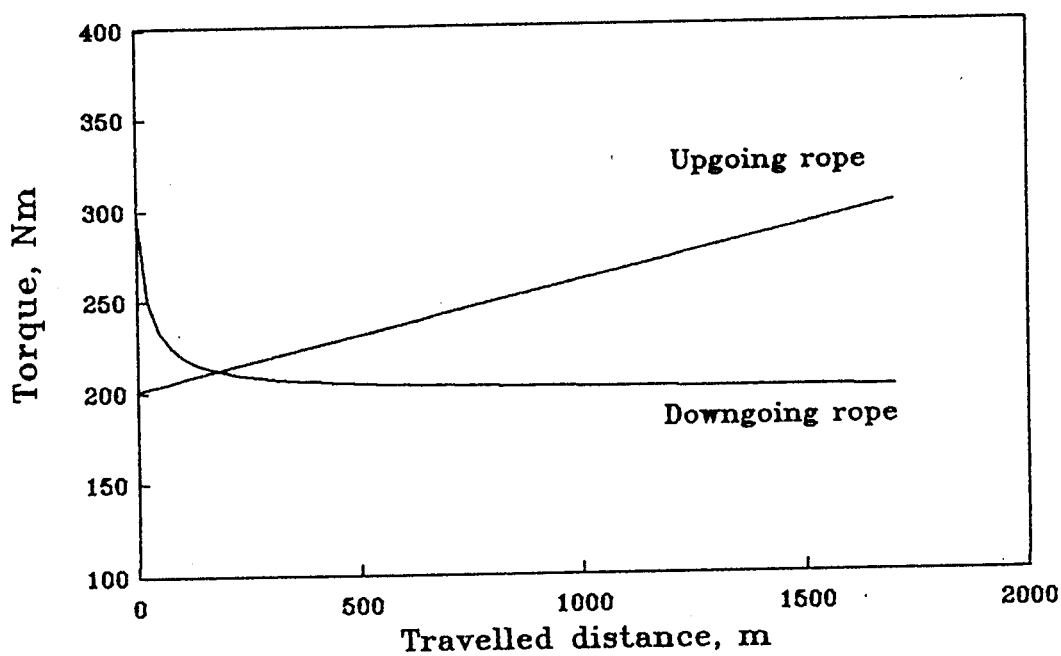

b. Theoretical (Constant C and T factors)

Figure 7.1 Head rope torque: experimental and theoretical results

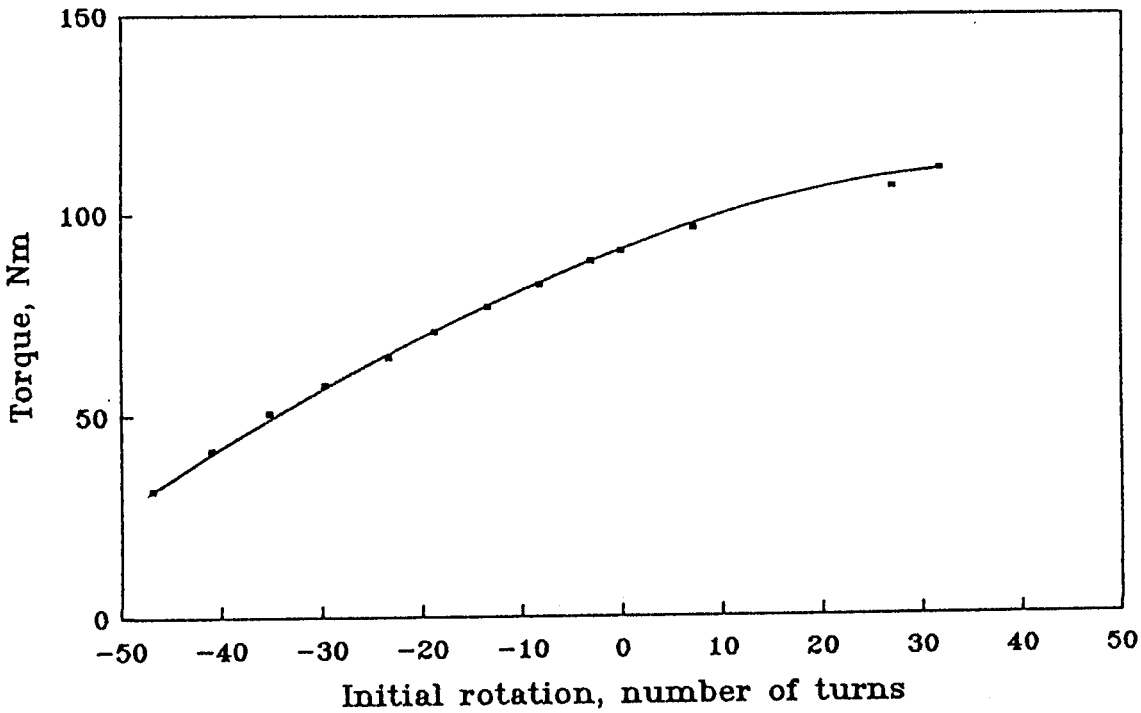

Figure 7.2 Torque difference at the beginning of the trip

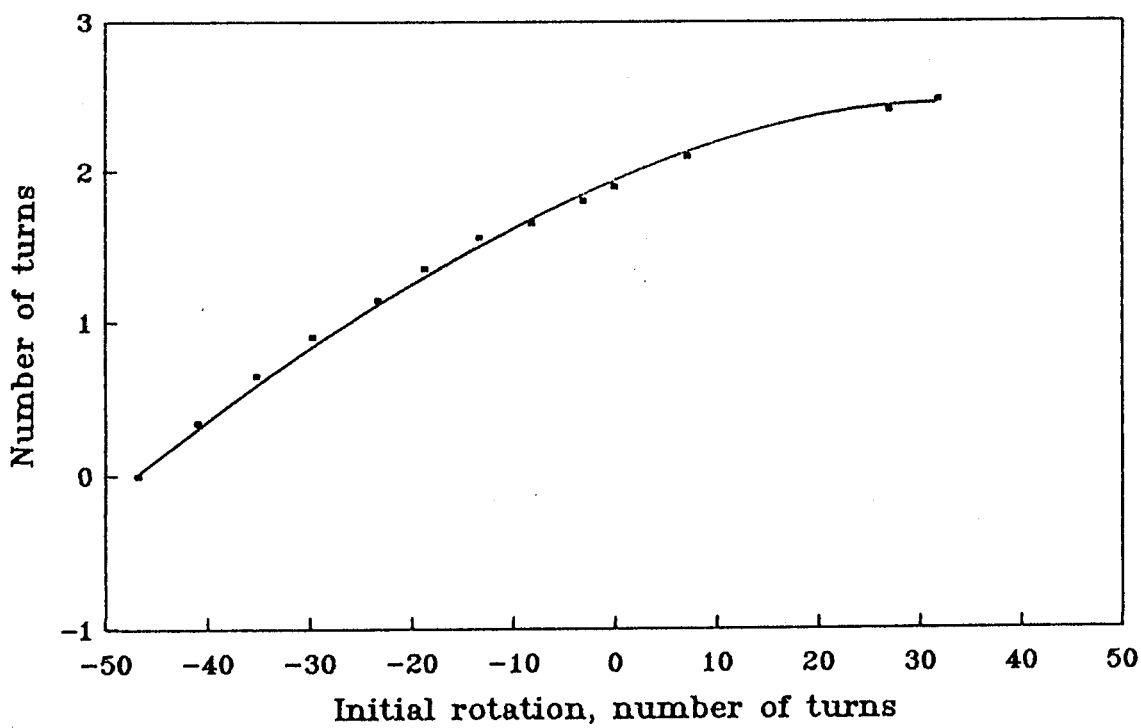

Figure 7.3 Chalk line test results for the middle section of the rope

c. The measured torque in the downgoing section of the head rope did not follow the rapid changes predicted by the theoretical model during the first stages of the trip.

7.1.1 Torque difference

The torque difference between the two sections of the rope at the start of the trip for the case of constant C and T factors, as was shown in Appendix B, is a function of the torque factor C:

$$M_{2,u} - M_{1,u} = Cqh \qquad (7.1)$$

The 20% difference between the measured and calculated values can therefore be justified by a similar difference between the assumed torque factor of 0,0007 Nm/N and the actual torque factor of the rope. Although a 20% difference appears to be high it is not unrealistic taking into account the number of assumptions made for the calculations.

The rope specimen tested in the laboratory to determine the torsional properties was cut from a discarded rope after completing 200.000 cycles. The rope installed on the winder at the time of the measurements had completed only 100.000 cycles.

As was shown by Yiassoumis and Stevenson[37] differences as high as 12% were found between the C factor of identical ropes manufactured at different times. Yiassoumis[38,39] has also shown that the torsional properties of the ropes change with cycling. Changes as high as 30% were found during laboratory tests after a new rope was subjected to tension torque loading for only a few cycles. A change of 30% after a few cycles is of course a result of the bedding-in process of the rope, but it is also indicative of the changes that can be expected after prolonged cycling in service.

7.1.2 Rope rotation

The calculated downgoing rope rotation (chalk test results) was approximately two turns while the measured value was only 45°. However the line drawn on the rope during the experiments had the same shape as the line predicted by the theoretical model, i.e. it was a parabola:

$$N = \alpha\, u(h - u)$$

with a maximum at $u = h/2$ and zero rotation at the start and the end of the trip, i.e. for $u = 0$ and $u = h$ respectively. Where α a factor. As was shown by the theoretical model, for the case of constant C and T factors model, equation 3.9, the factor α is a function of the rope properties:

$$\alpha = k/360° = (Cq/T)/360°$$

It is therefore submitted that although there is a substantial difference between the measured and calculated rope rotation, this difference is due to assumptions made regarding the properties of the rope. Although properties were measured in the laboratory on samples of the same construction assumptions were made regarding the relevance of these measurements to the ropes at the West Driefontein shaft. Further assumptions were made regarding the variation of these properties as discussed below.

For the theoretical model calculations it was assumed that the shape of the torque-tension curves was the same during loading and unloading i.e. hysteresis was neglected. The loading curves were used for both the upgoing trip (during which the tensile load in each rope element is increasing) and for the downgoing trip (during which the tensile load is decreasing).

But because of torsional hysteresis the torque in a rope element of the downgoing rope can be decreased without or with little change of lay angle. This is illustrated in figure 7.4. A rope element at the torque-tension condition A is entering the downgoing section of the rope. After a distance Δu is travelled the element is at the torque tension condition B. If hysteresis is neglected the lay angle of this element will be readjusted from the twist condition t_1 to the twist condition t_2. But as a result of the torsional hysteresis the element

can reach the torque tension condition B without changing its lay angle. Therefore no rotation is induced in the downgoing rope during the travelled step Δu. The cumulative effect of this action is that the rotation of the downgoing rope is less than that predicted by the theoretical model.

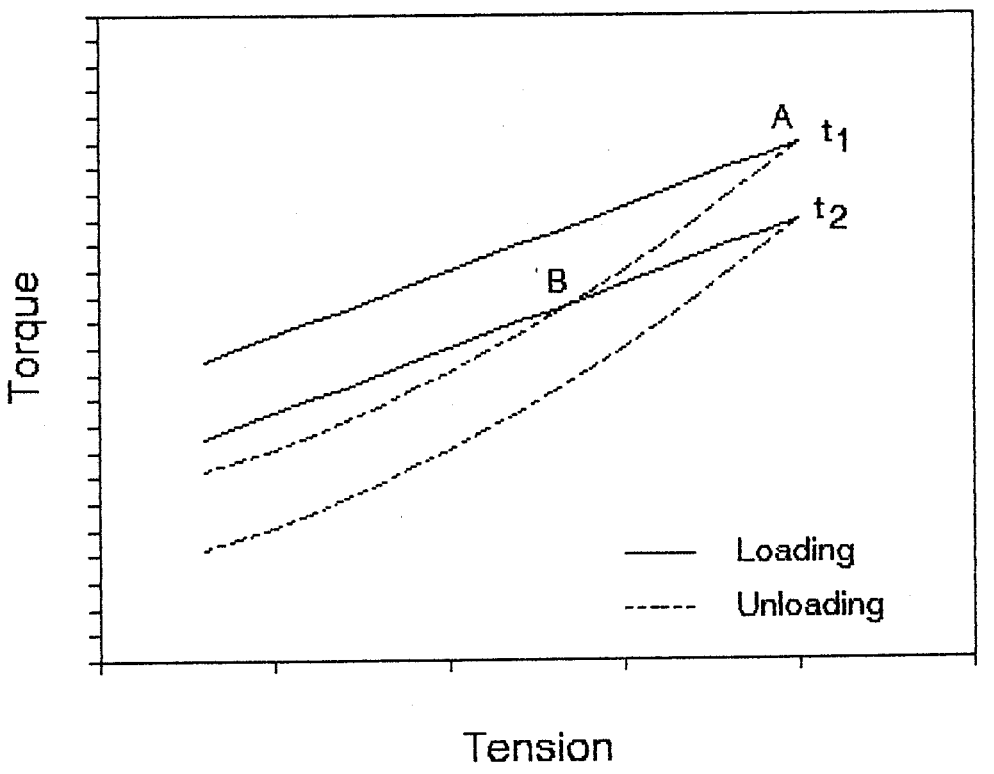

Figure 7.4 Effect of torsional hysteresis on rope rotation

As is illustrated in Fig. 2.5 the torque difference between loading and unloading curves for 0° end rotation at 250 kN is 70 Nm. The 70 Nm torque difference is more than 50% of the total torque variation in the rope during the trip. Hysteresis effects can therefore reduce considerably the downgoing rope rotation and could account for the full difference between the calculated and measured rope rotation values.

The assumption was made in the theoretical model calculations that the initial rotation on installation was zero. As was stated above, in order to match the theoretical results for the torque difference at the beginning of the trip with the experimental ones we must assume an initial rotation in excess of 50 positive turns. In order to match the calculated rope rotation of two full turns with the measured one of 45°, we must assume an initial rotation of 45 negative turns. This apparent discrepancy between the measured torque difference and rope rotation would have been significantly less if torsional hysteresis effects had not been ignored. The torsional stiffness of the rope, as discussed below, may also account for some of this discrepancy.

The torque difference in the two sections of the rope at the start of the trip is:

$$M_{2,0} - M_{1,0} = Cqh \qquad (7.1)$$

The rope rotation is calculated from equation 3.9

$$N = ku(h - u)/360° \qquad (3.9)$$

and for $u = h/2$

$$N = kh^2/1440° \qquad (3.10)$$

where $k = Cq/T$

Comparing equations 7.1 and 3.10 we see that while the torque difference is a function of the C factor only, the rope rotation is a function of both the C and T factors. The discrepancy between torque difference and rope rotation can therefore be explained if the T factor of the rope installed on the winder was higher than the T factor values used in the theoretical model. A higher T factor will not affect the torque difference calculations but it will reduce the calculated rope rotation.

Hobbs and Raoof[40] have shown that both the axial and torsional stiffness of a wire rope are significantly larger for small load changes than for large perturbations. In the case of small load changes a non-slip situation exists between the individual wires of a rope and therefore the rope is stiffer. Graphs of theoretical and experimental results for a single strand indicate that the non-slip torsional stiffness is three times higher than the full slip condition.

Work done by the author[37] has indicated a similar behaviour for the axial stiffness of a wire rope for very low tensile loads. The modulus of elasticity of a rope for very low loads is significantly higher than for moderate and higher loads. This is partially illustrated in Figs. 2.12 and 2.13. These results are in agreement with Raoof and Hobbs since the tensile load increment step for low tensile loads was only a fraction of the approximately 0,7 kN step for higher tensile loads.

Because of limitations of the available torque-tension machine this could not be experimentally confirmed for the torsional stiffness as well. The torsional stiffness measured according to the procedure of Chapter 2 is indicative of large load changes where the individual wires of the rope can slip on one another. Therefore it might not be representative of the rope behaviour in service. Because of the high torsional oscillations measured during the experiments at the West Driefontein winder it is not possible to reach a conclusion whether the rope operated in the slip or non-slip condition.

7.1.3 Rate of torque change

The third difference between theoretical and experimental results i.e. the absence of rapid torque changes in the downgoing rope during the first stages of the trip can be attributed to a number of reasons such as:

a. Experimental errors introduced due to the high level of torsional oscillations.

b. The fact that the West Driefontein winder incorporates a deflection sheave while the model assumes that there is no deflection sheave. Although the measurements were done on the side of the winder where there is no deflection sheave the torque and especially the torque in the downgoing rope might have been affected by the additional restriction imposed by the deflection sheave.

c. Differences in the shape of the torque-tension curves that were used for the theoretical model calculations and the torsional properties of the rope installed on the winder. As discussed the torsional properties of ropes vary with cycling and may also vary between ropes of the same construction but different manufactures. Since each section of the rope is subjected to a different tensile, torsional, and bending load cycling, the torsional properties of the rope possibly vary along its length. In such a case the shape of the torque-tension curves will vary along the length of the rope.

   Variations in the torsional properties along the length of the rope are also caused by non uniform wear. As was mentioned in Chapter 5, the diameter of the two rope portions close to the conveyances that do not pass over the driving wheel was 5% larger than portions that pass over driving wheel. At the start of the trip the downgoing rope has a length equal to the overrun distance, 25 m for the West Driefontein winder. These 25 m of rope are of larger diameter than the rest of the rope since they are not subjected to any external wear. During the trip, rope of smaller diameter and therefore different torsional properties is entering the downgoing section. The difference in the torsional properties will affect the torsional behaviour and the effect will be more pronounced at the beginning of the downgoing trip when the rope portions with different torsional properties are of similar lengths.

d. The fact that hysteresis was neglected. As was discussed in the previous paragraphs, in the theoretical model calculations it was assumed that the shape of the torque-tension curves was the same during loading and unloading and in fact the loading curves were used for the calculations. This assumption does not affect the upgoing rope since the tensile load in each element is increasing during the trip, but it does affect the downgoing section where the tension in each element is continually decreasing.

7.1.4 Torsional oscillations

The high level of torsional oscillations in the head rope could not be attributed with certainty to any particular reason. Further analysis in that respect was beyond the scope of the present dissertation due to the complexity of the matter[41].

7.2 Comparison Between Theoretical and Experimental Results: Tail Rope

7.2.1 Locked swivels

The torque measured in the tail rope during a trip and the values predicted by the theoretical model (constant C and T factors) were plotted in Fig. 7.5. The differences between the theoretical and experimental results are outlined and discussed below.

a. The measured torque difference between the two sections of the tail rope was approximately 200 Nm. The value predicted by the theoretical model with constant C and T factors was double the measured value i.e. 400 Nm. The value predicted by the variable C and T factors model, for zero initial rotation introduced in the rope, was slightly lower at 350 Nm. Since the tail rope operates at low tensile loads, approximately 5 kN to 150 kN, where the shape of the torque-tension curves is not linear it was expected that the constant C and T model will overestimate the torque values. On the other hand for the case of the variable C and T model, as was discussed in Chapter 4, because the available data for the rope torsional properties did not extend to the very low tensile load the rope operates, the weight of the tail sheave was assumed higher than its actual value. This assumption also causes the theoretical model to overestimate the torque values. In addition to these reasons the discrepancy can be attributed to the fact that rotation is periodically released from the tail rope by unlocking the swivels.

b. Although the torque in the upgoing rope followed generally the pattern predicted by the model, a drop in the torque during the first 100 m of the trip was measured which was not predicted by the theoretical model.

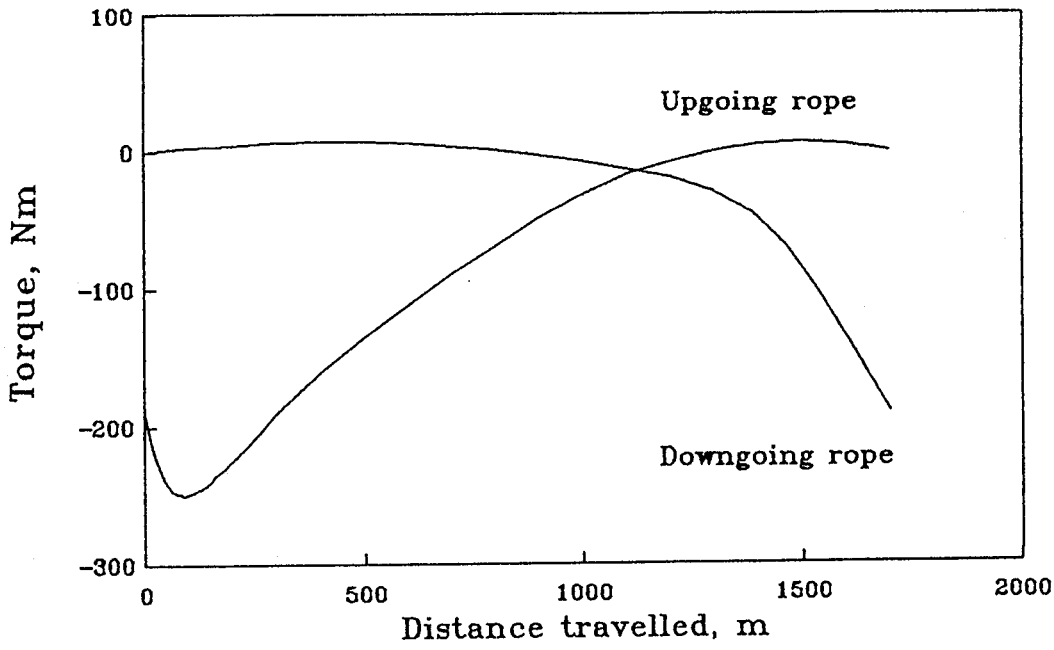

a. Experimental

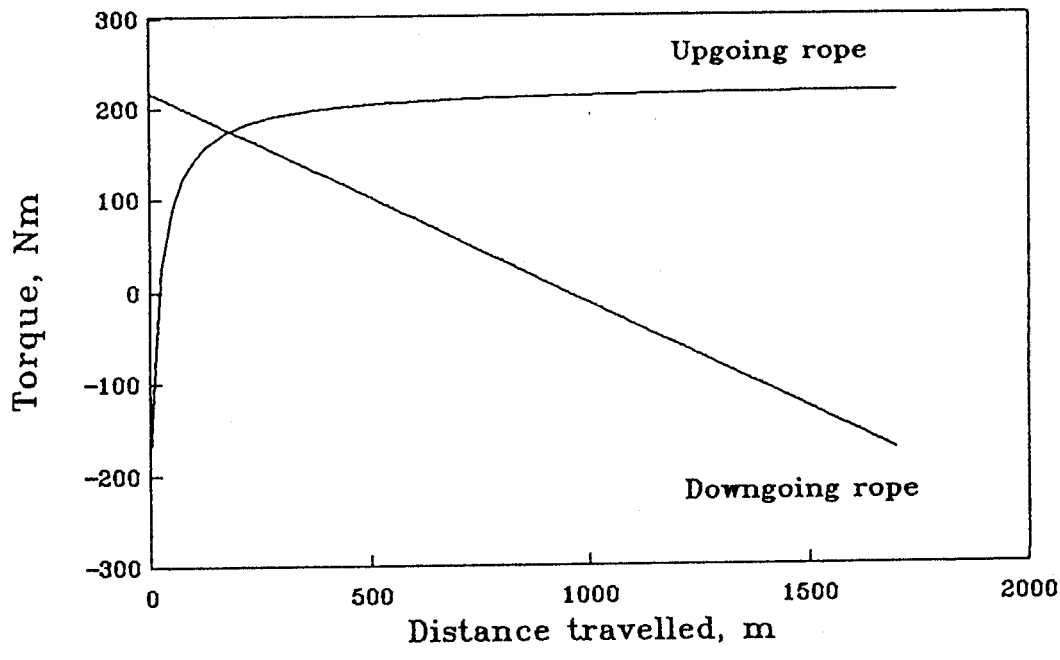

b. Theoretical (Constant C and T factors)

Figure 7.5 Tail rope torque: experimental and theoretical results

c. For the first 900 m of the trip the measured torque in the downgoing section of the rope remained almost constant while for the following 800 m it reduced by approximately 190Nm. The constant C and T factors model predicted a linear decrease of the torque in the downgoing section of the rope during the entire trip.

The last two differences imply significant differences between the actual shape of the torque-tension curves and the shape of the curves utilized for the theoretical model i.e. inaccurate C and T factors. One source for this inaccuracy is the length of the test specimen. Aust[42] has shown that the length of the test specimen has an effect on torque-tension test results. Because of the restriction of any movement of the wires at the end fittings a variation of the level of stresses was measured along the length of the rope sample. Therefore a short specimen length, like the one used during the laboratory tests, is expected to give less accurate results than a long specimen. The effects of the specimen's length are currently under investigation by the author.

7.2.2 Free swivels

The validity of the theoretical model of the tail rope where swivels are free and no tail sheave is installed, was proven by observations at the Mount Isa Koepe winder in Australia. The loop rotation was video-taped by Mr. E.J. Wainwright of Haggie Rand Ltd and the tape was made available to the author. The tail loop rotation follows the pattern predicted in Fig. 4.6.

7.3 Summary of Discussion on the Differences Between Theoretical and Experimental Results

The theoretical models have not been fully verified by the experiments at West Driefontein. The models have predicted correctly the trend and the direction of variation for both the torque in the ropes and the rope rotation but they did not accurately predicted the magnitude of these variations. The theoretical models have therefore correctly qualified but not accurately quantified the ropes' behaviour.

From the discussion in the preceding paragraphs 7.1 and 7.2 the discrepancies can be attributed to two groups of factors:

a. Assumptions made in the theoretical model, such as the assumption that the shape of the torque tension curves is the same during loading and unloading.

b. Experimental errors, either during the tests at West Driefontein or during the laboratory test to measure the rope properties.

The discussion on the ropes' behaviour that follows and the conclusions and recommendations that were reached are primarily based on the findings of the theoretical models.

7.4 Discussion on the Behaviour of the Head Rope

The number of turns that the head rope rotates during the downgoing trip (chalk test), as shown by equation 3.10, is a function of two parameters: the hoisting depth, h and the factor k which combines the rope properties.

$$N = kh^2/1440^\circ \qquad (3.10)$$

Since the rotation of the rope is a function of the square of the hoisting depth, h, it will be significantly higher for deeper shafts. This explains why problems manifested themselves in the deep South African shafts.

7.4.1 Comparison with the previous theoretical model

Equation 3.10 is the same as the one derived during the first attempt to study the torsional behaviour of Koepe head ropes in the late nineteen fifties[2]. Despite the fact that the wrong assumptions were used at the time, the equations that calculate the rope rotation in that report are right because two errors introduced in the analysis cancelled each other.

Firstly it was assumed that the the torque in each rope element is proportional to the tensile load in the element:

$M = CP + Cq(z + u)$ (Equation 3 in reference 2)

from were $dM = Cq.dz$

Secondly it was assumed that the variation of the relative rotation along the rope is a function of the torque variation along its length:

$d\Phi/dz = 1/T\int dM$ (Equation 4 in reference 2)

combining the two equations leads to the correct relation

$d\Phi = 1/T(Cqz + A)dz$ (Equation 5 in reference 2)

where A is an integration constant.

No attempt is made to calculate the torque in the head rope in that report.

7.4.2 Discussion on the C and T factors

As stated in Chapter 1 (Review of Literature) a reduction of the rope rotation is beneficial. This can be achieved by reducing the factor k which is a function of three rope properties: the torque factor, the torsional stiffness and the weight of the rope per meter length.

$k = Cq/T$

A rope with a zero torque factor ($C = \emptyset$) would eliminate torsional problems on Koepe winders. The torque in the upgoing and the downgoing ropes is calculated by equations 3.2 and 3.4 reproduced below:

$$M_{1,u} = CP + Cq(h/2 + a^2/L_h + u) + \Phi_{in}T/L_h \qquad (3.2)$$

$$M_{2,u} = CP + Cq(h/2 + a^2/L_h + a(h - u)/(a + u)) + \Phi_{in}T/L_h \qquad (3.4)$$

For a rope with zero torque factor the torque in both sections is a function of the rotation introduced on installation, Φ_{in}:

$$M_{1,u} = \Phi_{in}T/L_h \qquad (7.2)$$

If negative rotation is introduced in a multi-strand non-spin head rope on installation the inner strands of the rope will carry a higher percentage of the total tensile load, as shown in Chapter 2, Fig. 2.14. This will result in the outer strands becoming slack which, as was discussed in Chapter 2, will increase the probability of rope birdcaging. This is confirmed by field experience: Ropes with a very low torque factor are more susceptible to birdcaging.

A certain amount of positive torque, which tends to tighten the outer strands, is therefore desirable in the head rope. This is not incompatible with the desirability of low rope rotation. As is explained below, it is not the absolute value of the torque in the rope that creates the torsional problem but the torque difference in the two sections of the rope.

The change in lay angle of an element entering the downgoing section of the rope as was shown in Appendix B is:

$$\theta_2 - \theta_1 = ((M_{2,u} - M_{1,u})/T)r.\cos^2\beta \qquad (7.3)$$

This sudden change of the lay angle which in fact induces the rope rotation is proportional to the torque difference $M_{2,u} - M_{1,u}$ and not to the absolute value of the torque in the two sections of the rope. However, although the torque factor C does not appear explicitly in equation 7.3 it is embedded in the terms for $M_{2,u}$ and $M_{1,u}$. Therefore, for constant C and T factors, a low torque factor C reduces the torque difference and the change in lay angle occurring at the top of the descending rope.

For the case of variable C and T factors (which is the case for non-spin ropes) it may be feasible to shape the torque-tension curves in such a way that, although the individual torque values are high, the torque difference in the two sections of the head rope is maintained at reasonably low levels.

The same result i.e. high individual torque values in the two sections of the head rope but low lay angle changes can be achieved, according to equation 7.3, by a higher T factor.

The above discussion indicates that it is feasible to reduce the head rope rotation while a residual amount of torque is maintained in the head rope ($C \neq \emptyset$). It was also shown that a rope with such properties is either one with a high T factor and/or, perhaps, an appropriate shape of torque tension curves.

In the mining and rope manufacturing industry great concern is placed on the C factor of a non-spin rope. In fact non-spin ropes are designed and selected for applications on Koepe winders on the basis of the C factor. Through the theoretical model the significance of the T factor for the torsional behaviour of the head ropes has been demonstrated. In fact the improvements in rope performance achieved with the installation of non-spin ropes are primarily a result of their high T factor rather than their low C factor as shown below.

A typical value of the T factor for a non-spin rope is 50 Nm/(deg/m), Fig. 2.9. From Fig. 2.8 the T factor for an equivalent triangular strand rope is only 3 Nm/(deg/m). A typical value of the C factor for a non-spin rope is 0,7 Nm/kN, while for a triangular strand rope the equivalent value is 5 Nm/kN, Figs. 2.6 and 2.7. The T factor of a non-spin rope is therefore 17 times higher than that of a triangular strand rope while its C factor is only 7 times lower.

The k factor of a triangular strand rope is therefore approximately 120 times higher than that of a non-spin rope. The installation of non-spin ropes on Koepe winders has therefore reduced the rope rotation by a factor of 120. The T factor contributed 71% to the total reduction while the C factor only 29%.

7.4.3 Discussion on the rope weight, q

By definition the k factor is proportional to the weight of the rope per meter length. The head rope rotation, is therefore a function of the gradient of the tensile load along its length and not of the absolute value of the suspended load (for ropes with variable C and T factors the rope rotation can be a function of the suspended load as well). A lighter rope will therefore improve the torsional behaviour of the head rope.

In the case of two Koepe winders serving the same shaft, equipped with the same conveyances, carrying the same payload and operating with ropes of the same construction but different diameters i.e. different rope weights, the winder with the lighter rope will have better torsional behaviour. This winder will have a smaller factor of safety.

As shown by the author[41] non-spin ropes of identical construction but different tensile grades have similar torsional properties. Following the considerations of the above paragraph higher tensile grade ropes, and therefore lighter ropes, will improve the torsional behaviour of a head rope. Alternatively with higher tensile grade ropes higher payloads can be hoisted without affecting the torsional behaviour of the head rope detrimentally.

7.4.4 Discussion on the loading and unloading process of the conveyances

For the range of working tensions involved in this discussion i.e. above 200 Nm, the C factor of a triangular or non-spin head rope is practically constant (Figs 2.6 and 2.7). Therefore the k factor is inversely proportional to the torsional stiffness, T. The torsional stiffness of non-spin ropes is also relatively constant in that load range (Fig. 7.9). Therefore, in the case of a non-spin head rope the loading and unloading process does not influence the torsional behaviour, since the k factor remains constant.

In the case of a triangular strand head rope loading and unloading does affect the torsional behaviour. The torsional stiffness of a triangular strand rope increases linearly with tension as is shown in Fig. 2.8. Loading of the conveyance at the bottom of the shaft causes higher values for the torsional stiffness. The k factor therefore decreases and the relative rotation, equation 3.3 becomes smaller. A triangular strand head rope therefore rotates during loading or unloading.

7.4.5 Discussion on the lay angle variations

The chalk line test, which measures the total number of turns the rope rotates, is a good indicator of the torsional performance of a head rope. However, the lay angle deviation is the more adequate variable to study variations of the performance along the length of the rope. As was shown in Fig. 3.11 rope portions close to the two conveyances are subjected to more severe lay angle variations during a trip than the rest of the rope. Therefore, problems associated with the torsional behaviour of the ropes, such as internal wear due to inter-strand frictional movements or strand distortion are more likely to occur in those areas.

Rope portions close to the conveyances are also subjected to the worst conditions in terms of tension-tension fatigue. The tensile load amplitude in those sections is greater than in the rest of the rope. During rope inspection therefore special attention should be given to the two rope sections close to the conveyances, especially to the parts that are also subjected to bending as they pass over the driving wheel and the deflection sheave if there is one.

7.4.6 Discussion on rotation introduced in the rope

Introduction of end rotation into the rope during installation or during its service life would affect the area the winder operates in a torque-tension curves diagram. Introduction of negative end rotation as illustrated in Fig. 7.2 would, in general, reduce the variation of the torque during the trip. The number of turns the rope rotates according to a chalk line test would also become less if negative rotation is introduced to the head rope, Fig. 7.3.

Introduction of positive end rotation would, on the other hand, cause higher torque variation during a trip and would also increase the number of turns the head rope rotates. From Figs. 7.2 and 7.3 it is also concluded that the torsional behaviour is more sensitive to the introduction of negative end rotation. In other words greater variations in the torsional behaviour would happen if for example ten turns are introduced in the rope in the negative direction than if they are introduced in the positive direction. This conclusion depends on the shape of the torque-tension curves.

7.5 Discussion on the Behaviour of the Tail Rope

7.5.1 Tail loop formed freely without the use of a tail sheave.

The rotation of the loop is calculated by equation 4.10 reproduced below.

$$\begin{aligned}\Phi_t = \quad & -(\Phi_{s1}(h + b - u) + \Phi_{s2}(b + u))/L_t \\ & - 2CP_t(h + b - u)(b + u)/(TL_t) \\ & - Cq(h + b - u)(b + u)/(2T)\end{aligned} \tag{4.10}$$

It can easily be shown that if both swivels are locked ($\Phi_{s1} = \Phi_{s2} = 0$), the loop rotation is maximum for $u = h/2$ (see Fig. 4.2b). With $P_t = 0$ this maximum is:

$$\Phi_t = - CqL_t^2/(8T) \tag{7.4}$$

The tendency of the tail rope to deform into a figure of eight is therefore proportional to the square of the tail rope length. This observation is nevertheless only of theoretical importance since for all practical purposes in the deep South African shafts the two legs of the rope will intertwine

The use of free swivels is absolutely necessary in deep shafts. The loop rotations for two study cases of Chapter 4 are reproduced here in Fig. 7.6. In the first case both swivels are free and their frictional torque is constant and equal to 40 Nm. In the second case both swivels are also free but their frictional torque varies linearly with the applied tensile load from 20 Nm to 40 Nm. Although the maximum frictional torque is the same, the "more free" swivels in the second case cause five times more loop rotation and the rope will intertwine.

As discussed in Chapter 4 the greater rotation of the tail loop in the second case is due to the fact that the swivels do not rotate at the same time. In order to satisfy the torque equilibrium condition when only one swivel rotates, the loop is forced to rotate further.

The theoretical model indicates that for the case of a freely formed tail loop it is of paramount importance that the frictional torque of the swivels does not change significantly with the tensile load. In fact the term free swivel is misleading. A tail rope equipped with swivels of 40 Nm constant frictional torque will operate better than if it were equipped with swivels of frictional torque that varies with the tensile load between 20 Nm and 40 Nm and which would have been classified as a "more free" swivel.

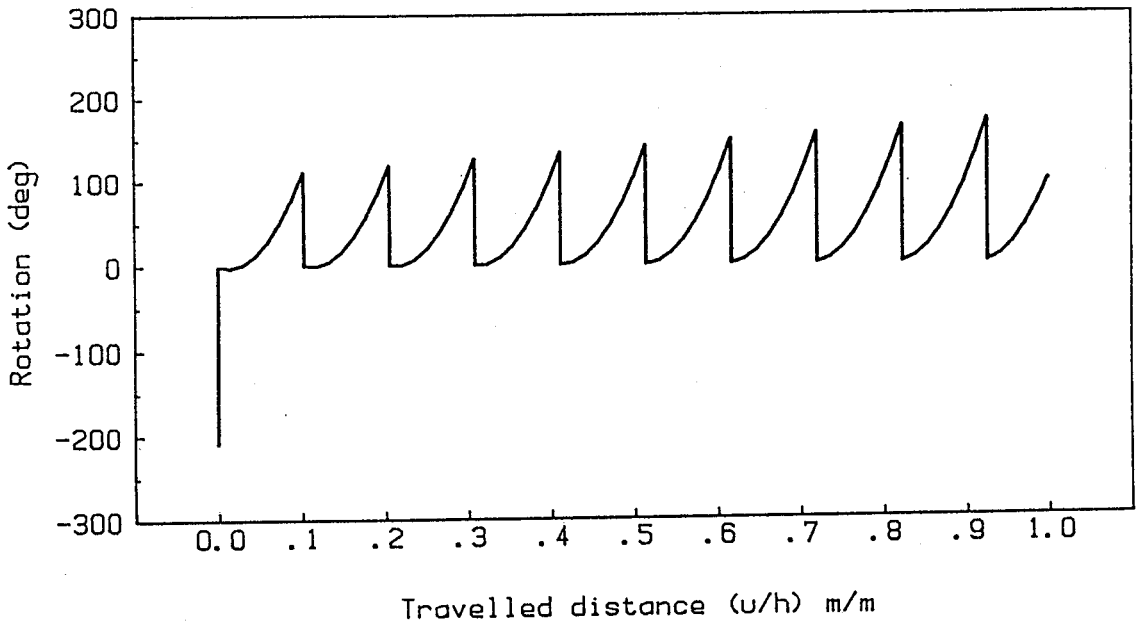

a.

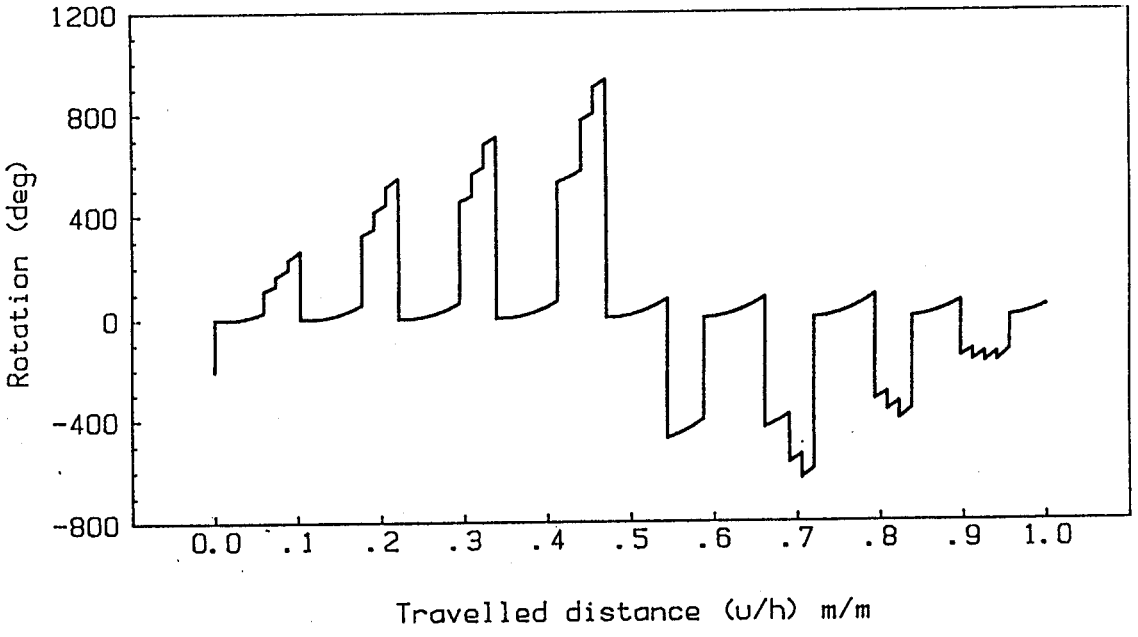

b.

Figure 7.6 Tail loop rotation
a. Swivels with constant frictional torque
b. Swivels with variable frictional torque

7.5.2 Tail loop formed by means of a tail sheave.

The torque in the two sections of the tail rope is calculated by equations 4.11 and 4.14. The torque difference in the two sections of the rope is proportional to the C and q factors.

$M_{1,u} - M_{2,u}$ proportional to Cq (7.5)

The change in the lay angle, $\theta_2 - \theta_1$, as a rope element enters the upgoing section of the rope is calculated from equations 4.13 and 4.16. and it is proportional to the k factor

$\theta_1 - \theta_2$ is proportional to k (7.6)

Equations 7.5 and 7.6 are of the same form as equations 7.1 and 7.3 of the head rope. It follows that the conclusions derived for the head rope regarding the torque factor, the torsional stiffness and the weight of the rope apply to the tail rope as well.

As in the case of the head rope it follows from figures 4.5b and 4.5c that the two rope portions close to the conveyances are subjected to more severe lay angle changes than the rest of the rope.

The tail rope is subjected to very low tensile loads. Since rotation is periodically taken out of the rope it is likely that its inner strands take a higher share of these low tensile load. The tail rope is therefore more susceptible to birdcaging problems than the head rope. As was discussed above the rope portions close to the conveyances are subjected to the highest lay angle changes which are happening under extremely low tensile loads. It is therefore more likely that birdcaging problems will occur in the two rope portions close to the conveyances.

7.6 Comparison Between Constant and Variable C and T Models

Modelling the behaviour of head and tail ropes with the assumption of constant C and T factors resulted in explicit equations for the torque, the lay angle deviation and the rope rotation. These equations have proved useful in understanding the manner in which rope and winder properties affect the rope behaviour. These equations are also help to understand the interactions between those properties.

The results calculated by the head rope constant C and T factors theoretical model were very similar to those of the variable C and T factors model. This is due to the fact that the C and T factors of non-spin ropes are almost constant at the relatively high tensile loads acting in a head rope. The constant C and T factors model is therefore a good approximation of the head rope's behaviour. The approximation is less satisfactory for tail ropes because the C and T factors for the majority of non-spin rope constructions are not constant at the low tensile loads acting in tail ropes. However both constant C and T factors models are useful tools for a quick assessment of a rope's behaviour.

The variable C and T factors models can be used for a more accurate analysis of a rope's behaviour. These models also provide a means of studying the effects of releasing or forcing rotations in a head or tail rope. The constant C and T factors models can not account fully for that because in equations 3.2, 3.4, 4.11 and 4.14 the initial rotation, Φ_{in}, affects only the level of the torque and rope rotation but not the variation during a trip.

A further advantage of the variable C and T factors models may be their use for identifying an optimum shape of the torque-tension curves for a particular winder. Appropriate ropes may then be selected or designed for that winder.

7.7 General Discussion

The findings of this study can not be seen or implemented in isolation of other factors that affect the general rope behaviour. Although the torsional behaviour of Koepe ropes is one of the most important parameters, especially in deep level mining, it is not the only one. A best solution for a problem related to the torsional behaviour is not necessarily the best solution for the general rope performance. For example, a zero C factor which eliminates rope rotation introduces other problems such as birdcaging.

On the other hand a best solution for one winder is not the best solution for every winder. This is implied by the great number of different rope constructions designed for Koepe winders.

The selection of the "best rope" for a given winder is based on past experience and a trial and error approach is adopted. It is often the case that this approach is extremely expensive and time consuming. A recent example is that of the Vaal Reefs number nine shaft Koepe winder tail rope. During the last few years a number of different rope constructions were tried, each one with limited success. This happens despite the fact that ropes of the same construction operate successfully on similar Koepe winders elsewhere.

Application of the theoretical model in such cases might reveal the reasons of the poor rope performance. These reasons might not necessarily relate to rope selection but could relate to rope installation and operation procedures such as selection of tail rope swivels and operating policy.

The principles developed during the course of the project have been successfully implemented by the author to model the torsional behaviour on triangular strand ropes on drum winders[43,44,45]. The generally held opinion that triangular strand ropes do not rotate on drum winders installations was disproved by the model. Their rotation was subsequently verified experimentally with on site measurements. Through use of the model certain aspects of the behaviour of triangular strand ropes on drum winders such as uniform wear pattern around the circumference of the rope and wear mechanics have been explained.

8 CONCLUSIONS AND RECOMMENDATIONS

As pointed out by Dr. J.T.D. Fritz previous research included an error in the assumption that the torque in hoisting ropes varies along their length. Assuming constant torque, new theoretical models were developed. The predictions of these models, based on laboratory measurements of rope properties were tested on a working Koepe winder.

Difficulties were encountered during some measurements on a working Koepe winder in the form of strong torsional vibrations. Such measurements involve considerable preparation and coordination with officers on the mine and could not be repeated. Nevertheless an attempt has been made to extract results by analytical manipulation to eliminate the effect of the vibrations.

8.1 Findings Related to the Measured and Calculated Results

Differences between measured and predicted behaviour involved the following:

- The head rope rotation measured by the chalk line test, was significantly lower than the calculated value. The difference is attributed to:
  a. The assumption made in the theoretical model that the loading and unloading torque tension curves were the same, i.e. hysteresis was neglected.
  b. Differences between actual torsional properties of the rope and those measured on a short sample in the laboratory.

- The differences between the measured and calculated torque values in both head and tail ropes were substantial. However, these differences could possibly be justified by:
  a. The assumptions made in the theoretical model.
  b. The fact that measurements were not done in a laboratory under controlled conditions, but on site with unknown factors and assumptions about the test conditions and the rope properties.

- Despite the differences between the measured and calculated values, the theoretical models have correctly predicted the trends and direction of the variation of the torque and the rope rotation. The models have therefore correctly qualified but not accurately quantified the ropes' behaviour.

8.2 Findings Related to Previous Work

The work presented in this dissertation has confirmed certain conclusions reached by previous researchers, namely:

- The rotation of both head and tail ropes is a function of the square of the hoisting depth.

- The head and tail rope portions close to the conveyances are subjected to the greatest lay angle changes. These portions are also subjected to the most severe fatigue loading. Special attention must therefore be given to those portions during rope inspection.

- A rope with a zero C factor will eliminate lay angle variations and rope rotation.

- On Koepe winders where the tail loop is formed freely without a tail sheave it is necessary to install low frictional torque swivels at both ends of the rope.

The present study has also given theoretical proof to certain opinions and practices adopted by rope users over the years such as the fact that:

- A rope with a zero or very low C factor is susceptible to birdcaging problems. A certain amount of positive torque, which tends to tighten the outer strands, is desirable in the head rope.

8.3 New Findings

The following findings, which the author believes to be new, follow from this research:

- The lay angle variations and therefore the rope rotation for both head and tail rope are a result of the torque difference in the two sections of the rope and not of the absolute value of the torque in the ropes.

- The torsional behaviour of multi-strand non-spin head ropes is more sensitive to the introduction of negative than positive rotation.

- Multi-strand non-spin head ropes do not rotate when the conveyances are loaded or unloaded. However triangular stand ropes rotate during these processes.

- The variation, with tensile load, of the frictional torque of the swivels on the two legs of a freely looped tail rope must be minimum. This will ensure that both swivels rotate simultaneously during the trip, preventing the two legs of the rope from intertwining.

The following additional findings, supported by the author, are a matter of controversy among rope users:

- The fact that both the head and tail rope rotation are functions of the square of the hoisting depth should not be seen as a limitation to the application of the Koepe system to deep level shafts. With proper rope design, rope selection and operating procedures, the problems associated with the torsional behaviour can be overcome.

- Lay angle variations and rope rotation can be minimised by appropriate rope design. A rope with a high torsional stiffness or an appropriate shape of torque-tension curves can give the desired results.

- Rope life improvements achieved with the installation of non-spin ropes are mainly due to the higher torsional stiffness of these ropes. Their lower torque factor has a lesser influence.

8.4 Recommendations for Further Work

Further research, aimed at improving the quantitative accuracy of predictions of rope behaviour, is recommended. In particular:

- Modelling of the torsional behaviour of the ropes taking into account hysteresis effects will increase the accuracy of the calculations. This however will result in a significantly more complex algorithm. The condition of each rope element will depend not only on the torque and tension in the element but also on the torque and tension history.

- Further experiments on Koepe winders are recommended to measure the torque variation in both head and tail ropes.

- Further investigation into the torsional properties of wire ropes is recommended. Aspects such as variation of the torsional properties of ropes along their length and effective torsional stiffness of a wire rope in service should be investigated.

Appendices in separate PDF file